I. A Theoretical Investigation of the Charge Transfer Process in Alkali-Atom Alkali-Ion Collisions

II. *Ab Initio* Effective Potentials for Use in Molecular Calculations

Thesis by

Carl Frederick Melius

In Partial Fulfillment of the Requirements

For the Degree of

Doctor of Philosophy

California Institute of Technology

Pasadena, California

1973

(Submitted November 13, 1972)

To my mother

ACKNOWLEDGEMENTS

It would be impossible to look back on the four years at Caltech and not mention the names of three people who took an active role in following my research progress at Caltech: Colonel Robert P. Knight, Minnesota State Director of Selective Service; Hazel Johnson, Executive Secretary of Local Board Number 90; and Dr. Curtis W. Tarr, Ex-National Director of Selective Service. I would have included in this list the names of the Local Board 90 members but I never could meet them despite two special trips back to Minnesota for personal appearances. It is too bad that Dr. Tarr was not able to hold his job very long. If only he were younger, I know of an organization which could have offered him a position with all expenses paid and travel to a foreign country. It is also unfortunate that there will be cut backs in the efforts of Col. Knight and Ms. Johnson to send out notices of "greeting" which have cheered the hearts of young men in America.

I would like to thank the following people who helped make my stay at Caltech possible: Dr. William Goddard, advisor; Harriett Buhai, Peter Marx, and David Brown, lawyers; David Huestis, colleague; Dean F. Bohnenblust; S. B. Lans, R. F. Leach, S. Winthrop, and E. S. Roeth, Government Appeal Agents; Senators Alan Cranston, Eugene McCarthy, and George Murphy; G. Ketabgian, D. Derauf, and D. W. Eisenstadt, Medical Doctors; innumerable secretaries including Yvonne Goddard; and last, but most important, an unknown doctor at the Los Angeles Induction Center.

ABSTRACT

PART I. The charge transfer processes occurring in collisions of alkali atoms with alkali ions have been studied theoretically using the molecular wavefunction approach. In Part A, we discuss the coupling process between electronic states as exemplified in collisions of $Li + Na^+$ and $Na + Li^+$. We find that the total transition process can be decomposed into a succession of simple two-state transition processes. The Σ-Σ two-state process can be described by a three-step process involving a coupling region, an uncoupled phase changing region, and a decoupling region. On the other hand, in the molecular wavefunction formulation, the Σ-Π two-state transition involves a continuous coupling process. The resulting transition probabilities for Σ-Π coupling differs from Σ-Σ coupling leading to different cross sections. In Part B, the molecular wavefunction approach is used to calculate the charge transfer cross sections of alkali-atoms and alkali-ions involving Li, Na, and K.

PART II. We have investigated the method of effective potentials in replacing the core electrons in molecular calculations. The effective potential method has been formulated in a way which will simplify computations while preserving ab initio quality results. The effective potential is expressed in an analytic form which represents the actual ab initio non-local potential (as defined by the matrix elements for a given basis set). Furthermore, this analytic form permits efficient computations of the effective potential integrals by incorporating the properties of Gaussian basis functions. To minimize the number of

basis functions required in the molecular calculations, we define a new ab initio effective potential derived from a modified HF orbital whose core character has been removed. The effective potential method as formulated becomes a very strong but reliable tool in attempting calculations on very large molecules.

TABLE OF CONTENTS

Page

PART I

The Charge Transfer Process Using the Molecular Wavefunction Approach

PART I-A

A Description of the Asymmetric Charge Transfer Process in $Li + Na^+$ and $Na + Li^+$

I. INTRODUCTION

Collisionally induced transitions between electronic states during slow atom-atom collisions (e.g., electronic excitation, electronic transfer, or electronic excitation transfer) are described in the near-adiabatic formalism in which the electronic wavefunction does not depend on the motion of the nuclei. Early investigations of the charge transfer process were carried out by Landau,[1] Zener,[2] and Stueckelberg.[3] They obtained an estimate of the two-state transition probability for two potential energy curves having a crossing or a near crossing (giving rise to the LZS approximation).[4] Estimates of the charge transfer probability between two near-resonant electronic states has been considered by Gurnee and Magee,[5] Rapp and Francis,[6] and others.[7-11] More recently, the importance of coupling to other states, in particular the rotational coupling to π states, has been considered.[12-14] These approaches usually take the electronic states to be atom eigenstates. On the other hand, one can take the electronic states to be molecular wavefunctions obtained from the Born-Oppenheimer approximation.[15] This molecular wavefunction approach has been applied to several charge transfer systems[12, 13, 16-19] However, difficulties exist in this procedure, both in the evaluation of the molecular wavefunctions and energy curves and in the evaluation of the coupling terms between the molecular states.[20]

Herein, we report the use of the multistate molecular wavefunction approach to obtain electronic transition cross sections for the collisions

$$Li + Na^+ \rightarrow Li^+ + Na \qquad (1)$$

and

$$Na + Li^+ \rightarrow Na^+ + Li \qquad (2)$$

The molecular wavefunctions and coupling terms are evaluated rigorously. We find that the molecular wavefunction approach leads to a simple picture of the charge transfer process involving a succession of two-state transition processes. The two-state coupling process is discussed and compared with existing models.

II. DETAILS OF THE METHOD

A. The Coupled Equations

The total wavefunction Ψ for the scattering system can be expressed in the time independent representation as a function of the internuclear distance R and the electronic coordinates, taken collectively as $\underset{\sim}{r}$. Since the nuclear masses are much greater than the electronic mass, we expand the total wavefunction as

$$\Psi = \sum_i F_i(\underset{\sim}{R})\psi_i(\underset{\sim}{r}, R) \qquad (3)$$

where ψ_i describes a given electronic state of the system (which may depend on the internuclear separation, but not on the orientation of the molecule in space), while F_i describes the nuclear motion for the given electronic state ψ_i.

Substituting Eq. (3) into the time-independent Schroedinger equation, multiplying on the left by ψ_j, and integrating over the electronic coordinates, we obtain the set of coupled equations for the nuclear motion[21]

$$\sum_i \{S_{ij}(-\frac{1}{2m}\nabla_R^2 - E) + V_{ij}(R) + \frac{J_{ji}}{M} - \frac{\vec{\Gamma}_{ji}}{M} \cdot \vec{\nabla}_R\} F_i(\underset{\sim}{R}) = 0 \qquad (4)$$

where

$$S_{ij} = \langle \psi_i | \psi_j \rangle \tag{5a}$$

$$V_{ij} = S_{ij} \frac{Z_A Z_B}{R} + \langle \psi_i | H_{e\ell} | \psi_j \rangle \tag{5b}$$

$$\vec{\Gamma}_{ij} = \langle \psi_i | \vec{\nabla}_R | \psi_j \rangle \tag{5c}$$

$$J_{ij} = \langle \psi_i | -\tfrac{1}{2} \nabla_R^2 | \psi_i \rangle \tag{5d}$$

and $H_{e\ell}$ is the electronic Hamiltonian.

While Eq. (4) is exact, it involves an infinite number of states (including the continuum). To be computationally feasible, it is necessary to choose a representation for ψ_i so that Eq. (3) can be approximated in terms of a small number of states. One approach is to take ψ_i to be the atomic eigenfunctions of the separated atoms. This is a good approximation for very high nuclear velocities since the nuclei would typically be moving as fast as the valence electrons (e.g., $v \sim 10^8$ cm/sec corresponding to a Na^+ ion energy of $\sim$ 120 KeV). For slower velocities, the electron is best described in terms of molecular wavefunctions. One uses the Born-Oppenheimer approximation[15] to define each ψ_i as the solution of the electronic Hamiltonian

$$\mathcal{H}_{e\ell} \psi_i(\underset{\sim}{r}, R) = E_i(R) \psi_i(\underset{\sim}{r}, R) \quad . \tag{6}$$

In this case $S_{ij} = \delta_{ij}$ and $V_{ij} = V_i \delta_{ij}$. The V_i's represent adiabatic potential energy curves along which the nuclei move.

For the energy range we are considering, $E \gg V_i(R) - V_i(\infty)$ [i.e., $E > 100$ eV]. We can therefore assume that the projectile travels in a straight line (this should be valid except for very small impact

parameters, which contribute little to the total cross section.) Using this impact parameter approach,[22] the nuclear wavefunction can be taken as

$$F_i(\underset{\sim}{R}) = a_i(z) \exp[i \int_{-\infty}^{z} k_i(z')dz'] \tag{7}$$

where $z^2 + b^2 = R^2$, b is the impact parameter, R is the internuclear distance, $k_i = [2m(E - V_i)]^{\frac{1}{2}}$, E is the translational energy for the separated system ($E = \frac{1}{2} Mv^2$), and V_i is the potential energy of the i^{th} molecular state (see Fig. 1). Substituting Eq. (6) into Eq. (3), taking $k_i = k_j \approx k = Mv$, and ignoring terms of order $1/M$ compared to unity, we obtain[23]

$$\frac{da_i(z)}{dz} = -\sum_j \Gamma_{ij}(z) \exp[-i\omega_{ij}(z)]a_j(z) \tag{8}$$

where

$$\omega_{ij}(z) = \int_{-\infty}^{z} (V_j - V_i)dz' \tag{9}$$

and

$$\Gamma_{ij}(z) = \langle \psi_i | \frac{d}{dz} | \psi_j \rangle \quad . \tag{10}$$

Eq. (8) represents the usual set of close coupled equations to be solved in the impact parameter method.[22]

The Γ_{ij}'s represent the non-adiabatic coupling terms between molecular states due to the breakdown of the Born-Oppenheimer approximation:

$$\Gamma_{ij} = \frac{z}{R} M_{ij} + \frac{b}{R} N_{ij} \tag{11}$$

where

$$M_{ij} = \langle \psi_i | \frac{\partial}{\partial R} | \psi_i \rangle \tag{12a}$$

$$N_{ij} = \langle \psi_i | \frac{1}{R} \frac{\partial}{\partial \theta} | \psi_j \rangle \cdot \tag{12b}$$

M_{ij} will couple states of the same symmetry (i.e., Σ-Σ, Π-Π etc.) while N_{ij} will couple states whose angular momentum differs by one, (i.e., Σ-Π).

B. The Molecular Eigenstates

The molecular wavefunction ψ_i [Eq.(6)] were evaluated using the effective potential method.[24] The angular-dependent effective potentials were obtained from modified Hartree-Fock orbitals and were designed to provide ab initio quality results with minimal computational effort. The method should reproduce the HF description of the wavefunctions which should be appropriate for the single valence electron of $LiNa^+$. The HF description of the alkali atoms leads to a small error in the ionization energies for the various atomic states. However, this error is very serious for small energy differences between different atoms (e.g., the energy defect for Li(2s) and Na(3s) should be .0093 h = .25 eV rather than 0.0141 h). To alleviate this difficulty, the effective potentials have been modified to reproduce the experimental ionization energies. The basis set for the Σ states consisted of three s, three p and one d contracted Gaussians on each center, appropriate for describing the lowest ^2S and ^2P states of each atom. For the Π states, the basis set was modified by deleting the s functions and adding a d function to each center.

The effective potential method breaks down for small R ($<3.5a_0$) since it assumes that the core orbitals do not change with R. However, the dominant charge transfer processes occur at long range, so a detailed knowledge of the potential energy curves and coupling terms at small R are not necessary. We found that modification of the potential energy curves and coupling terms for $R < 3.5\ a_0$ did not significantly change the charge transfer cross sections.

C. Evaluation of the Coupling Matrix Elements

The coupling terms M_{ij} and N_{ij} are evaluated by substituting the solutions of Eq.(6) into Eqs.(12a) and (12b). However, a difficulty exists in the M_{ij} and N_{ij} since they are not translationally invariant.[20,22] That is, the evaluation of the matrix elements depends upon the origin used to define the coordinate system. As an example, in Fig. 2 we show the coupling term between the $1\ ^2\Sigma^+$ and $2\ ^2\Sigma^+$ states of $LiNa^+$ with the origin taken at the Li atom ($\langle 1 | \frac{\partial}{\partial R} | 2 \rangle_{Li}$) and with the origin taken at the Na atom ($\langle 1 | \frac{\partial}{\partial R} | 2 \rangle_{Na}$). To counteract the lack of translational invariance, travelling phase factors have been introduced into the basis functions used to describe the ψ_i's.[25-28] While traveling phase factors are appropriate for the atomic eigenfunction approximation,[29] this method results in non-symmetric matrix elements (i.e., $\Gamma_{ij} \neq -\Gamma_{ji}$) even when the velocity goes to zero.[30] The corresponding coupling

terms for $LiNa^+$ for small velocity obtained from the translational phase factor method are shown by dashed lines in Fig. 2. Since $\Gamma_{ij} \neq \Gamma_{ji}$, probability conservation and detailed balancing are not satisfied in Eq. (6).[31] While translational phase factors are important for taking into account the translational momentum of the electron and should be included for high velocities (for which the electron's translational energy is comparable to the energy separation between states,[32] the method does not yield the correct coupling terms for the molecular wavefunction approach.

We have, therefore, formulated a simple and straightforward method for obtaining the coupling matrix elements between molecular wavefunctions which does not involve phase factors.[33] For example, the coupling between the 2s and 2p states of an atom when the other

nucleus is at infinity should be zero, which corresponds to the origin being located on the atom. If one were to take the origin as the center of mass, for example, the coupling term would be non-zero. Thus, the origin for evaluating Γ should depend on the position of the electron and not on the positions of the nuclei. One can consider the electronic transition as occurring instantaneously (i.e., the electron does not shift its position during the transition). The transition represents the change in the evolution operator describing the electron's motion. Thus, the transition depends on the probability of both states finding the electron at the same point in space. We therefore define the origin for evaluating the matrix element as the position $\underset{\sim}{r}$ of the electron during the transition. Since there are various positions of the electron for which a transition can take place (due to the wave nature of the electron), we define a weighted value $\overline{\Gamma}_{ij}$ for the matrix element as

$$\overline{\Gamma}_{ij} = \int d^3r\, \rho_{ij}(\underset{\sim}{r})\, \Gamma_{ij}(\underset{\sim}{r}) / \int d^3r\, \rho_{ij}(\underset{\sim}{r}) \tag{13}$$

where $\Gamma_{ij}(\underset{\sim}{r})$ is the coupling term evaluated with the origin taken at point $\underset{\sim}{r}$ and $\rho_{ij}(\underset{\sim}{r})$ is the weighting function $[\rho_{ij}(\underset{\sim}{r}) = |\psi_i^*(\underset{\sim}{r})\, \psi_j(\underset{\sim}{r})|]$ for that point $\underset{\sim}{r}$.

For diatomic molecules, $\Gamma_{ij}(\underset{\sim}{r})$ is a linear function of the distance z along the internuclear axis (not to be confused with z of the impact parameter method). One can then find a point $\underset{\sim}{\overline{r}} = \overline{z}$ ($\overline{x} = 0$, $\overline{y} = 0$) such that

$$\int d^3r\, \rho_{ij}(\underset{\sim}{r})\, (z - \overline{z}) = 0. \tag{14}$$

$\overline{\Gamma}_{ij}$ of Eq. (13) can therefore be replaced by

$$\Gamma_{ij} = \Gamma_{ij}(\overline{z}) \tag{15}$$

where $\overline{z}$ specifies the origin of the coordinate system in which Γ_{ij} is evaluated. The corresponding coupling term for $LiNa^+$ ($\langle 1 | \frac{\partial}{\partial R} | 2 \rangle_{\overline{z}}$) is shown in Fig. 2.

The definition of Γ_{ij}, as formulated, depends only on the position of the electron and is independent of the masses of the nuclei. That is, the coupling term due to the breakdown of the Born-Oppenheimer approximation results from the motion of the nuclei which are taken as infinitely massive. This is consistent with the derivation of Eq. (8) which assumes the motion of the nuclei to be independent of the instantaneous position or velocity of the electron.

In actually evaluating Γ_{ij} on the computer, N_{ij} can be evaluated by direct operation of the $\frac{\partial}{\partial \theta}$ upon the basis functions (since the coefficients depend only upon R). For M_{ij}, however, the operation of $\frac{\partial}{\partial R}$ upon the coefficient is not known. Therefore, we used

$$M_{ij} = \langle \psi_i | \frac{\partial}{\partial R} | \psi_j \rangle = \lim_{\delta \to 0} \frac{1}{\delta} \langle \psi_i(R) | \psi_j(R+\delta) \rangle \tag{16}$$

since $\langle \psi_i(R) | \psi_j(R) \rangle = 0$. A value of 0.001 a_0 was used for δ.

D. Solutions of the Coupled Equations

The N-state coupled equations in (8) were solved by transforming to a new set of variables depending only on the ratio of each state, i, to some reference state, o. Letting

$$a_i = a_0 \rho_i e^{i\phi_i} \tag{17a}$$

$$C_i^{Re} = Re[\rho_i e^{i(\phi_i + \omega_{io})}] \tag{17b}$$

and

$$C_i^{Im} = Im[\rho_i e^{i(\phi_i + \omega_{io})}] \tag{17c}$$

where ρ_i and ϕ_i are real, and taking the initial conditions to be

$$a_i = \delta_{io}, \tag{18}$$

we obtain in place of (8) a new set of 2(N-1) coupled equations involving only real functions, i.e.,

$$\begin{aligned}
\frac{\partial C_i^{Re}}{\partial z} &= \sum_{j=0}^{N-1} \{\Gamma_{ij} C_j^{Re} - \Gamma_{oj}(C_i^{Re} C_j^{Re} - C_i^{Im} C_j^{Im})\} + C_i^{Im} \frac{\Delta E_{io}}{v} \\
\frac{\partial C_i^{Im}}{\partial z} &= \sum_{j=0}^{N-1} \{\Gamma_{ij} C_j^{Im} - \Gamma_{oj}(C_i^{Re} C_j^{Im} + C_j^{Re} C_i^{Im})\} - C_i^{Re} \frac{\Delta E_{io}}{v}.
\end{aligned} \tag{19}$$

The coupled equations (19) were solved for various impact parameters and energies using an integration scheme by Bulirsch and Stoer.[34] The equations were integrated from $z = -30\ a_0$ to $z = +30\ a_0$, transforming first to a new variable

$$u = \alpha z / \sqrt{1 + \alpha^2 z^2} \tag{20}$$

so that $-1 < u < 1$. [α was taken to be $z(\text{initial})^{-1}$.][35] A fixed step

size was taken in u, using 200 to 300 points, the resulting $a_i(+\infty)$ being accurate to three places.[36]

The transition probability is given by

$$\rho_{o\to i}(v,b) = |a_i(\infty)|^2 = \rho_i^2(\infty)/(1 + \sum_{j=1}^{N-1} \rho_j^2(\infty)) \tag{20}$$

while the cross section for going from state o to state i is given by

$$\sigma_{o\to i}(v) = 2\pi \int_0^\infty P_{o\to i}(v,b)\, b\, db. \tag{21}$$

The impact parameter was varied by increments of 0.25 a_0 to 0.5 a_0 from b = 0 a_0 to b = 20 a_0, while the velocity was incremented by 1.0 atomic units of inverse velocity. Spline interpolation was used to obtain the transition probabilities for other impact parameters and velocities.

III. RESULTS

In order to describe the charge transfer processes which occur between electronic states, we use as an example the collisional processes involved in $Li + Na^+$ and $Na + Li^+$.[37] The six lowest molecular states of the $LiNa^+$ molecule (four $^2\Sigma^+$ states and two $^2\Pi$ states) dissociating to the Li 2s and Li 2p states and to the Na 3s and Na 3p states, were used in the calculations. The potential energy curves used to evaluate the ω_{ij} [Eq.(6)] are shown in Fig. 3. The coupling terms M_{ij} [Eq.(12a)] are shown in Fig. 4 while the coupling terms N_{ij} [Eq.(12b)] without the $\frac{1}{R}$ factor (i.e., $\langle\Sigma|\frac{\partial}{\partial\theta}|\Pi\rangle$) are shown in Fig. 5.

The resulting total charge transfer cross section for $Li + Na^+$ and $Na + Li^+$ are shown in Fig. 6 and compared with the experimental results of Daley and Perel.[38] We see that the theoretical and experimental results are in very good agreement. In particular, the phases and amplitudes of the oscillatory structure are in excellent agreement. Furthermore, the cross sections for processes $Li + Na^+$ and $Na + Li^+$ are correctly distinguished. The estimated uncertainty in the absolute magnitude for either experimental cross sections is 10%.[39] Inclusion of the six molecular states should adequately represent the total charge transfer process. Hence the main error in the theoretical cross sections is due to the neglect of translational momentum of the electrons. Neglecting translational momentum will lead to an overestimate of the transition probability between states, the error increasing with the ion velocity.[40]

IV. DISCUSSION

A. Cross Sections for Transitions to Individual States

We have shown that the molecular wavefunction approach can provide quite accurate charge transfer cross sections (including the detailed structure). It can also distinguish between such similar collisions as $Li + Na^+$ and $Na + Li^+$. However, if one hopes to obtain estimates for cross sections of electronic transitions occurring in other collisions for which the exact potential energy curves or coupling terms are not known, then the nature of the coupling processes between electronic states must be understood. We, therefore, present an

analysis of the coupling processes occurring in the $Li + Na^+$ and $Na + Li^+$ collisions, the conclusions of which should be of general applicability.

The $LiNa^+$ molecular system represents an ideal system to study theoretically since the energy defect $|\Delta E|$ between the ground states for the two atoms (Li 2s and Na 3s) is 0.0093 h (= 0.25 eV) while the next higher state is 0.0586 h above the Na 3s. Thus, we have a near-resonance between the Li 2s and Na 3s. As a result the 2-state approximation (involving the $1\,^2\Sigma^+$ and $2\,^2\Sigma^+$ states) should yield a reasonable estimation of the charge transfer cross section.

In order to determine the relative importance of the $1\,^2\Sigma^+ \rightarrow 2\,^2\Sigma^+$ transition to the other transitions which could occur, we carried out three sets of calculations:

(i) 2 states $(1\,^2\Sigma^+,\ 2\,^2\Sigma^+)$

(ii) 3 states $(1\,^3\Sigma^+,\ 2\,^2\Sigma^+,\ 1\,^2\Pi)$

(iii) 6 states $(1\,^2\Sigma^+,\ 2\,^2\Sigma^+,\ 3\,^2\Sigma^+,\ 4\,^2\Sigma^+,\ 1\,^2\Pi,\ 2\,^2\Pi)$

for both (1) and (2). The resulting cross sections are given in Fig. 7. We see that the cross sections are dominated by transition between the two lowest $^2\Sigma^+$ states. The transition to the Li $2p_\pi$ state is, to a certain extent, also important, particularly for the exothermic process $Na + Li^+$, where the transition Na 3s → Li $2p_\pi$ eventually dominates the Na 3s → Li 2s for low energies. Cross sections to other states are considerably smaller. Comparing the 2 state, 3 state, and 6 state results, we see that the oscillations in the total cross section arise from the $1\,^2\Sigma^+ \rightarrow 2\,^2\Sigma^+$ transition. However, the oscillations in the 2-state

calculations are out of phase with the 3- and 6-state calculations which include the $1\,^2\Pi$ state. The difference in the total cross sections for processes (1) and (2) (Fig. 6) result essentially from the added contribution of the transition to the $1\,^2\Pi$ state for process (2), which the two-state approximation does not include.

From Fig. 7 we see that the three- and six-state calculations lead to essentially identical cross sections for the $1\,^2\Sigma^+ \rightarrow 2\,^2\Sigma^+$ transition, both in amplitude and oscillatory structure. On the other hand, the cross section for transition to the $1\,^2\Pi$ state in the 3-state approximation represents the sum of the cross sections for transition into the $1\,^2\Pi$, $2\,^3\Pi$, $3\,^2\Sigma^+$, and $4\,^2\Sigma^+$ states in the 6-state approximation. [For high velocities ($v > .2$ a.u.), the 3-state approximation breaks down as transitions to the higher lying states become important.]

To understand these results, we must first understand the coupling process. We therefore discuss the two different types of two-state coupling processes which occur in the molecular wavefunction approach: (a) radially induced transitions between states of the same symmetry (e.g., Σ - Σ and Π - Π) and (b) rotationally induced transitions between states of different symmetries (e.g., Σ - Π).

B. The Two-State Σ-Σ Coupling Process

The simplest 2-state process involves symmetric, resonant charge transfer.[5, 6, 41] For the symmetric case, there is no coupling between states because the two Σ states have different symmetries (i.e., g and u) leading to $M_{ij} = 0$.

However, since each state represents motion on a different potential energy curve, the resulting nuclear wavefunctions differ in phase [see Eq.(7)] leading to oscillation in the charge transfer cross section as a function of impact parameter (for a given velocity). This may be seen more clearly from Eq.(19) where the phase factors of Eq.(7) have been incorporated into the coupled equations. The initial boundary conditions are $\rho = 1$, $\phi = 0$ in Eq.(17a). The resulting transition probability is

$$P(v,b) = \sin^2(\tfrac{1}{2}\Delta\phi) \tag{22}$$

where

$$\Delta\phi = \frac{1}{v}\int_{-\infty}^{\infty}(V_2 - V_1)dz \tag{23}$$

We see that P for a given b and v depends only upon the energy difference between the adiabatic states. As an example, we show the energy difference between the $1\,^2\Sigma_g^+$ and $1\,^2\Sigma_u^+$ states for Na_2^+ in Fig. 8. The resulting P(v,b) for

$$Na + Na^+ \rightarrow Na^+ + Na \tag{24}$$

is shown in Fig. 9a as a function of b for various v. As the impact parameter decreases, the energy difference for the minimum distance of approach increases and P oscillates rather uniformly. However, due to a maximum in the energy difference ($R_{max}(Na_2^+) = 11.4a_0$), the rate of oscillation is decreased for impact parameters smaller than this R_{max}, leading to oscillations in the total cross section.[42,43] The total cross section for process (24) in the 2-state approximation is shown in Fig. 10.

As expected from (23), the oscillation varies as v^{-1}.

We now consider the near-resonant 2-state charge transfer process. The coupling term between states [$M_{12} = \langle \psi_1 | \frac{\partial}{\partial R} | \psi_2 \rangle$] represents the transformation of the orbitals from being left and right atomic orbitals at infinity ($R > 20\ a_0$) to being bonding and antibonding molecular orbitals at small internuclear distances ($R < 6\ a_0$). M_{12} for $LiNa^+$ is plotted in Fig. 8. For finite velocities one might expect transitions between these adiabatic states throughout the entire region ($R = 6\ a_0$ to $22\ a_0$). However, the energy difference between states (shown in Fig. 8) grows exponentially as the atomic orbitals begin to overlap, preventing any net transfer between the states for smaller R [due to the rapid oscillation of the exponential terms in Eq. (8)]. [Note that translational energy needed to cause an appreciable transition probability is much greater than the energy difference between electronic states (10^3 eV compared to 1 eV)]. Transitions between states occur only at large R, (between ~12 a_0 and 22 a_0 for $LiNa^+$, the actual width depending on the velocity) where M_{12} is large while ΔE is still small. We denote this region as the transition region. For smaller R, the nuclei enter an intermediate region in which no net transitions occur between the states. However, since each state represents motion on a different potential energy curve, the phase factors of Eq. (7) will differ, the resulting phase difference being

$$\Delta\phi = \int_{-R_0}^{R_0} \frac{1}{v}\, \Delta E\, dz \qquad (25)$$

where R_0 is a representative internuclear distance of the transition region. As the nuclei separate, they again pass through the transition region, where the states decouple. The different regions are depicted in Fig. 11. If there were no change in phase ($\Delta\phi = 0$), then the states would reverse the transition process yielding the original starting state [since Γ has changed sign($\Gamma(-z) = -\Gamma(z)$)]. However, $\Delta\phi$ is not zero, in general, leading to a charge transfer probability which depends on the relative phase change (27) between the two intermediate states.

We thus find that in the molecular wavefunction framework the description of the near-resonant charge transfer process is quite comparable to that of the symmetric resonant charge transfer process (where $R_0 = \infty$).[44] Initially the electron starts out localized on one atom. As the nuclei approach, they pass through a transition region after which the electron has a certain probability $|\bar{a}_i(R_I)|^2$ of being in either of the two molecular states ($|\bar{a}_1|^2 + |\bar{a}_2|^2 = 1$). [For the symmetric case, $|\bar{a}_1(R_I)|^2 = |a_2(R_I)|^2 = \frac{1}{2}$.] The magnitudes $|\bar{a}_1|$ and $|\bar{a}_2|$ remain constant in the intermediate region but the phase factors change, leading to a relative phase change of $\Delta\phi$ as in Eq. (25). The nuclei upon separating re-enter the transition region where the states are decoupled. Phase interference yields a resulting transition probability

$$P(v,b) \approx 4\,|\bar{a}_1\bar{a}_2|^2\,\sin^2[\tfrac{1}{2}\Delta\phi] \qquad (26)$$

where $\Delta\phi$ is defined in (25). Eq. (26) reduces to Eq. (22) for the resonant case. Since $|\bar{a}_1|^2 + |\bar{a}_2|^2 = 1$, we will denote $|a_2|^2$ as p (which depends

upon v and b) and rewrite (26) as

$$P(v,b) = 4\ p(1 - p)\ \sin^2[\tfrac{1}{2}\Delta\phi]. \qquad (26')$$

While P represents the transition probability for the entire process, p represents the transition probability after crossing the transition region only once.

The actual transition probabilities for $LiNa^+$ as obtained from Eq. 8) in the two-state approximation are shown in Fig.9b. In particular, we have superimposed the transition probabilities P, for v^{-1}=6, 12, and 18 a.u. in Fig. 12 which shows that P(v,b) does depend on $\sin^2[\frac{1}{2}\Delta\phi]$ where $\Delta\phi$ is proportional to v^{-1}. The values of p(v,b) for v^{-1} = 6, 12, and 18 a.u. are shown in Fig. 13. [The p's were obtained by integrating Eq. (8)from z = - ∞ to z = 0.] Note that no oscillations occur in p since the transition region has only been crossed once.

The process involving Π-Π coupling is equivalent to the Σ-Σ coupling process, with Eqn. 26 representing the transition probability.

C. A Two-State Model for Σ-Σ Coupling

In order to better understand the 2-state coupling, we will consider a simple model. Using a 2-state atomic eigenfunction model for the molecular wavefunctions, an approximate functional dependence of p and $\Delta\phi$ on the velocity and the impact parameter can be derived.

We assume that the molecular wavefunctions can be expressed as a linear combination of the two atomic orbitals (at least in the transition region). We further assume that the overlap between the

two atomic orbitals can be ignored in this region. The transformation from atomic orbitals ϕ to molecular orbitals ψ is given by

$$\begin{pmatrix} \psi_1(z) \\ \psi_2(z) \end{pmatrix} = \begin{pmatrix} \cos\theta & \sin\theta \\ -\sin\theta & \cos\theta \end{pmatrix} \begin{pmatrix} \phi_A \\ \phi_B \end{pmatrix} \tag{27}$$

where θ is a function of z. Letting ϵ_A and ϵ_B be the eigenenergies of ϕ_A and ϕ_B respectively, and H_{AB} the interaction hamiltonian, we have

$$\Delta E = 2\, H_{AB} \sqrt{\alpha^2 + 1} \tag{28}$$

$$\tan\theta = \alpha \pm \sqrt{\alpha^2 + 1} \tag{29}$$

where

$$\alpha = \frac{\Delta V_\infty}{2\, H_{AB}} \quad \text{and} \quad \Delta V_\infty = |\epsilon_B - \epsilon_A|.$$

Using Eq.(27) the coupling term for b = 0 is just

$$M_{12} = \langle \psi_1 | \frac{\partial}{\partial R} | \psi_2 \rangle = \frac{\partial \theta}{\partial R}. \tag{31}$$

That is, the Born-Oppenheimer coupling term for the molecular wavefunction represents the rate of rotation of the two atomic wavefunctions between themselves to form the molecular wavefunctions. The final molecular wavefunction (R = 0) corresponds to a rotation of $\pi/4$.

To obtain an estimate of M_{12} we take H_{AB} to be decreasing exponentially in the transition region, i.e.,

$$H_{AB} = \kappa\, e^{-\beta R}. \tag{32}$$

We define the point R_M as the midway point in the rotation [i.e., $\theta(R_M) - \theta(\infty) = \pi/8$], which occurs when $2\, H_{AB} = \Delta V_\infty$ or $\alpha = 1$. Using Eq.(31) and Eq. (29), we obtain

$$M_{12} = \frac{\beta}{4}\ \mathrm{sech}\ \beta\ (R - R_M). \tag{33}$$

For $LiNa^+$, we find from Fig. 8 that M_{12} does indeed have the general form of Eq. (33)in the transition region where $R_M \approx 12.8\ a_0$ and $\beta \approx .42$,[45] [corresponding to K = 1.4 in Eq. (32)]. [Note that the value of M_{12} at the maximum ($\beta/4$) is related to the exponential decay rate β since the total area under curve for M_{12} must equal the total $\Delta\theta = \theta(R=0) - \theta(\infty) \approx \pi/4$.[45]]

Substituting Eq. (33)and Eq. (28)into Eq. (8)and integrating from $z = -\infty$ to $z = 0$, we obtain $p(v, b)$. The resulting $p(v, b)$ are shown in Fig. 15 (solid lines). These can be compared with the actual p's in Fig. 14.

Analytic forms for $p(v, b)$ can be obtained in two limiting cases. For zero impact parameter ($b = 0$), $\Gamma_{12} = -M_{12}$ since $z = -R$. The solution of Eq. (8)then yields

$$p(v, o) = \tfrac{1}{2}\ \mathrm{sech}\ \gamma\ e^{-\gamma} \tag{34}$$

where

$$\gamma = \frac{\pi \Delta V_\infty}{2 \beta v} .$$

At high velocities ($\frac{\Delta V_\infty}{v} \ll 1$) $p(v, o)$ equals $\frac{1}{2}$ (which is equivalent to the symmetric case for which $\frac{\Delta V_\infty}{v} \equiv 0$). As the velocity goes to zero, $p(v, o)$ goes to zero exponentially as v^{-1}.

The other case which can be solved analytically is the high energy limit. In this case, the exponential terms in Eq. (8)can be ignored and we obtain

$$p(\infty, b) = \sin^2\left[\tfrac{1}{4} \arctan\left(\sinh \beta(R_m - b)\right) + \frac{\pi}{8}\right]. \tag{35}$$

We see that $p(\infty, b)$ has a value of $\frac{1}{2}$ at $b = 0$ and eventually dies exponentially to zero at large b. This decrease in p with increasing impact parameter results from the z/R dependence of Γ_{12} (i.e., $\Gamma_{12} = z/R\ M_{12}$). Thus, for large impacts, $z = \sqrt{R^2 - b^2} \ll R$ in the transition region (see Fig. 11).

To obtain an approximate analytical form for $p(v, b)$, we can take p to be a product of $p(v, o)$ and $p(\infty, b)$, i.e.,

$$p(v, b) \approx 2\ p(v, o)\, p(\infty, b) \tag{36}$$

where $p(v, o)$ is defined in Eq. (34)and $p(\infty, b)$ is defined in Eq. (35). This approximate p is shown in Fig. 14 (dashed line) and compared with the p obtained from substituting the 2-state model into Eq.(8). To complete the atomic eigenfunction model of Eq. (26′), we can obtain an estimate of the phase difference $\Delta\phi$. Ignoring the ΔV_∞ compared to H_{AB} and

$k_0 \to \infty$ yields

$$\Delta\phi = \frac{1}{v} 4kb\, K_1(b\beta) \tag{37}$$

where K_1 is a Bessel function of the second kind. Since K_1 rapidly goes to infinity as $b \to 0$, $\sin^2[\frac{1}{2}\Delta\phi]$ oscillates very rapidly at small b and can be approximated by its average value of $\frac{1}{2}$. However, since K_1 does not possess a maximum, no oscillations are present in the total cross section. The exponential decrease of the cross section results from the velocity dependence of p in Eq. 34. The high energy limit is proportional to v^{-2} due to the v^{-1} dependence of $\Delta\phi$.[47] From Eq. (6) we would expect the minimum in the cross section to occur when both the cosine and sine parts of the exponential term can maintain the same sign throughout the transition region, i.e., when

$$\frac{\Delta V_\infty \Delta z}{V_{max}} \approx \frac{\pi}{4} \tag{38}$$

where Δz is a measure of the width of the transition region. For $LiNa^+$ $\Delta V_\infty = .0093$ a.u. and $v_{max} \approx 0.14$ a.u. and hence (38) leads to $\Delta z \approx 12\ a_0$. Eq. (38) is the basis of the "near-adiabatic" theory proposed by Massey.[48] From Eq. (33), we see that Δz is inversely proportional to β. This property is reflected in the transition probability p [Eq. (34)] which is a function of $\frac{\Delta V_\infty}{\beta v}$. One can interpret p as $\sin^2(\Delta\theta)$ where $\Delta\theta$ represents the area under the part of the M_{12} curve that can remain in phase during

the evolution through the transition region.

D. The Two-State Σ-Π Coupling Process

The coupling between Σ and Π states results from the rotation of the nuclear axis with respect to the space fixed axis. The Σ-Π coupling process has been studied in detail in a recent paper by Russek.[14] Russek's model assumed a constant coupling term and intersecting straight line potential energy curves. From Fig. 3 and Fig. 5, we see that these approximations are quite good for the $LiNa^+$ $2\,^2\Sigma^+ - 1\,^2\Pi$ transition (for $LiNa^+$, $\langle 2\,^2\Sigma^+ | \frac{\partial}{\partial\theta} | 1\,^2\Pi \rangle \approx .95$, $R_c \approx 5.1\ a_0$). The actual 2-state transition probabilities between the $2\,^2\Sigma^+$ and $1\,^2\Pi$ states of $LiNa^+$ are shown in Fig. 9c for various velocities. We see that transitions can occur for impacts larger than the curve crossing. A maximum in the transition probability, $P_{\Sigma-\Pi}$ occurs at an impact parameter which is just inside the curve crossing. For smaller b, $P_{\Sigma-\Pi}$ decreases, eventually becoming zero at $b = 0$.[48] Oscillations appear in $P_{\Sigma-\Pi}$ for small b as the velocity decreases. However, the maximum in $P_{\Sigma-\Pi}$ remains close to unity, decreasing very slowly at smaller velocities. Therefore, the total cross section for Σ-Π coupling (see Fig. 10) decreases very slowly as v goes to zero (due essentially to the narrowing of $P_{\Sigma-\Pi}$ about its maximum). The cross section for very low velocities can be estimated from Fig. 7 of Russek's paper. Since $P_{\Sigma-\Pi}$ for small b does not contribute significantly to the total cross section (because $P_{\Sigma-\Pi}$ is small and is weighted by b), no significant oscillations occur in the total cross section due to the oscillation in $P_{\Sigma-\Pi}$ (see Fig. 9c).

The resulting Σ-Π transition probability differs from the Σ-Σ transition probability due to the different nature of the Σ-Σ and the Σ-Π coupling processes. The Σ-Σ coupling process could be divided into three steps involving a transition region and an intermediate region. On the other hand the Σ-Π coupling process in the molecular wavefunction approach is more appropriately treated as one continuous process. The difference results from the different nature of the coupling terms. While $\Gamma_{\Sigma\text{-}\Sigma}$ has the general form

$$\Gamma_{\Sigma\text{-}\Sigma} \approx \frac{z}{R}\frac{\beta}{4} \operatorname{sech} \beta(R - R_M) \tag{39}$$

[see Eq.(33)], $\Gamma_{\Sigma\text{-}\Pi}$ has the form (in the coupling region)

$$\Gamma_{\Sigma\text{-}\Pi} \approx \frac{b}{R^2} L \tag{40}$$

where L is a constant. Thus, $\Gamma_{\Sigma\text{-}\Pi}$ does not go to zero for small R, but rather, increases. This growth in Γ as R becomes smaller compensates for the corresponding increase in the energy difference, leading to a continuous coupling between the states. Thus, the phase interference between states is an integral part of the coupling process and oscillations occur throughout the transition [see Ref. (14)]. While $\Gamma_{\Sigma\text{-}\Sigma}$ is zero at the half-way point in the collision (i.e., z = 0), $\Gamma_{\Sigma\text{-}\Pi}$ reaches its maximum value at this point. Furthermore, $\Gamma_{\Sigma\text{-}\Pi}$ maintains the same sign throughout the collision. Thus, unlike Σ-Σ coupling, large transition probabilities occur for collision trajectories which are tangential to and even outside the curve crossing [see Fig.(9c)]. Due to the curve crossing, $P_{\Sigma\text{-}\Pi}$ can be large even for small velocities, unlike $P_{\Sigma\text{-}\Sigma}$

which decreases exponentially as v^{-1} (see Fig. 10).

At high velocities, the total cross section does not go to zero, but increases instead (see Fig. 10). This results from the neglect of the translational momentum of the electron. This neglect is much more serious for Σ-Π coupling than for Σ-Σ coupling because of the different nature of the coupling process. The Σ-Σ coupling term [eq. (39)] is antisymmetric with respect to z, which reverses the transition process at high energies, leading to zero charge transfer. On the other hand, $\Gamma_{\Sigma-\Pi}$ [Eq. (40)] maintains the same sign during the collision, leading to twice the rotation $\Delta\theta$ between states as occurred at $z = 0$. Thus, the Σ-Π cross section eventually goes to a constant at infinite velocity since $\langle 2\,^2\Sigma^+ | \frac{\partial}{\partial\theta} | 1\,^2\Pi \rangle$ does not remain constant but goes to zero at large R. In the model used by Russek, the coupling term is assumed constant for all R, but the energy difference is assumed to be infinite at large R, so his cross section remains flat at high energy. However, neither cross section is really meaningful at this high energy limit, since the molecular wavefunction approach is not appropriate for such high velocities.

The neglect of the electronic translational momentum along the z axis causes the Σ-Π transition probability to be overestimated at lower energies as well, though to a lesser extent. This error in $\sigma_{\Sigma-\Pi}$ is much greater than the error in $\sigma_{\Sigma-\Sigma}$ for equivalent ion velocities, due to the high angular velocities reached at small impact parameters.

D. The Multistate Coupling Process

Having considered the 2-state processes, we now consider the entire coupling process involved in the scattering processes (1a) and

(1b). We find that the multistate coupling process can be interpreted as a series of 2-state coupling processes.[50] We showed that transitions between two Σ states occur only at long range where the potential energy curves are close together; for smaller R, the two Σ states were uncoupled. On the other hand, Σ-Π transitions occur in the region of the curve crossing between the Σ and Π states. From the potential energy curves for the $LiNa^+$ quasimolecule (Fig. 3), we see that the $1\,^2\Sigma^+$ and $2\,^2\Sigma^+$ potential energy curves are nearly degenerate at large R ($R \gtrsim 12 a_0$), permitting a strong Σ-Σ coupling between these states. The other $^2\Sigma^+$ states are much higher in energy, so that no direct transitions will occur to these higher lying Σ states [except at high energies (v > .2 a.u.)]. On the other hand, the $1\,^2\Pi$ state crosses the $2\,^2\Sigma^+$ state at 5.1 a_0, permitting transitions to occur between the $2\,^2\Sigma^+$ and $1\,^2\Pi$ states at small R. There is a curve crossing of the $1\,^2\Pi$ curve and $3\,^2\Sigma^+$ curve at 10.7 a_0, allowing a 2-state coupling between these two states. And finally, the $3\,^2\Sigma^+$ and $4\,^2\Sigma^+$ states and the $1\,^2\Pi$ and $2\,^2\Pi$ states have a near resonance at large R permitting Σ-Σ and Π-Π coupling to occur respectively between these two pairs of states. Coupling will not occur between other pairs of states because the energy difference is too large. Since Σ-Σ transitions (or Π-Π transitions) occur at large R while Σ-Π transitions occur at small R for which the Σ states are uncoupled, we can decompose the multistate process into separate 2-state processes.

First, as the nuclei approach each, the electron entering on the $1^2\Sigma^+$ or $2\,^2\Sigma^+$ state passes through the transition region coupling the $1\,^2\Sigma^+$ and $2\,^2\Sigma^+$ states. The probability for a transition is given by Eq. 36. For smaller R, an electron in the $1\,^2\Sigma^+$ is not coupled with any

other state, until the nuclei separate and re-enter the $1\,^2\Sigma^+ - 2\,^2\Sigma^+$ transition region. On the other hand, an electron in the $2\,^2\Sigma^+$ is coupled to the $1\,^2\Pi$ state at smaller R. The transition between the $2\,^2\Sigma^+$ and $1\,^2\Pi$ states can be treated by the 2-state process considered in part D. Thus, as the nuclei begin to separate, there is a probability for being in the $1\,^2\Sigma^+$, $2\,^2\Sigma^+$ and $1\,^2\Pi$ states. As the nuclei separate further, a transition can occur between the $1\,^2\Pi$ state and the $3\,^2\Sigma^+$ state (at ~ 10.7 a_0). Finally, for $R > 12\ a_0$ the separating nuclei enter the transition regions for the $1\,^2\Sigma^+ - 2\,^2\Sigma^+$ coupling, $1\,^2\Pi - 2\,^2\Pi$ coupling, and $3\,^2\Sigma^+ - 4\,^2\Sigma^+$ coupling. For the $1\,^2\Sigma^+ - 2\,^2\Sigma^+$ coupling, the resulting transition probability is no longer given by Eq. (26), but the basic principles still hold. The probability amplitude on the $2\,^2\Sigma^+$ state in the intermediate region has been reduced. Thus, when the atoms depart there is a smaller component of $2\,^2S$ to interfere with the $1\,^2\Sigma^+$ state, giving rise to smaller oscillations in p. Also, $\Delta\phi$ has been changed due to the new possible trajectories created by addition of the $1\,^2\Pi$ state.

If p′ represents the probability to remain on the $2\,^2\Sigma^+$ state during the intermediate step, then Eq. (26) becomes

$$P = 4p(1-p)\left[p' \sin^2\left(\tfrac{1}{2}\Delta\phi'\right) + \tfrac{1}{4}(1-p')\right] \qquad (41)$$

This can be best shown for the symmetric Na_2^+ charge transfer whose transition probabilities for the 3-state process ($1\,\Sigma_g$, $1\,\Sigma_u$, $1\,\Pi_u$) are shown in Fig. 9d [in this case, $p = \frac{1}{2}$ in Eq. (41)]. Since the $\Delta\phi$ has changed, the oscillations in the total cross section for Na_2^+ have changed (see Fig. 10). The corresponding transition probabilities for $Na + Li^+$ in the 3-state approximation are shown in Fig. 9e. Again, the change

in $\Delta\phi$ leads to a shift in the oscillations in the $1\,^2\Sigma^+ \rightarrow 2\,^2\Sigma^+$ cross sections (see Fig. 7, Fig. 10). Note that the $2\,^2\Sigma^+ \rightarrow 1\,^2\Pi$ transition probabilities are similar for the 2- and 3-state approximations except for a scaling factor (1-p) where p is defined in Eq. (31). [For Na_2^+, $(1-p) \equiv \frac{1}{2}$, so the 2-state Σ-Π transition probability (not shown) is equivalent to the Σ-Π transition probability in the 3-state approximation scaled by a factor of two.]

For the 3-state approximation, the $1\,^2\Pi$ state was not allowed to interact with the other higher lying states. However, as we saw from the potential energy curves, transitions could occur from the $1\,^2\Pi$ state to the $3\,^2\Sigma^+$ and $2\,^2\Pi$ states and then from the $3\,^2\Sigma^+$ state to the $4\,^2\Sigma^+$ state. However, since small impact parameters are required to populate the $1\,^2\Pi$ state, the $1\,^2\Pi \rightarrow 3\,^2\Sigma^+$ transition probability will be small. Also, since the Li 2p - Na 3p energy splitting (0.0187h) is larger than the Li 2s - Na 3s energy splitting, the $3\,^2\Sigma^+ \rightarrow 4\,^2\Sigma^+$ and $1\,^2\Pi \rightarrow 2\,^2\Pi$ transition probabilities are small. The resulting transitions do not involve any interference (as in 1Σ - 2Σ coupling) since the transition region is only crossed once.

E. A Comparison of the Molecular Wavefunction and the Atomic Eigenfunction Formulations

We have used the molecular wavefunction formulation (MWF) to obtain charge transfer cross sections. In this approach, the $\underset{\sim}{S}$ and $\underset{\sim}{V}$ matrices of Eq. (4) were taken as diagonal so that the coupling between (molecular) states results from the $\underset{\sim}{\Gamma}$ matrix [Eq. (11)]. One could

have used, instead, the diabatic representation involving frozen atomic orbitals in Eq. (4), and would have obtained an equivalent solution (assuming an infinite number of states). In this atomic eigenfunction formulation (AEF), $\vec{\underset{\sim}{T}}$ is equal to zero (neglecting the overlap between atomic states), with the coupling between (atomic) states resulting from the non-zero $\underset{\sim}{V}$ matrix. Using the impact parameter method, the resulting 2-state coupled equations in the diabatic representation are [6]

$$\frac{d}{dz}(a_1) = \frac{-i}{v} \frac{H_{AB} - S H_{BB}}{(1 - S^2)} e^{-i\Omega(z)} a_2$$

$$\frac{d}{dz}(a_2) = \frac{-i}{v} \frac{H_{AB} - S H_{AA}}{(1 - S^2)} e^{+i\Omega(z)} a_1 \qquad (42)$$

where $\Omega(z) = \int_{-\infty}^{z} (H_{BB} - H_{AA})/(1 - S^2) \frac{dz}{v}$, $S = \langle \phi_A | \phi_B \rangle$, $H_{AB} = \langle \phi_A | H_{e\ell} | \phi_B \rangle$, etc. Usually, one further assumes that $S \approx 0$ and, for systems like $A + B^+ \rightarrow A^+ + B$, assumes that $H_{BB} - H_{AA} \approx \epsilon_B - \epsilon_A$. The resulting equations look very similar to Eq. (8), but differ in two essential respects. First, since $\epsilon_B - \epsilon_A$ is a constant, the exponential terms in Eq. (42) oscillate uniformly along the entire trajectory. And second, the coupling term, $\frac{H_{AB}}{v}$, increases rapidly as the internuclear distance decreases and depends inversely upon the velocity. Thus, in the AEF, we have transitions throughout the entire interaction region, with the strongest coupling for smaller R. This gives rise to strong oscillations in the transition probability during the entire collision.

If one were to make the approximations presented in Part D of this section (i.e., the two-molecular states must be linear combinations of the two atomic orbitals, the overlap is zero, and straight line trajectories are used), then the resulting transition probabilities for the MWF would be identical for either formulation. For example, substituting Eq. (34) into Eq. (26′), we obtain the same transition probability for zero impact as Demkov[8] [Eq. (11) of this paper] obtained using the AEF.[51]

However, in general, ψ_i wants to include polarization and also wants to become more contracted. This requires many atomic orbitals, including those in the continuum. To see what effect this restriction has on the cross section, we carried out a frozen Li 2s and Na 3s basis set calculation to obtain $\Delta E'$ and M_{12}'. These are compared with the actual ΔE and M_{12} in Fig. 15. We see that $\Delta E'$ is smaller, and that M_{12}' has been shifted inward. The difference results essentially from polarization of the orbitals, allowing them to interact at longer range. The resulting values for β and R_M of Eq. (33) are $\beta' = .38$ and $R_M = 11.8\ a_0$ compared with $\beta = .42$ and $R_M = 12.8\ a_0$ for the actual molecular wavefunctions. This error results in a cross section which is too small.

Further approximating M_{12} and ΔE by the model presented in section IV-C, one usually takes $\beta = \sqrt{2I}$ (defined in a.u.'s) where I is the smaller of the ionization energies for atoms A and B.[6,8] For $LiNa^+$, $\beta = .62$ which makes the resulting cross section even smaller. Olson[11] uses this method to obtain an estimate of the $LiNa^+$ charge transfer cross section.[52] As expected, the cross section is too small since

R_M is too small and β is too large. This does not mean that the model presented in IV-C is poor. Using $\beta = 0.42$ and $R_M = 12.8\, a_0$, we in fact obtained a very good approximation to the cross section. The only difficulty is that one needs a better empirical formula for estimating β and R_M. Using the appropriate β and R_M, obtained perhaps from a simple MO calculation, the reduced cross section presented in Olson's paper[11] should be very useful for estimating charge transfer cross sections.

A further difficulty arises in the atomic eigenfunction formulation. For the multistate process the AEF does not provide a simple picture of the transition process representing a succession of 2-state processes as occurs in the MWF (section IV-D) because the transition region in the AEF extends throughout the entire interaction region. To obtain an estimate of the transition probability to other states in the MWF, we need to know p, the probability for being in an intermediate molecular state [Eq. (36)]. The AEF provides only the total transition probability, P. One can extract p from P if P is put in the form of [Eq. (26′)]. This form of P has been estimated by Rapp and Francis[6] and by Demkov.[8] Using Eq. (51) of Ref. 6, we obtain

$$p_{RF} = \tfrac{1}{2}\, \mathrm{sech}\,[\gamma_{RF}]\, \exp[-\gamma_{RF}]$$

$$\gamma_{RF} = \frac{\pi\, \Delta V_\infty}{2\, \beta v} \left(\frac{2\beta b}{\pi}\right)^{\frac{1}{2}} \tag{43}$$

while from Eq. (11) of Ref. 8, we obtain

$$p_D = \tfrac{1}{2} \operatorname{sech} [\gamma_D] \exp [-\gamma_D]$$

$$\gamma_D = \frac{\pi \Delta V_\infty}{2\beta v} (1 - b^2/R_M^2)^{-\frac{1}{2}} \tag{44}$$

where R_M is the same as used in Eq. (33). These estimates of p are compared with our estimate of p (denoted p_{MG}) [Eq. (36)] in Fig. 16 for $v = 12$, $\beta = .42$, $R_M = 12.8a_0$ and $\Delta V_\infty = 0.0093h$ and also compared with the p obtained from numerical calculation (p_N). We see that p_N, p_D, and p_{MG} agree for small b. However, p_D goes to zero at R_M. On the other hand, p_{RF} is an asymptotic approximation for large b, so is not expected to be good as small b. However, even for large b, p_D decreases too slowly.

Another case where differences occur between the MWF and the AEF is when the rectilinear trajectory restriction is lifted. As we have shown, when the energy difference between states is large the nuclei will move on one or the other of the adiabatic potential energy curves with no coupling between states. On the other hand, no simple picture is obtained in the diabatic representation. Transitions occur constantly between the diabatic states. These "transitions" really mean that the electron does not want to be in a diabatic atomic state, but rather it wants to be in an adiabatic molecular state. Each molecular state in itself can be considered to have an electron jumping back and forth between the two atoms. The resulting oscillations in the transition probability [Eq. (23)] represent the difference in the electron jumping rates for the two different molecular states. This is much like the mechanism for an interferometer.

In the region where transitions occur, we found that the translational energy must be much greater than the potential energy difference. Thus, for small energy differences it doesn't matter which potential energy curves the nuclei move on since the change in potential energy is negligible compared to the nuclear kinetic energy [this is pointed out very clearly in a paper by Delos, Thorson, and Knudson].[53] In the transition region, therefore, we can treat the trajectories for either state as being identical. Inside the transition region, however, we must use two different trajectories defined by the adiabatic potentials.

We, therefore, strongly disagree with the conclusions reached by Penner and Wallace[54] and by Corrigall, Kuppers, and Wallace.[55] While the actual charge transfer process occurs through two different trajectories with a given probability for being on each state [$|\bar{a}_1|^2$ and $|\bar{a}_2|^2$ of Eq. (23)], Wallace et al. attempt to define a single trajectory for the entire process. Their erroneous conclusion results from a misinterpretation of the meaning of a molecular wavefunction and from a misinterpretation of the transition probability as a function of the trajectory. The conclusion of the results presented in this paper indicate that semiclassical trajectories defined by adiabatic potential energy curves from molecular wavefunctions can correctly describe most collisional processes.[56]

The reason the molecular wavefunction approach is appropriate is that for energies such that the electron is moving much faster than the nuclei, the electron has time to adjust its motion in order to define a particular energy state (within energy limits resulting from the uncertainty

principle). Generally, the energy splitting between states will be larger than the energy uncertainty. Therefore, the states will be essentially uncoupled. Only for pseudo curve crossings and near-resonances will the energy uncertainty be of the same size as the energy splitting to allow transitions.

References

1. L. Landau, Phys. Z. Sowjetunion 2, 46 (1932).
2. C. Zener, Proc. Roy. Soc. (London) A137, 696 (1932).
3. E. C. G. Stueckelberg, Helv. Phys. Acta 5, 369 (1932).
4. For a recent discussion of the LZS method, see W. R. Thorson, J. B. Delos, and S. A. Boorstein, Phys. Rev. A4, 1052 (1971).
5. E. G. Gurnee and J. L. Magee, J. Chem. Phys. 26, 1237 (1956).
6. D. Rapp and W. E. Francis, J. Chem. Phys. 37, 2631 (1962).
7. D. R. Bates, Dis. Faraday Soc. 33, 7 (1962).
8. Y. N. Demkov, Sov. Phys. JETP. 18, 138 (1964).
9. A. R. Lee and J. B. Hasted, Proc. Phys. Soc. 85, 673 (1965).
10. W. Lichten, Phys. Rev. 139, A27 (1965).
11. R. E. Olson, Phys. Rev. (to be published).
12. D. R. Bates and D. A. Williams, Proc. Phys. Soc. 83, 425 (1964).
13. R. McCarroll and R. D. Piacentini, J. Phys. B. 4, 1026 (1971).
14. A. Russek, Phys. Rev. A. 4, 1918 (1971).
15. M. Born and J. R. Oppenheimer, Ann. Phys. 84, 457 (1927).
16. R. K. Colegrave and D. B. L. Stephens, J. Phys. B. 1, 856 (1968).
17. S. A. Evens, J. S. Cohen, and N. F. Lane. Phys. Rev. A. 4, 2235 (1971).
18. W. L. McMillan, Phys. Rev. A. 4, 69 (1971).
19. C. Bottcher and M. Oppenheimer, J. Phys. B. 5, 492 (1972).
20. D. W. Jepsen and J. O. Hirschfelder, J. Chem. Phys. 32, 1323 (1960).

21. See, for example, D. R. Bates and A. R. Holt, Proc. Roy. Soc. A292, 168 (1966).

22. D. R. Bates, H. S. Massey, and A. L. Stewart, Proc. Roy. Soc. (London) A216, 437 (1953).

23. One could have started with $F_i(\underset{\sim}{R}) = a_i'(z)e^{ikz}$. After making the substitution $a_i(z) = a_i'(z) \exp[\, i \int_{-\infty}^{z} (k_i^2 - k^2)\, dz'$ to remove the diagonal terms, one would also obtain Eq. (8).

24. See (a) C. F. Melius, W. A. Goddard III, and L. R. Kahn, J. Chem. Phys. 56, 3342 (1972); (b) C. F. Melius and W. A. Goddard III, to be published; (c) L. R. Kahn, and W. A. Goddard III, J. Chem. Phys. 56, 2685 (1972).

25. D. R. Bates and R. McCarroll, Proc. Roy. Soc. A245, 175 (1958).

26. S. B. Schneiderman and A. Russek, Phys. Rev. 181, 311 (1969).

27. H. Levy II, and W. R. Thorson, Phys. Rev. 181, 252 (1969).

28. M. E. Riley and T. A. Green, Phys. Rev. A4, 619 (1971).

29. R. McCarroll, Proc. Roy. Soc. A284, 547 (1961).

30. Expressing the molecular wavefunction as

$$\psi_i(\underset{\sim}{r}, R) = \sum_k \phi_k(r, R)\, C_{ki}(R)$$

where ϕ_k is an atomic eigenfunction containing the translational phase factor, then using the method of traveling orbitals, we would have for $v \approx 0$,

$$M_{ij} = \underset{\sim}{C}^t_{(i)}\, \underset{\sim}{S}\, \underset{\sim}{C}'_{(j)}$$

while

$$M_{ji} = \underset{\sim}{C}^{t}_{(j)} \underset{\sim}{S} \underset{\sim}{C}'_{(i)}$$

where $C'_{ij}(R) = \partial/\partial R(C_{ij}(R))$ and $S_{k\ell} = \langle \phi_k | \phi_\ell \rangle$. But

$$\underset{\sim}{C}^{t} \underset{\sim}{S} \underset{\sim}{C}' + \underset{\sim}{C}'^{t} \underset{\sim}{S} \underset{\sim}{C} + \underset{\sim}{C}^{t} \frac{\partial \underset{\sim}{S}}{\partial R} \underset{\sim}{C} = 0$$

and $\underset{\sim}{C}^{t} \frac{\partial \underset{\sim}{S}}{\partial R} \underset{\sim}{C}$ is non-zero, in general, so $M_{ij} \neq - M_{ji}$.

31. T. A. Green, Proc. Phys. Soc. 86, 1017 (1965).

32. The translational momentum of the electron will be important when the energy difference, ΔE, between states is zero. For large R, $\Delta E = 0$ in the symmetric resonant case. In this case, neglect of translational momentum prevents the symmetric molecular states from dissociating correctly to left and right atomic states, resulting in a non-zero coupling between states. For Σ-Π coupling, $\Delta E = 0$ at the curve crossing. In this case, neglect of the electron's momentum leads to an overestimate of the transition probability.

33. C. F. Melius and W. A. Goddard III, Chem. Phys. Lett. 15, 524 (1972).

34. R. Bulirsch and J. Stoer, Numerische Mathematik 8, 1 (1966).

35. Normally, α can be taken as an arbitrary small number (e.g., (z initial)$^{-1}$). It is useful in Σ-Π coupling, where by increasing α, a higher density points can be placed at small z where the angular rotation is fastest.

36. For small impact parameters, Σ-Π coupling would cause ρ_i to become very large, causing an overflow in the computer. Such points were deleted from the spline interpolation scheme in obtaining the transition probabilities.

37. The results for collisions of other alkalis are presented in a separate paper [C. F. Melius and W. A. Goddard III, to be published].

38. H. L. Daley and J. Perel, VIth ICPEAC, MIT, Cambridge, (The MIT Press, Cambridge, Massachusetts, 1969) p. 051.

39. J. Perel, private communication.

40. The error is more serious for transitions to Π states than to Σ states (see discussion). Thus, the total cross section for the endothermic process (e.g., $LiNa^+$) can be too small at low velocity.

41. O. B. Firsov, Zh. Eksp, Teor, Fiz., 21, 1001 (1951).

42. F. J. Smith, Phys. Lett. 20, 271 (1966).

43. J. Perel, Phys. Rev. A1, 369 (1970).

44. When electron momentum is included, R_0 for the symmetric case also becomes finite.

45. For small R, the actual M_{12} differs from Eq.(30) due to the interaction with the core. However, since it is inside the transition region, it does not significantly affect the results.

46. For near curve crossings, $\Delta\theta \approx \pi/2$. However, Eq. (33) is no longer appropriate.

47. Since the electron's translational momentum has been ignored, the v^{-2} dependence is incorrect for high energies.

48. H. S. W. Massey, Rept. Progr. Phys. 12, 248 (1949).

49. The reason the transition probability is small for small impact parameters is that the wavefunction tends to remain space-fixed

while the nuclei rotate. Since the rotation is almost 180°; the resulting wavefunction still has the original symmetry (though the molecular wavefunction's phase may be changed).

50. C. F. Melius and W. A. Goddard III, Phys. Rev. Lett. 29, 975 (1972).

51. For the $\sin^2 \Delta\phi$ term, Demkov neglects the ΔV_∞ term while we leave it in but require a finite range of integration. Demkov in his derivation uses the diabatic representation [rather than the adiabatic representation as he implies in Eq. (6)]. Also, as we showed, the transition region occurs over a wide region; this region is generally outside Demkov's R_0 (≡ our R_M) since the energy difference is smaller. Instead of Eq. (11) of Demkov's paper (which implies that the transition occurs at a discrete point), one should use Eq. (36) substituted into Eq. (26′) (which was obtained using the molecular wavefunction approach). The basic ideas presented in Demkov's paper however, are correct, as we have shown. Demkov estimates β of Eq. (32) to be $\beta = \sqrt{2I}$ (= .62 a_0^{-1} for LiNa) while we find that β = .42 a_0^{-1}. However, this error in Demkov's values results from approximating H_{AB} and does not reflect on the interpretation of the results in his paper.

52. Olson's (Ref. 11) attempts to improve upon the approximation for β by taking $\beta = .86\sqrt{2I}$ where the factor (.86) is obtained from experimental observation. He obtains an $R_M = 10.63\ a_0$. Though H_{AB} could have been put in the form (32) with $\kappa = 1.3$ and $\beta = .535$ (by taking $R \approx R_M$), Olson takes $\kappa \equiv 1.0$ and obtains a final value $\beta = .506$.

53. J. B. Delos, W. R. Thorson, and S. K. Knudson, Phys. Rev. A6, 709 (1972).

54. A. Penner and R. Wallace, Phys. Rev. A5, 639 (1972).

55. B. Corrigall, K. Kuppers, and R. Wallace, Phys. Rev. A4, 977 (1971).

56. For Σ-Π coupling, we found that the molecular wavefunction approach leads to coupling throughout the entire coupling region. The reason is that the molecular wavefunctions are not the correct representation. The correct representation involves angular momentum states defined by $(\Sigma + i\lambda\Pi)/(1 + \lambda^2)$ and $(\lambda\Sigma - i\Pi)/(1 + \lambda^2)$ where λ depends on R and v. In this new representation, the coupling process would then involve a transition region (near the pseudo-curve crossing) and an intermediate region. The resulting potential energy curves would provide the appropriate trajectory paths.

FIGURE CAPTIONS

Fig. 1. Collision geometry. The projectile (B) moves with a constant velocity along the z axis from $z = -\infty$ to $z = +\infty$ past the target (A) at an impact parameter b.

Fig. 2. The coupling term M_{12} between the $1^2\Sigma^+$ and $2\,^2\Sigma^+$ states of $LiNa^+$. $\langle 1 \mid {}^{\partial}/_{\partial R} \mid 2 \rangle_{Li}$, $\langle 1 \mid {}^{\partial}/_{\partial R} \mid 2 \rangle_{Na}$ and $\langle 1 \mid {}^{\partial}/_{\partial R} \mid 2 \rangle_{\bar{z}}$ represent M_{12} evaluated with the origin taken at the Li atom, Na atom, and $\bar{z}$, respectively. $\langle C_1 \mid S \mid \frac{\partial C_2}{\partial R} \rangle$ and $-\langle \frac{\partial C_1}{\partial R} \mid S \mid C_2 \rangle$ represent M_{12} when the overlap of basis functions is ignored.

Fig. 3. The potential energy curves for the $LiNa^+$ molecule [atomic united ($\hbar = 1$, $e = 1$, $m_e = 1$) are used; 1 hartree = 27.211 eV, 1 Bohr = 0.52917Å].

Fig. 4. The coupling terms $M_{ij} = \langle \Psi_i \mid {}^{\partial}/_{\partial R} \mid \Psi_j \rangle$ between the various molecular states of $LiNa^+$.

Fig. 5. The coupling terms $RN_{ij} = \langle \Psi_i \mid {}^{\partial}/_{\partial \Theta} \mid \Psi_j \rangle$ between the various molecular states of $LiNa^+$.

Fig. 6. Comparison of the theoretical (six-state) and experimental cross sections for $Li^+Na^+ \rightarrow Li^+Na$ and $Na + Li^+ \rightarrow Na^+ + Li$ [—— theoretical; ----- experimental]. Estimated error in the absolute values of the experimental total cross sections is 10%.

Fig. 7. Comparison of the theoretical cross sections to individual atomic states using six-state (———), three-state (---), and two-state (----) approximations for collisions of $Na + Li^+$ and $Li + Na^+$ (1 a.u. velocity = 2.18×10^8 cm/sec; $\pi a_0^2 = 0.879 \times 10^{-16}$ cm^2).

Fig. 8. The potential energy difference curves [$\Delta E = V_2(R) - V_1(R)$] for Na_2^+ (dotted line), $LiNa^+$ (solid line), and the two-state model for $LiNa^+$ (dashed line). Also plotted are the coupling terms M_{12} for $LiNa^+$ (solid line) and the two-state model for $LiNa^+$ (dashed line).

Fig. 9. The transition probabilities P(v, b) as a function of impact parameter b for various velocities for (a) $Na+Na^+$ ($1\,^2\Sigma_g^+$, $1\,^2\Sigma_u^+$ two-state); (b) $Na+Li^+$ ($1\,^2\Sigma^+$, $2\,^2\Sigma^+$ two-state); (c) $Na+Li^+$ ($2\,^2\Sigma^+$, $1\,^2\Pi$ two-state); (d) $Na+Na^+$ ($1\,^2\Sigma_g^+$, $1\,^2\Sigma_u^+$, $1\,^2\Pi_u$ three-state), and (e) $Na+Li^+$ ($1\,^2\Sigma^+$, $2\,^2\Sigma^+$, $1\,^2\Pi$ three-state).

Fig. 10. Total charge transfer cross sections for $Na + Na^+$ and $Na + Li^+$ in the three-state approximation (solid lines) and in the two-state approximation (dashed line). Also plotted are cross sections for transitions to the $1\,^2\Pi$ (or $1\,^2\Pi_u$) state in the three-state approximation.

Fig. 11. A diagram of the transition region and the intermediate region of the charge transfer process.

Fig. 12. The transition probabilities P(v, b) for the two-state $Li + Na^+ \rightarrow Li^+ + Na$ charge transfer process for inverse velocities v^{-1} = 6, 12, and 18 a.u.

Fig. 13. The transition probabilities p at z = 0 for the two-state Li + $Na^+ \rightarrow Li^+$ + Na charge transfer process for v^{-1} = 6, 12, and 18.

Fig. 14. The transition probabilities p at z = 0 for the two-state Li + $Na^+ \rightarrow Li^+$ + Na charge transfer process using the two-state model (———) and Eqn. 36 (---) for v^{-1} = 6, 12, and 18 (β = .42, ΔV_∞ = .0093 h, and $R_M = 12.9\ a_0$).

Fig. 15. A comparison of the coupling term M and energy difference ΔE for the frozen orbital (FO) and the complete basis set calculations on $LiNa^+$.

Fig. 16. A comparison of the transition probabilities p using Eq. (36) (p_{MG}), Eq. (43) (p_{RF}) and Eq. (44) (p_D) with the actual theoretical transition probability p_A for v^{-1} = 12 a.u. (see Figs. 13 and 14).

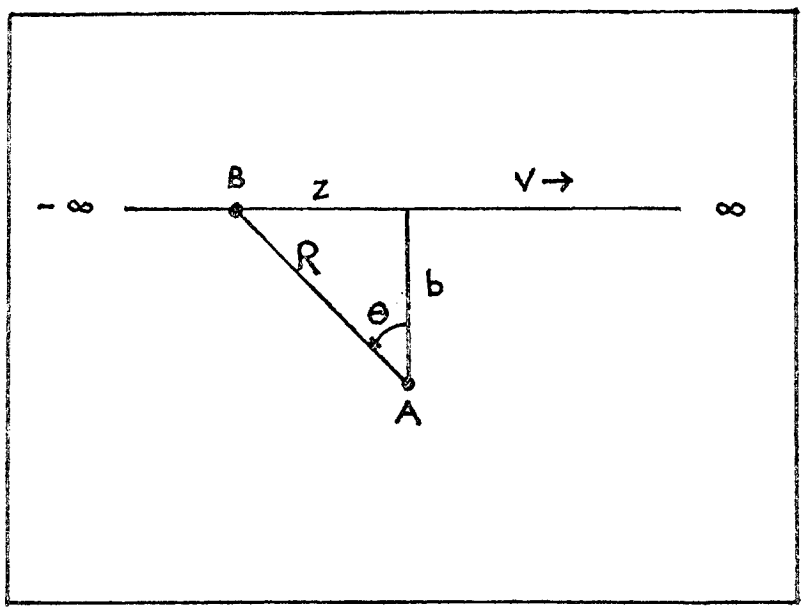
B
z
V→
- ∞
∞
R
b
θ
A

Fig. 1

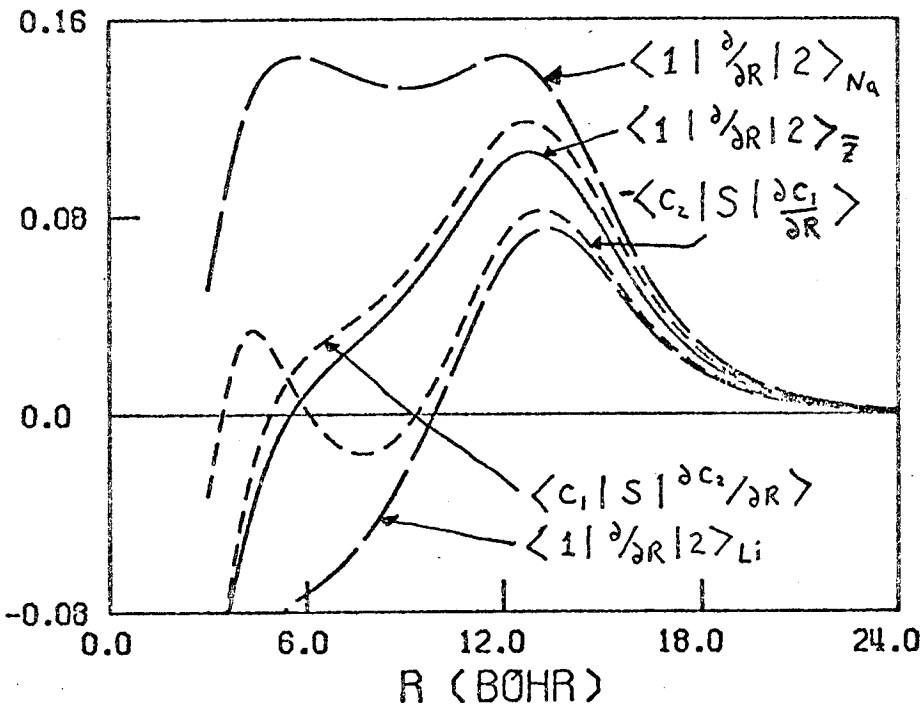
0.16
0.08
0.0
-0.08
0.0
6.0
12.0
18.0
24.0
R (BØHR)
⟨1 | ∂/∂R | 2⟩Na
⟨1 | ∂/∂R | 2⟩z̄
-⟨c2 | S | ∂c1/∂R⟩
⟨c1 | S | ∂c2/∂R⟩
⟨1 | ∂/∂R | 2⟩Li

Fig. 2

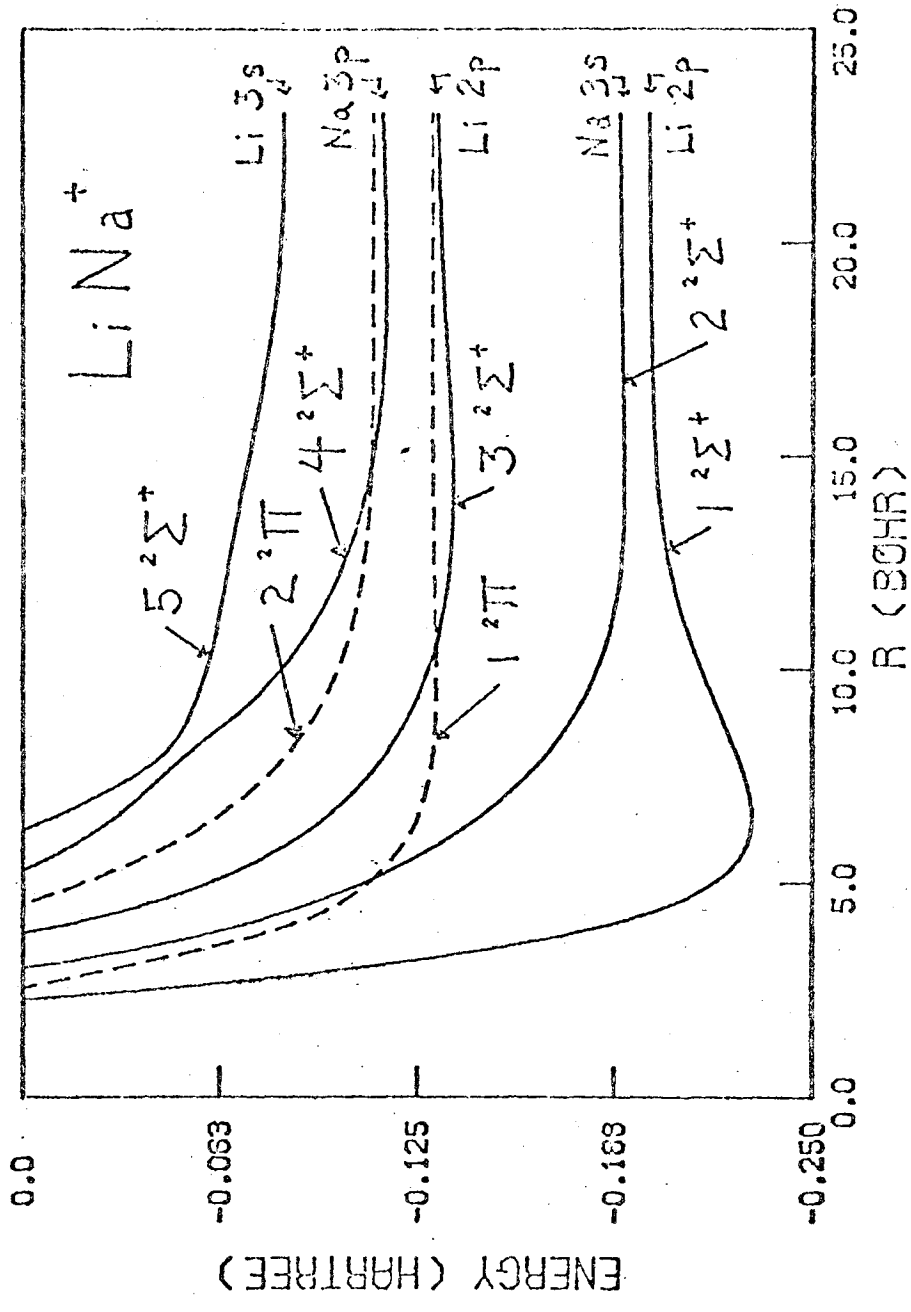
LiNa+
Li 3s
Na 3p
Li 2p
Na 3s
Li 2p
5 ²Σ+
2 ²Π
4 ²Σ+
3 ²Σ+
1 ²Π
2 ²Σ+
1 ²Σ+
0.0
-0.063
-0.125
-0.188
-0.250
ENERGY (HARTREE)
0.0
5.0
10.0
15.0
20.0
25.0
R (BOHR)

Fig. 3

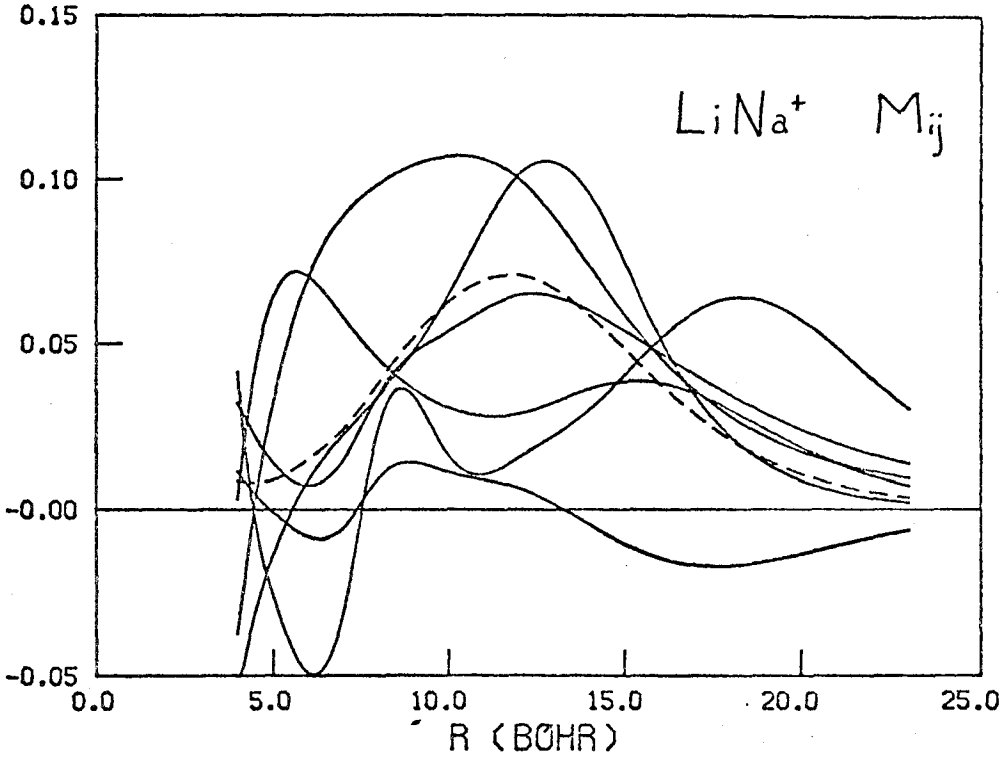
0.15
0.10
0.05
-0.00
-0.05
LiNa+ Mij
0.0
5.0
10.0
15.0
20.0
25.0
R (BOHR)

Fig. 4

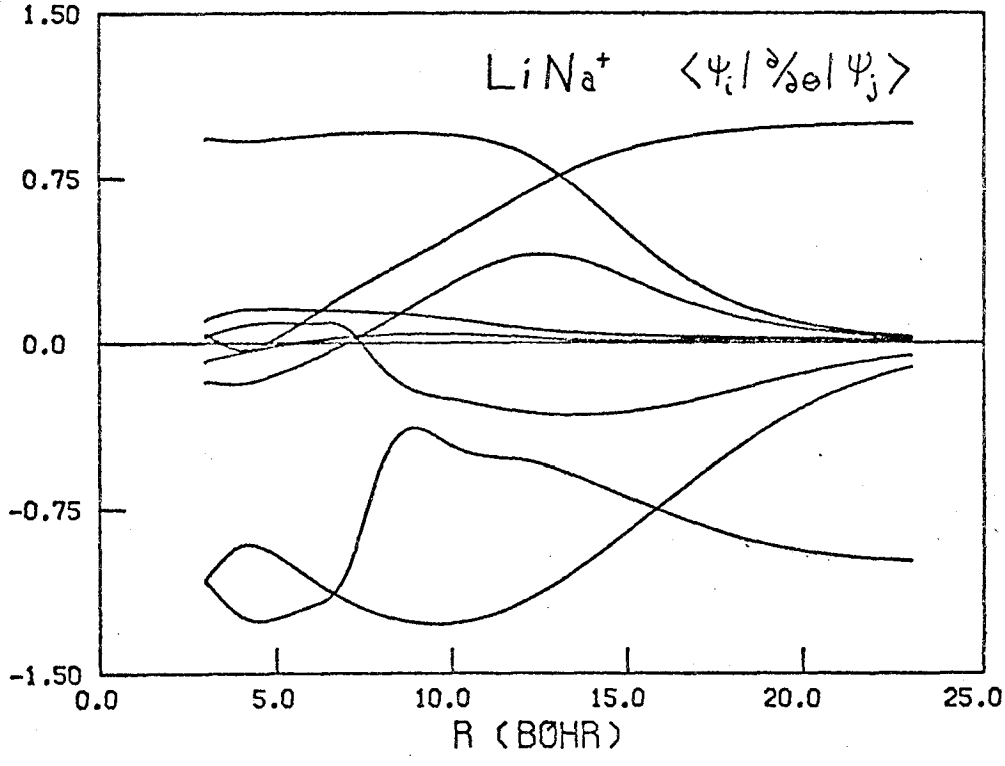
1.50
0.75
0.0
-0.75
-1.50
LiNa+ <Ψi| ∂/∂θ |Ψj>
0.0
5.0
10.0
15.0
20.0
25.0
R (BOHR)

Fig. 5

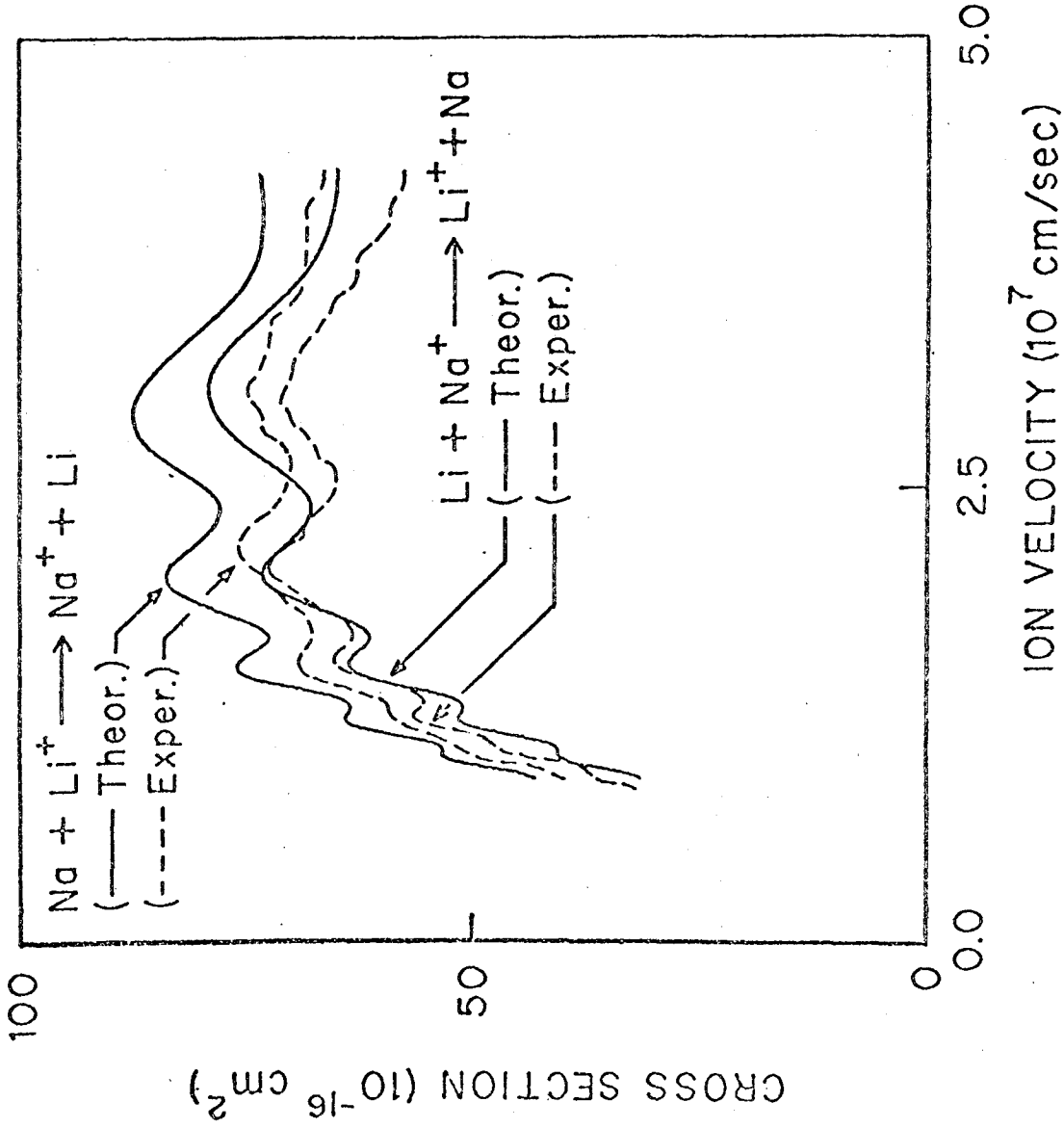
Na + Li+ ⟶ Na+ + Li
(——— Theor.)
(- - - - Exper.)
Li + Na+ ⟶ Li+ + Na
(——— Theor.)
(- - - - Exper.)
CROSS SECTION (10-16 cm2)
100
50
0
0.0
2.5
5.0
ION VELOCITY (10^7 cm/sec)

Fig. 6

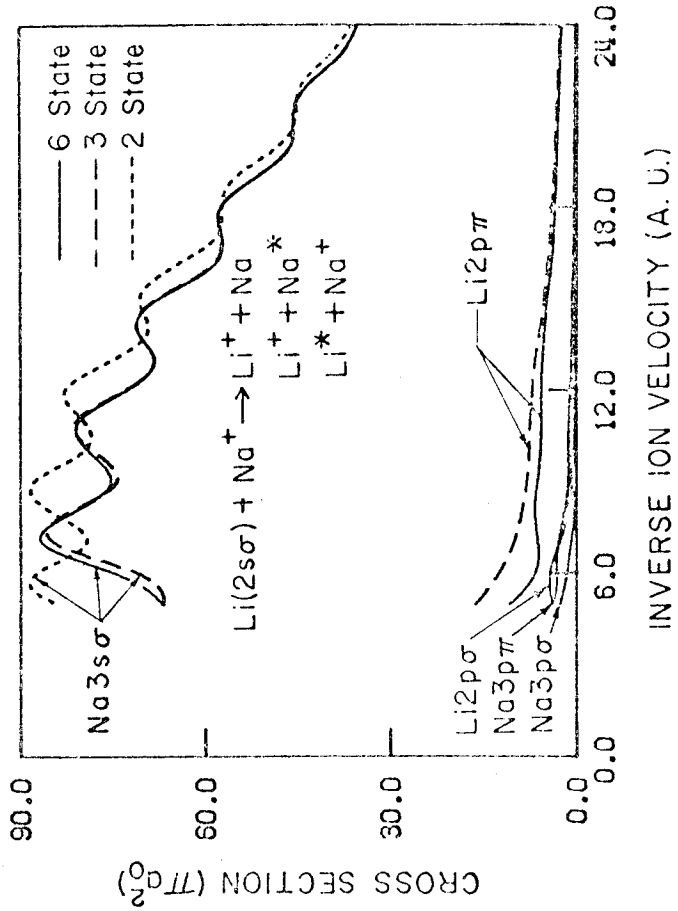
6 State
3 State
2 State
Na3sσ
Li(2sσ) + Na+ → Li+ + Na
Li+ + Na*
Li* + Na+
Li2pπ
Li2pσ
Na3pπ
Na3pσ
90.0
60.0
30.0
0.0
6.0
12.0
18.0
24.0
CROSS SECTION (πa0²)
INVERSE ION VELOCITY (A. U.)

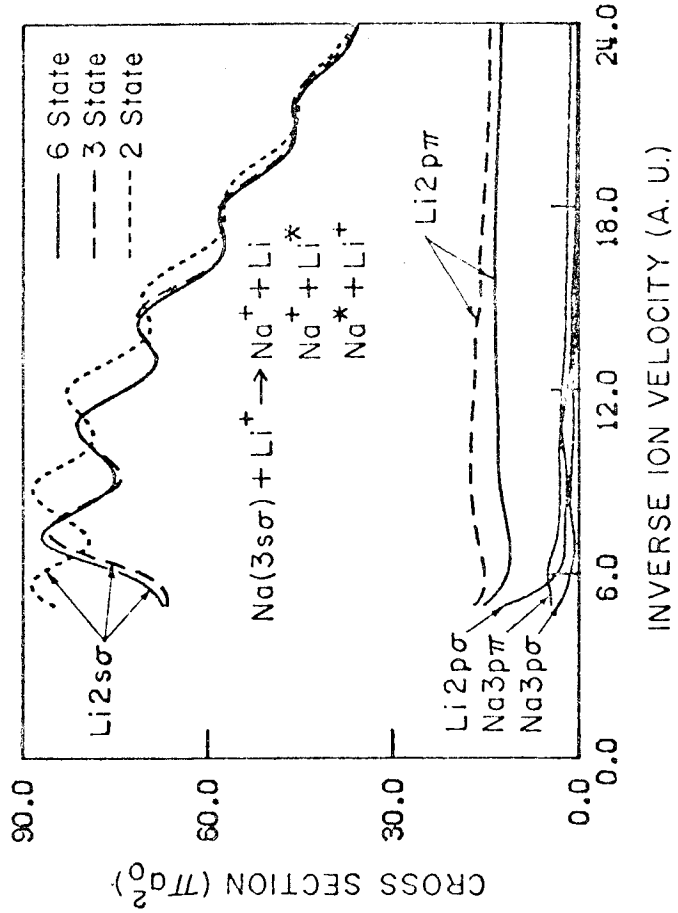
6 State
3 State
2 State
Li2sσ
Na(3sσ) + Li+ → Na+ + Li
Na+ + Li*
Na* + Li+
Li2pπ
Li2pσ
Na3pπ
Na3pσ
90.0
60.0
30.0
0.0
6.0
12.0
18.0
24.0
CROSS SECTION (πa0²)
INVERSE ION VELOCITY (A. U.)

Fig. 7

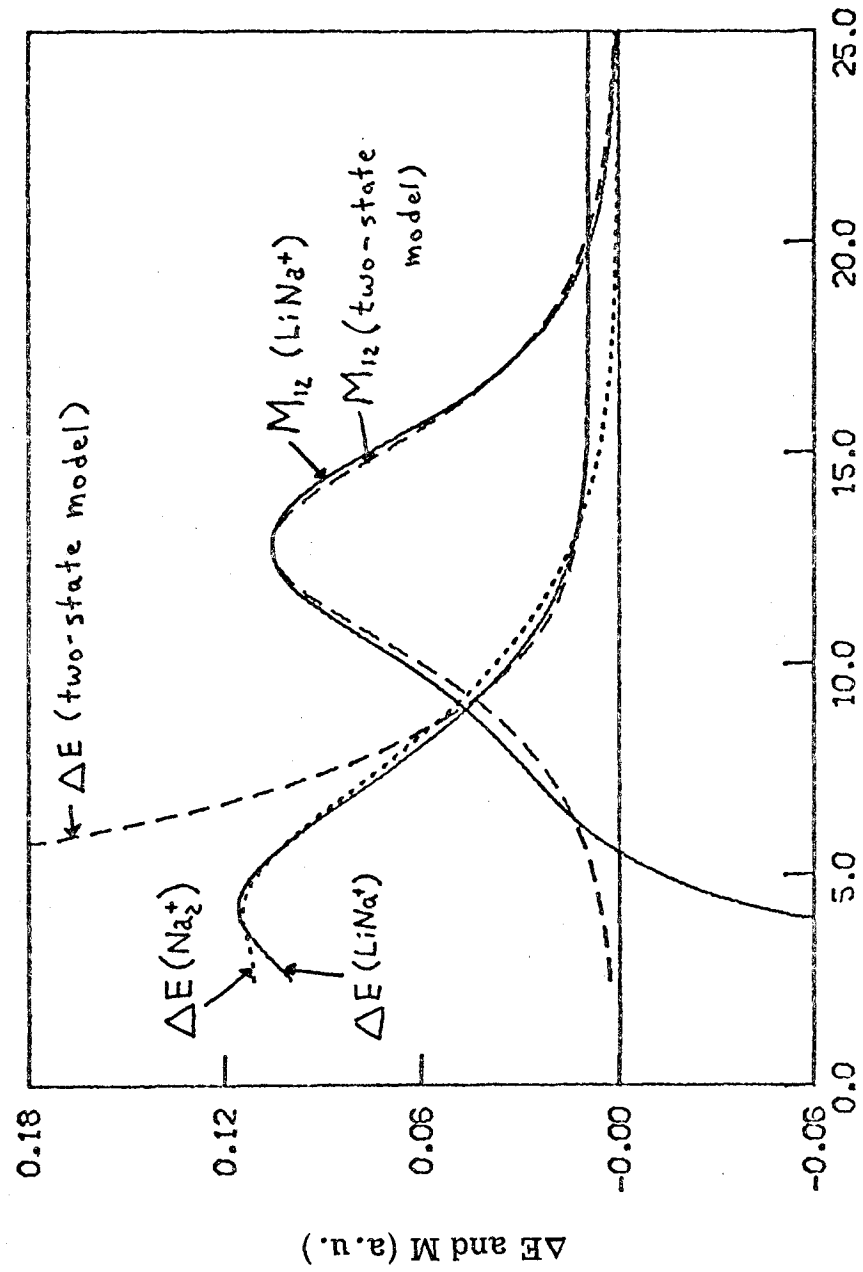
ΔE (two-state model)
M_{12} ($LiNa^+$)
M_{12} (two-state model)
$\Delta E(Na_2^+)$
$\Delta E(LiNa^+)$
0.18
0.12
0.06
-0.00
-0.06
0.0
5.0
10.0
15.0
20.0
25.0
R (BOHR)
ΔE and M (a.u.)

Fig. 8

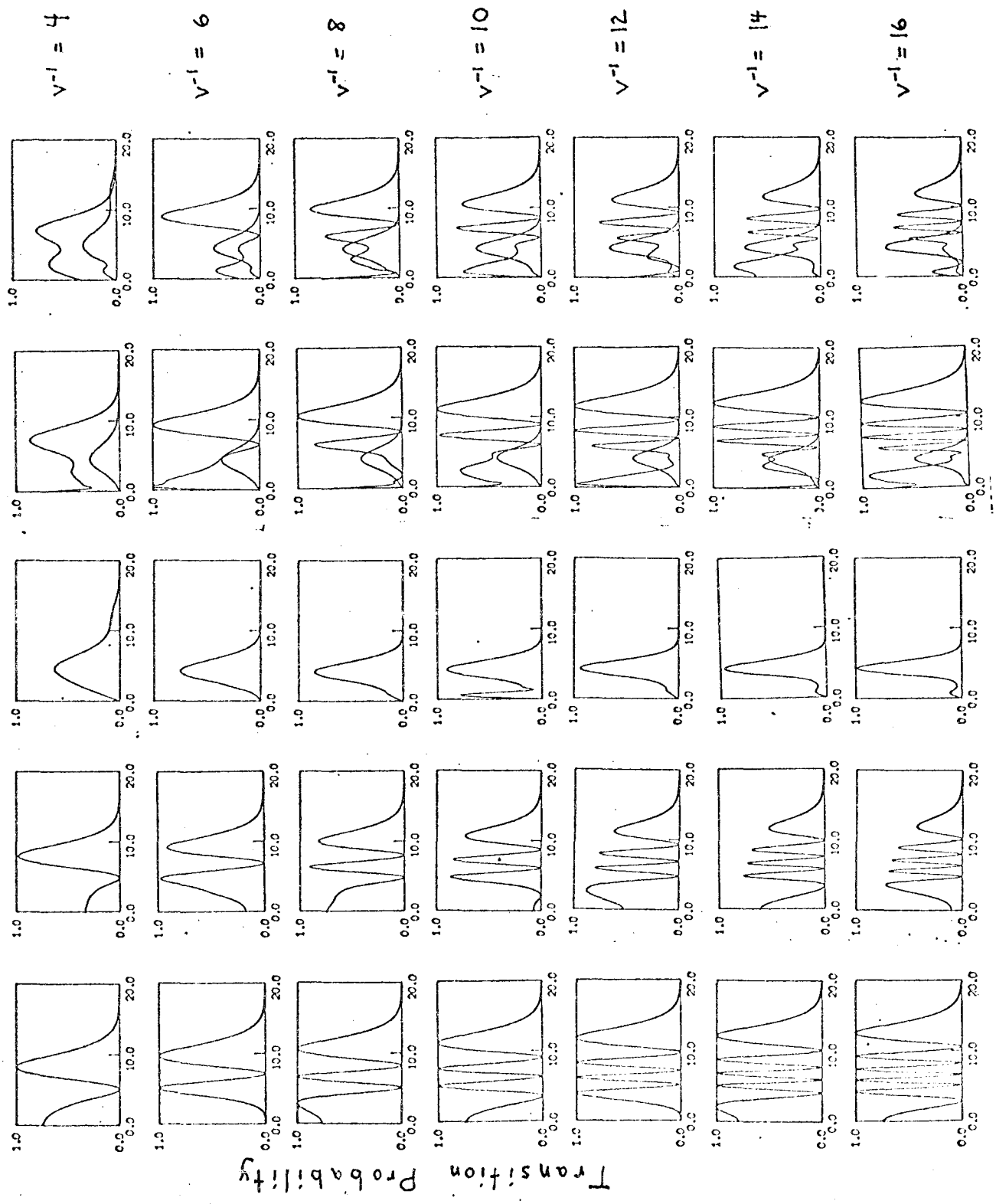
$v^{-1} = 4$
$v^{-1} = 6$
$v^{-1} = 8$
$v^{-1} = 10$
$v^{-1} = 12$
$v^{-1} = 14$
$v^{-1} = 16$
Transition Probability
Impact Parameter (a_0)

Fig. 9

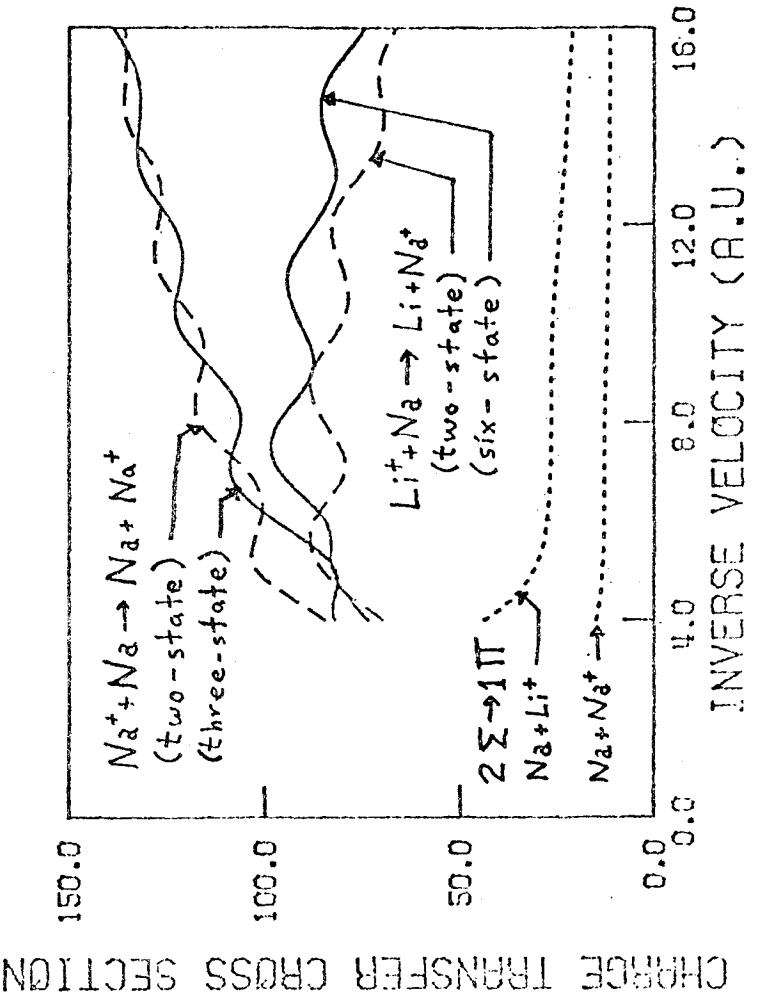
CHARGE TRANSFER CROSS SECTION
150.0
100.0
50.0
0.0
0.0
4.0
8.0
12.0
16.0
INVERSE VELOCITY (A.U.)
$Na^+ + Na \rightarrow Na + Na^+$
(two-state)
(three-state)
$Li^+ + Na \rightarrow Li + Na^+$
(two-state)
(six-state)
$2\Sigma \rightarrow 1\Pi$
$Na + Li^+$
$Na + Na^+ \rightarrow$

Fig. 10

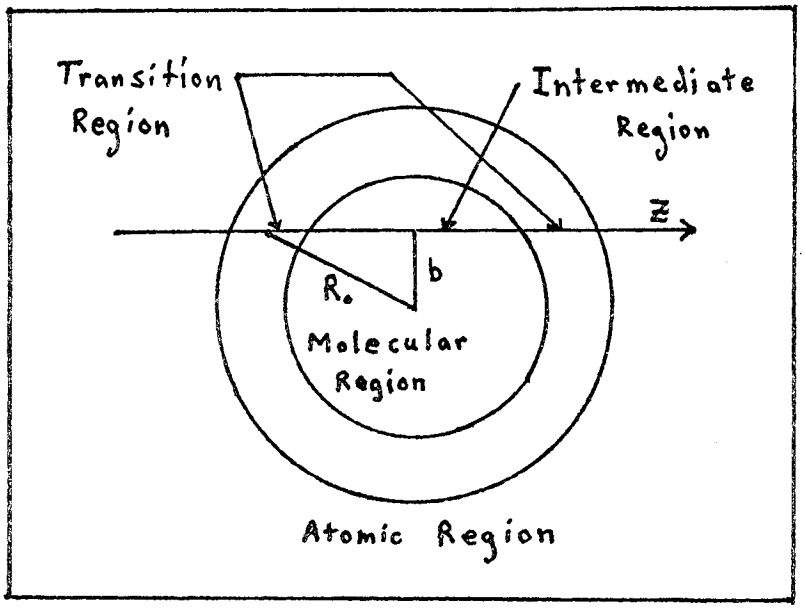
Transition
Region
Intermediate
Region
z
b
R.
Molecular
Region
Atomic Region

Fig. 11

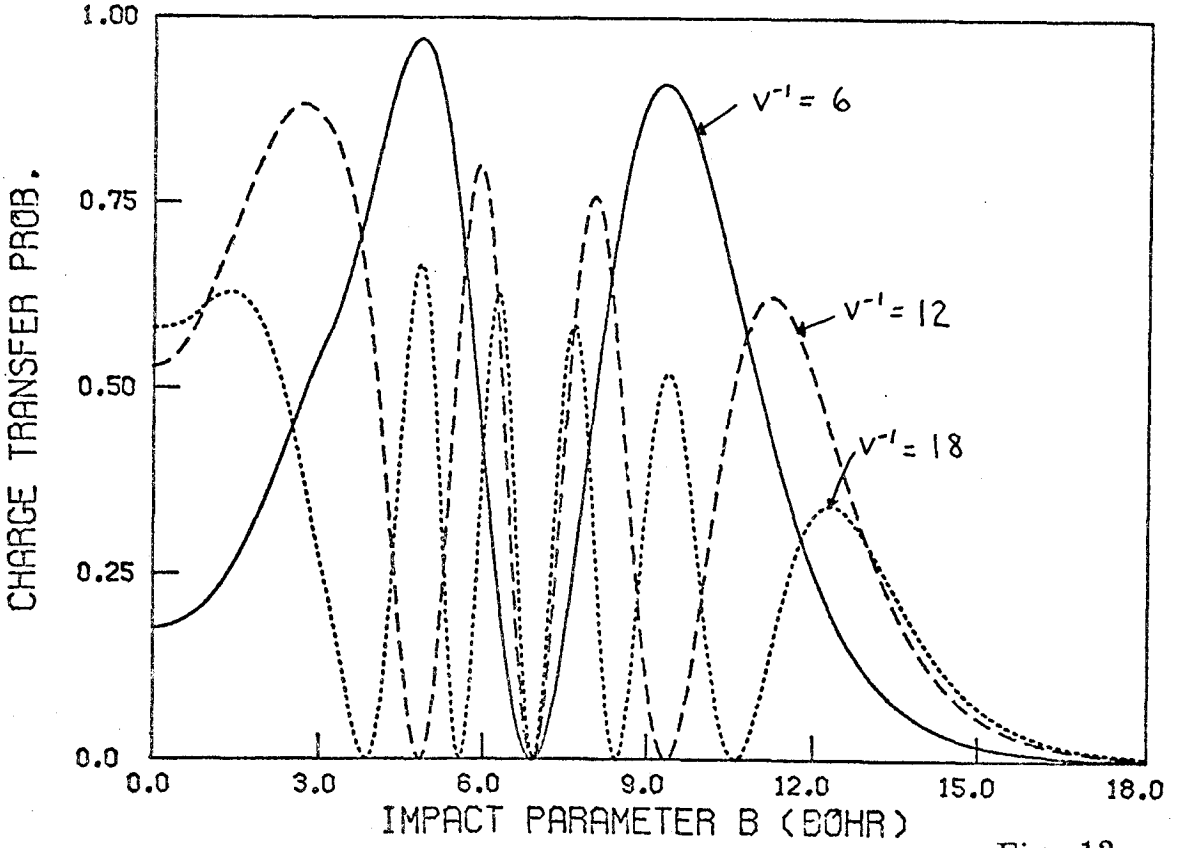
1.00
0.75
0.50
0.25
0.0
CHARGE TRANSFER PROB.
$V^{-1} = 6$
$V^{-1} = 12$
$V^{-1} = 18$
0.0
3.0
6.0
9.0
12.0
15.0
18.0
IMPACT PARAMETER B (BOHR)

Fig. 12

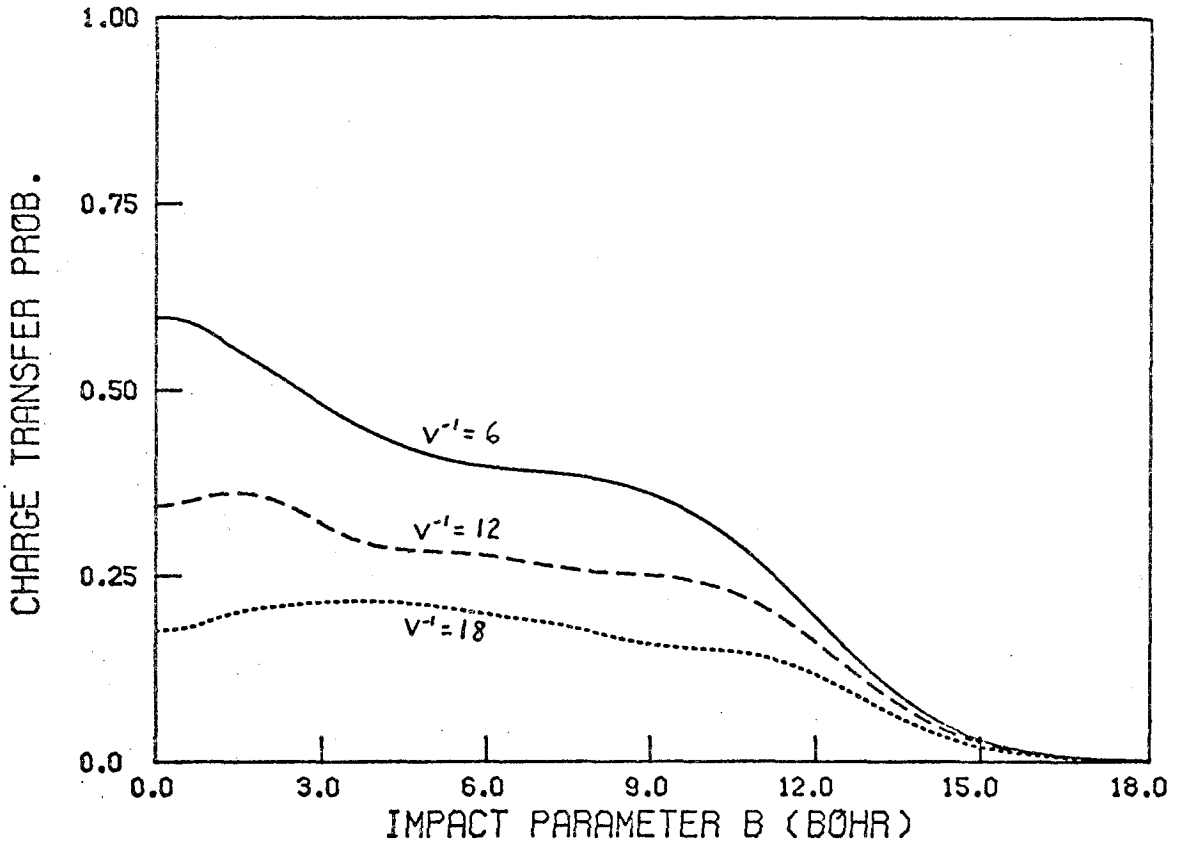
1.00
0.75
0.50
0.25
0.0
CHARGE TRANSFER PROB.
$V^{-1} = 6$
$V^{-1} = 12$
$V^{-1} = 18$
0.0
3.0
6.0
9.0
12.0
15.0
18.0
IMPACT PARAMETER B (BOHR)

Fig. 13

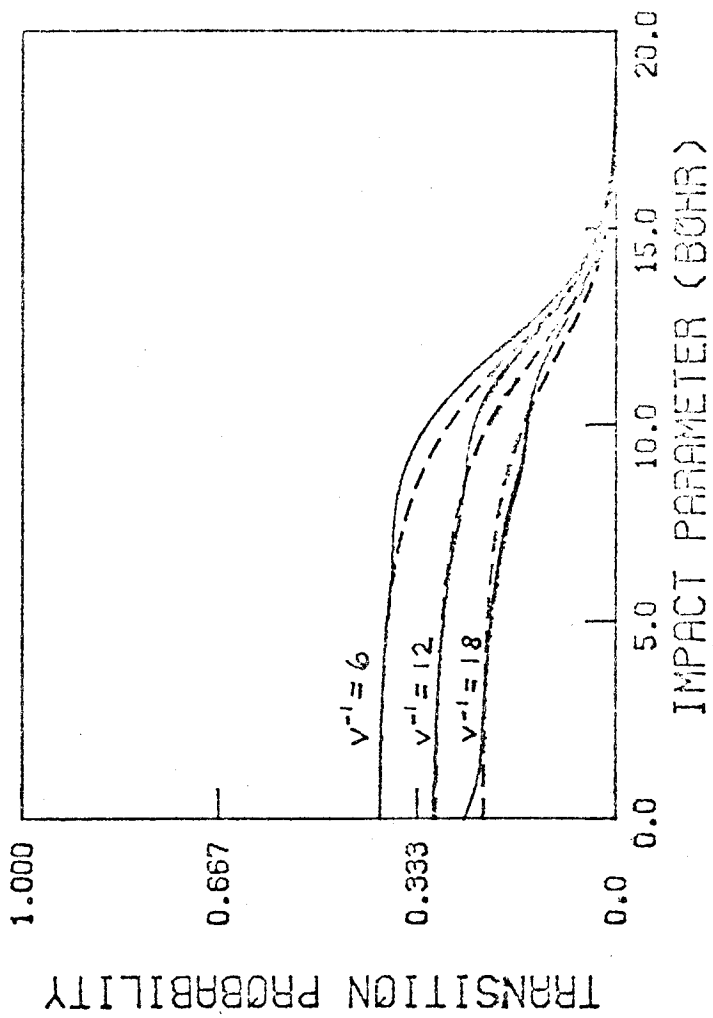
TRANSITION PROBABILITY
1.000
0.667
0.333
0.0
0.0
5.0
10.0
15.0
20.0
IMPACT PARAMETER (BOHR)
v⁻¹ = 6
v⁻¹ = 12
v⁻¹ = 18

Fig. 14

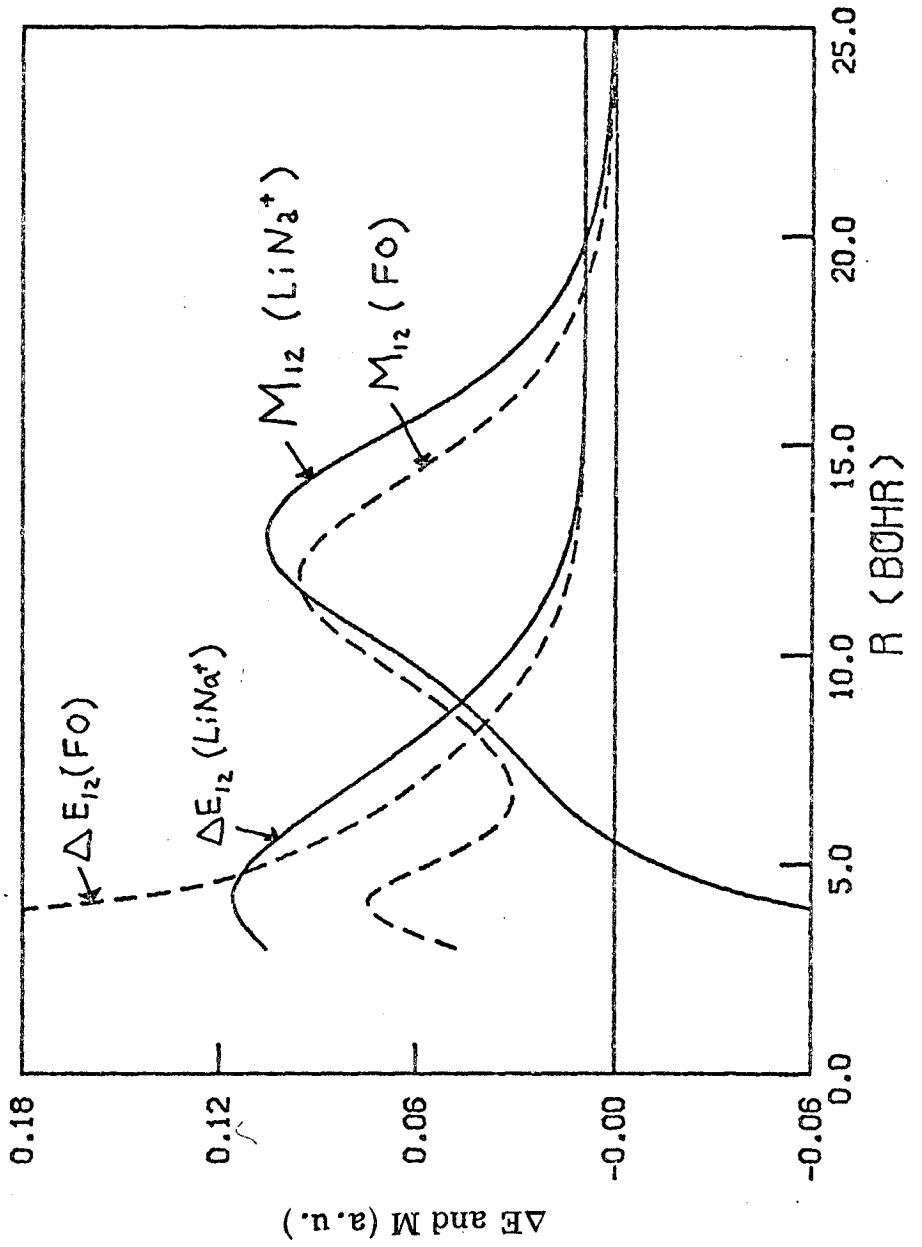
ΔE and M (a.u.)
0.18
0.12
0.06
-0.00
-0.06
0.0
5.0
10.0
15.0
20.0
25.0
R (BØHR)
$\Delta E_{12}(FO)$
$\Delta E_{12}(LiNa^+)$
$M_{12}(LiNa^+)$
$M_{12}(FO)$

Fig. 15

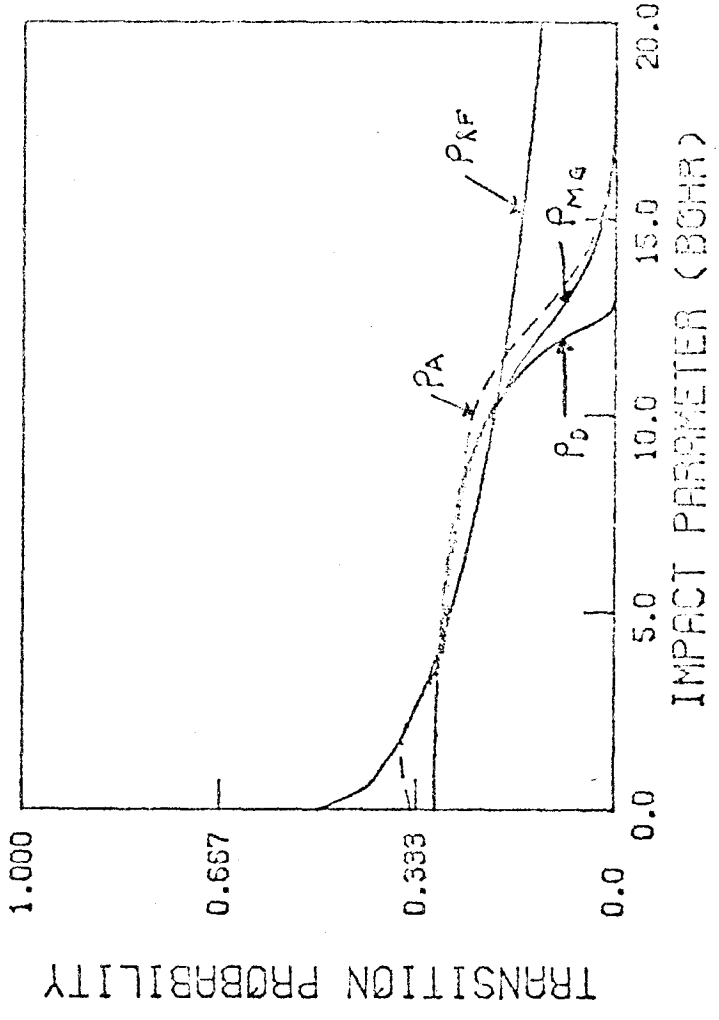
TRANSITION PROBABILITY
1.000
0.667
0.333
0.0
0.0
5.0
10.0
15.0
20.0
IMPACT PARAMETER (BOHR)
P_{KF}
P_{MG}
P_A
P_b

Fig. 16

PART I

The Charge Transfer Process Using the Molecular Wavefunction Approach

PART I-B

An Application to Alkali-Atom Alkali-Ion Collisions Involving Li, Na, and K

I. INTRODUCTION

Collisions of atoms or molecules involving the change of the electron from one electronic state to another (i.e., charge transfer, electronic excitation, electronic excitation transfer) can be described in the molecular wavefunction representation[1] whereby coupling between electronic states of the quasimolecule is caused by a collisionally induced breakdown of the Born-Oppenheimer approximation.[2] This molecular wavefunction approach has been used to study the resonant and near-resonant charge transfer process for a number of systems.[3-9] Though a two-state approximation is usually employed, several studies have included the effect of other states, in particular, Π states which are rotational coupled.[7-9]

However, difficulties have existed both in the evaluation of the Born-Oppenheimer breakdown terms[10] and in the determination of the molecular wavefunctions for a number of excited states. As a result, little has been reported on multistate excitations in various systems using the molecular wavefunction approach.

Herein we report multistate calculations on the charge transfer processes involved in collisions of $Li + Na^+$, $Na + Li^+$, $Li + K^+$, $K + Li^+$, $Na + K^+$, and $K + Na^+$. The potential energy curves and Born-Oppenheimer breakdown terms were rigorously evaluated. The results are in good agreement with experimental results. Furthermore, we find that the results can be explained very simply in the molecular wavefunction approach from simple considerations of the potential energy curves. The dominant processes involve $1\,^2\Sigma^+ \rightleftharpoons 2\,^2\Sigma^+$ coupling, $2\,^2\Sigma \rightleftharpoons 1\,^2\Pi$

coupling and, for $K + Li^+$, $2\,^2\Sigma^+ \rightarrow 3\,^2\Sigma^+$ coupling. The relative importance of each of these processes depends on the relative velocity of the nuclei and on the potential energy differences.

II. DETAILS OF THE METHOD

The molecular wavefunction approach is used to obtain the transition probabilities and cross sections between the various electronic states of the colliding atoms. Details of this method are presented in an earlier paper (Paper I).[11] In this approach, the total wavefunction is expressed as

$$\Psi = \sum_i F_i(\underset{\sim}{R})\, \psi_i(\underset{\sim}{r}, R) \tag{1}$$

where R is the internuclear distance and $\underset{\sim}{r}$ represents all the electronic coordinates. F_i describes the nuclear wavefunction while ψ_i is the solution of the electronic Hamiltonian for the molecule

$$\mathcal{H}_{e\ell}\, \psi_i(\underset{\sim}{r}, R) = E_i(R)\, \psi_i(\underset{\sim}{r}, R). \tag{2}$$

Using the impact parameter approach [which should be valid for the energies we consider (e.g., $E > 100$ eV)], we take the nuclear wavefunction to be

$$F_i(\underset{\sim}{k}) = a_i(z) \exp\left[i \int_{-\infty}^{z} k_i(z')dz' \right]$$

where $z^2 + b^2 = R^2$, b is the impact parameter, R is the internuclear distance, $k_i = [2M(E-V_i)]^{\frac{1}{2}}$, E is the translational energy for the

separated atoms ($E = \frac{1}{2}M v^2$), and V_i is the energy of the i^{th} molecular state. The resulting coupled equations to be solved in the molecular wavefunction approach are[1]

$$\frac{d\, a_i(z)}{dz} = - \sum_j \Gamma_{ij}(z) \exp[- i\, \omega_{ij}(z)]\, a_j(z) \tag{3}$$

where

$$\omega_{ij} = \frac{1}{v} \int_{-\infty}^{z} (V_j - V_i)\, dz' \tag{4}$$

and

$$\Gamma_{ij} = \frac{z}{R} M_{ij} + \frac{b}{R} N_{ij} \tag{5a}$$

$$M_{ij} = \langle \psi_i | \frac{\partial}{\partial R} | \psi_j \rangle \tag{5b}$$

$$N_{ij} = \langle \psi_i | \frac{1}{R} \frac{\partial}{\partial \theta} | \psi_j \rangle . \tag{5c}$$

The Γ_{ij}'s are the Born-Oppenheimer breakdown terms which couple the states together. A difficulty exists in the evaluation of these terms since they are not translationally invariant.[2, 10] A method has been developed to overcome this difficulty and has been presented in Paper I.

The molecular wavefunctions ψ_i were calculated using the effective potential method.[12] The effective potentials were derived from coreless Hartree-Fock orbitals (CHF) and designed to provide ab initio quality results with minimal computational effort. The method should reproduce the HF description of the wavefunction and therefore should be appropriate for the single valence electron of the alkali-atom alkali-ion molecular

system. The HF description leads to a small error in the ionization energies for the various atomic states. However, this error is very serious for small energy differences between different atoms (e.g., the energy defect for Li(2s) and Na(3s) should be .0093 h = .25 eV rather than 0.141 h as obtained from HF). To alleviate this difficulty, the effective potentials were modified to reproduce the experimental ionization energies. The basis set for each molecular calculation included three s, three p and one d contracted Gaussians on each center to describe the Σ states, and three p and two d contracted Gaussians on each center to describe the Π states.

The effective potential method assumes that the cores remain frozen. Therefore, the method breaks down for small R when the cores from different atoms begin to overlap (R ~3.5 a_0 to 5 a_0, being smallest for those molecules containing Li and largest for those molecules containing K). However, since the charge transfer process for alkali-atom alkali-ion collision is dominated by large impact parameter collisions, the resulting cross sections are not significantly affected.[13]

III. RESULTS

Using the coupled equations of (6) we have calculated the charge transfer cross sections for collisions of $Li + Na^+$, $Na + Li^+$, $Li + K^+$, $K + Li^+$, $Na + K^+$, and $K + Li^+$.

A. Potential Curves

The six lowest molecular states (4 Σ and 2 Π states) dissociating to the lowest ^2S and ^2P states of each atom were used in the calculations.

The resulting potential energy curves for $LiNa^+$, LiK^+, and NaK^+ are shown in Fig. 1.[14] For comparison, we also show in Fig. 1 the corresponding potential energy curves for Li_2^+, Na_2^+ and K_2^+.

For the homonuclear systems the degenerate states of the separated atoms form bonding and antibonding g and u states which split in energy as the energy decreases. This splitting is sufficiently large to cause a crossing of the $3\,^2\Sigma_g^+$ and $2\,^2\Sigma_u^+$ states. For the heteronuclear dialkalis, the potential energy curves represent wavefunctions which start off localized on one or the other of the atoms at infinity but eventually change to bonding and antibonding orbitals at smaller R as the interaction energy between the atomic eigenfunctions becomes much larger than the energy difference at infinity.

We see, for example, that the $1\,^2\Sigma^+$ curve of $LiNa^+$ is bounded by the $1\,^2\Sigma_g^+$ curves of Li_2^+ and Na_2^+, with similar bounds for the internuclear dialkalis. The crossing of the Σ_u and Σ_g curves of the homonuclear molecules are replaced in the heteronuclear molecules by near crossings. For LiK^+, the K 4s energy is close enough to the Li 2p energy to allow considerable mixing between these two states, though at smaller R mixing of the K 4s and the Li 2s becomes more important.

The long-range behavior of the two lowest potential energy curves for each molecule are proportional to $\alpha_i/2R^4$ where α_i is the polarizability for each atom ($\alpha_{Li} \approx 166\ a_0^3$, $\alpha_{Na} \approx 186\ a_0^3$, and $\alpha_K \approx 282\ a_0^3$ from the theoretical calculations). The excited states do not exhibit this R^{-4} behavior with the Π states being repulsive at long-range. As far as the charge transfer process is concerned, however, this long range behavior is not important and the potential energy curves can be considered to be flat at large R.

The important part of the potential energy curves involves smaller R where the atomic wavefunctions overlap, causing large changes in the potential energy curves.

B. The Coupling Term

The coupling terms M_{ij} between the various Σ states and between the Π states for $LiNa^+$, LiK^+, and NaK^+ are shown in Fig. 2. The M_{ij}'s reflect the changes in the wavefunctions as a function of R as they go from being atomic orbitals at large R to molecular bonding and anti-bonding orbitals at smaller R. At very small R ($<4\ a_0$) the rapid change in the M_{ij}'s represent the interaction of the core orbitals with each other. For large R, coupling terms between wavefunctions dissociating to different atoms (e.g., Li 2s and Na 3s) go to zero exponentially as the overlap of the atomic eigenfunctions. On the other hand, the coupling term between wavefunctions dissociating to the same atom (e.g., Li 2s and Li 2p) go to zero as R^{-3} due to polarization of the atom by the positive charge of the other atom.

The coupling terms N_{ij} which couple the Σ states to Π states are shown in Fig. 3 (the actual functions plotted are $R\ N_{ij}(R) = \langle \Sigma_i \left| \frac{\partial}{\partial \theta} \right| \Pi_j \rangle$). The coupling results from rotation in space of the internuclear axis along which the molecular states have been quantized.[15] At infinity, the rotation will couple the degenerate pairs of angular momentum states of the atom (e.g., Li $2p_x$ and Li $2p_z$ for rotation about the y axis). Likewise, as the atoms come together, rotation will couple together those molecular states which have a similar shape but are rotated by 90°

[e.g., the $2\,^2\Sigma^+$ and $1\,^2\Pi$ states of $LiNa^+$ at small R both resemble hydrogenic 2p orbitals (ignoring orthogonality to the cores)].

C. Total Cross-Sections

The resulting total cross sections for the various alkali-atom alkali-ion collisions are shown in Fig. 4 as a function of velocity. We see that the cross sections are small at low velocity, increase with increasing velocity, pass through a maximum, and then fall off to zero at higher velocity. The charge transfer cross sections for the exothermic reactions are larger than for the endothermic reactions. While the cross sections for $Li + Na^+$ and $Na + Li^+$ are quite similar, we see that the cross section for $K + Li^+$ is much larger than the cross section for $Li^+ + K$. The ratio of the cross sections for $Na + K^+$ and $K + Na^+$ lie between these two extremes. For most of the cross sections, we find an oscillatory structure imposed on the overall shape. The oscillations for $K + Li^+$ are difficult to see due to the rapid rise in the cross section. The oscillatory structures for $Li + Na^+$ and $Na + Li^+$ and for $Na + K^+$ and $K + Na^+$ are nearly equivalent both in amplitude and phase.

In Figs. 5, 6, and 7 we compare the theoretical cross sections with the experimental results of Perel and Daley.[16] The experimental results are estimated to have an accuracy of 10% in the absolute magnitude of the cross section.[17] The accuracy in the experimental results decreases at either extreme of the experimental range, particularly for the low energy end. We see that the theoretical and experimental cross sections for $Li + Na^+$ and $Na + Li^+$ are in very good agreement, both in the total

magnitude and in the oscillatory structure. For the other endothermic reactions ($Li + K^+$ and $Na + K^+$) the cross sections are also in fairly good agreement, the oscillatory structure agreeing quite well, but the theoretical magnitude being somewhat small. For the exothermic processes $K + Li^+$ and $K + Na^+$, however, the theoretical cross sections are too large in total magnitude, though the oscillatory structure is quite good. The velocities at which the cross sections reach a maximum for the theoretical and experimental results are in good agreement for all the collisional cross sections studied.

While there is some error in the experimental results, particularly in $Na + K^+$ and $K + Na^+$ measurements, the main disagreement between the experimental and theoretical results probably lies in the approximations made in the theoretical calculations. The molecular wavefunctions used in the calculations form a sufficiently complete basis set (see discussion) to provide an accurate description. Also, the assumption of linear trajectories is valid except at small impact parameters which do not contribute significantly to the cross section. However, the approximation which neglects the translational momentum of the electron leads to cross sections which are over estimated. This error increases with increasing velocity. The neglect of translational momentum is particularly significant for the Σ-Π coupling process which leads to the overestimate of the cross-sections for $K + Li^+$ and $K + Na^+$.

Overall, however, we find that the theoretical calculations provide a good description of the charge transfer cross sections. Furthermore, as we shall see, the various alkali-atom alkali-ion cross sections can be explained very simply in terms of transitions between the molecular states of the quasimolecule formed during the collision.

IV. DISCUSSION

A. $Li + Na^+$ and $Na + Li^+$

As mentioned in the previous section, $Li + Na^+$ and $Na + Li^+$ have very similar charge transfer cross sections, both in total magnitude and in the oscillatory structure (see Fig. 4). To see why, we have plotted in Fig. 8 the cross sections for transitions to the individual states (using the six-state approximation). We see that the cross-sections are dominated by transitions between the two lowest $^2\Sigma^+$ states [note that $\sigma_{Li\ 2s \rightarrow Na\ 3s} = \sigma_{Na\ 3s \rightarrow Li\ 2s}$ due to the detailed balancing]. The transition to the Li $2p_\pi$ state is, to a certain extent, also important, particularly for the exothermic process $Na + Li^+$. In fact the Na 3s → Li $2p_\pi$ transition eventually dominates the Na 3s → Li 2s at low energies due to its slower rate of decrease. Cross sections for transitions to other states are considerably smaller.

Given an understanding of the coupling process between molecular states, the explanation for these results becomes readily obvious and even predictable from simple considerations of potential energy curves. A detailed discussion of the coupling process between states in the molecular wavefunction approach is given in Part I. A brief summary of the process is presented below.

In the molecular wavefunction approach, the transition between two states (of the separated quasimolecule) involves a three-step process. First, as the atoms approach, they enter a transition region where the two molecular states couple. This region (where the wavefunctions change their character from atomic to molecular) is defined as the

range over which the energy difference is small while the coupling term is large. Second, as the atoms approach closer, they enter an intermediate region where the two states are uncoupled. Finally, as the atoms separate, they re-enter the transition region and decouple. However, due to the different evolution of their phase factors [see Eq. (5)] in the intermediate region, interference occurs in the decoupling region leading, in general, to a non-zero probability for a transition.

From the potential energy curves for the $LiNa^+$ quasimolecule (Fig. 1), we see that the lowest two $^2\Sigma^+$ states are nearly degenerate at large R. Thus, we expect a strong coupling between these two states at large R (the actual transition region is roughly $12\ a_0 \lesssim R < 22\ a_0$). On the other hand, the energy difference to the higher-lying $^2\Sigma^+$ states is too large to allow significant transitions [except for $v \gtrsim 0.2$ a.u. ($v = 4 \times 10^7$ cm/sec or E = 7 keV for $Li^+ + Na$)]. From the potential energy curve, we see that the Π states also have large energy differences at large R. However, the $1\ ^2\Pi$ state crosses the $2\ ^2\Sigma^+$ state at $5.1\ a_0$. Thus, transitions can occur from the $2\ ^2\Sigma^+$ state to the $1\ ^2\Pi$ state at small impact parameters due to rotational coupling.

Transitions to the other higher-lying states occur by first populating the $1\ ^2\Pi$ state and then transferring to the other states which are close in energy to the $1\ ^2\Pi$ state. For collisions involving $Li + Na^+$, the electron must first transfer from the $1\ ^2\Sigma^+$ state to the $2\ ^2\Sigma^+$ state. Thus the Li 2s → Li $2p_\pi$ cross section is much smaller than the Na 3s → Li $2p_\pi$ cross section at small velocities. We see that the total cross section for the process $Na + Li^+ \rightarrow Na^+ + Li$ is larger than for the

reverse process $Li + Na^+ \rightarrow Li^+ + Na$ due to the added cross section for the $2\,^2\Sigma^+ \rightarrow 1\,^2\Pi$ transition.

From Fig. 8, we see that the oscillatory structure in the total charge transfer cross section is due to the $1\,^2\Sigma^+ \leftrightarrow 2\,^2\Sigma^+$ transition, resulting from a maximum in the energy difference between these two states.[6] The phase of the oscillatory structure differs from that obtained in a simple two-state calculation due to the other trajectory available in the $1\,^2\Pi$ state. No significant oscillatory structure is present in the Σ-Π transitions due to the different nature of the Σ-Π rotational coupling process. [For a detailed discussion, see Part I.]

Experimental results have been obtained for transitions to the excited states by Aquilanti et al.[18] The cross sections for $Na(3s) + Li^+ \rightarrow Na(3p) + Li^+$ is of the same order of magnitude as our theoretical cross section. However, for $Na(3s) + Li^+ \rightarrow Na^+ + Li(2p)$, their experimental cross section is several orders of magnitude smaller than we predict. From the potential energy curves of $LiNa^+$ and Na_2^+ (Fig. 1) one finds curve crossings of the second $^2\Sigma^+$ state with the first $^2\Pi$ state. One would, therefore, expect the cross section $Na(3s) + Li^+ \rightarrow Na^+ + Li(2p)$ to be nearly as large as the $Na(3s) + Na^+ \rightarrow Na^+ + Na(3p)$ cross section (for which their results are in good agreement with ours). We therefore believe their experimental cross sections for $Na(3s) + Li^+ \rightarrow Na^+ + Li(2p)$ to be in error.

B. $Li + K^+$ and $K + Li^+$

Unlike the $Li + Na^+$ and $Na^+ + Li$ charge transfer cross sections, the cross section for $K + Li^+$ is quite different from the $Li + K^+$ cross section. To see why the difference occurs, we have plotted the cross sections for transitions to the individual states in Fig. 9. We see that the $Li + K^+$ charge transfer process is very similar to the $Li + Na^+$ charge transfer process being dominated by the transition between the two lowest Σ states. On the other hand, the $K + Li^+$ charge transfer process is dominated by transitions between the $2\,^2\Sigma^+$ state and the $1\,^2\Pi$ state. Also, transitions between the $2\,^2\Sigma^+$ and $3\,^2\Sigma^+$ states play an important role similar to that between the $1\,^2\Sigma^+$ and $2\,^2\Sigma^+$ states. The oscillations in the total cross section result from the Σ-Σ transitions. However, since the $K + Li^+ \rightarrow K^+ + Li$ cross section represents two different Σ-Σ transitions, the oscillations for each process slightly interfere leading to smaller net oscillations than in the $Li + K \rightarrow Li^+ + K$ cross section. As was done for $Li + Na^+$ and $Na + Li^+$, these results can be readily explained by looking at the molecular potential energy curves for LiK^+ and using the simple concepts for molecular transition processes. From Fig. 1 we see that the energy defect $[\Delta E(\infty)]$ between the two lowest Σ states of LiK^+ ($0.039\,h = 1.06$eV) is much larger than in $LiNa^+$ while it is comparable to the energy defect between the $2\,^2\Sigma^+$ and $3\,^2\Sigma^+$ states ($0.029h = 0.79$ eV).

For an electron starting on the $1\,^2\Sigma^+$ state ($Li + K^+$), only the $2\,^2\Sigma^+$ state is close in energy. Therefore, one would expect and, in fact, finds that the charge transfer process is dominated by the

$1\,^2\Sigma^+ \rightarrow 2\,^2\Sigma^+$ two-state coupling process. However, as expected, the cross section is much smaller than for $Li + Na^+$, due to the larger energy defect. The minimum in the energy difference (0.037 h) occurs at 14.5 a_0 rather than at infinity (excluding effects of polarizability) due to mixing of the K 4s and the Li 2p atomic states. The net effect, though, is rather negligible. At smaller R, the K 4s and the Li 2s interact strongly to split the $1\,^2\Sigma^+$ and $2\,^2\Sigma^+$ states apart.

For an electron starting on the $2\,^2\Sigma^+$ state ($K + Li^+$), both the $1\,^2\Sigma^+$ state and the $3\,^2\Sigma^+$ state are close in energy, allowing coupling to both states. As mentioned though, the energy difference to either is considerably larger than for $LiNa^+$ so that transitions to either state will be small at low velocities. [At higher velocities ($v > \sim .2$ a.u.) (7 keV for Li^+ or 39 keV for K^+) these transition processes become important.] On the other hand, a curve crossing exists between the $2\,^2\Sigma^+$ and the $1\,^2\Pi$ states. Therefore, significant charge transfer can occur from the K atom to the Li atom through rotational coupling of the molecular Σ and Π states of the quasi-molecule. The cross section for transitions to the $3\,^2\Sigma^+$ state does not exhibit the characteristic shape of the $1\,^2\Sigma^+ \rightarrow 2\,^2\Sigma^+$ cross section because in addition to the direct $2\,^2\Sigma^+ \rightarrow 3\,^2\Sigma^+$ transition, we also have transitions from the $1\,^2\Pi$ state to the $3\,^2\Sigma^+$ state due to a curve crossing of these two potential energy curves at $R = 12.5\ a_0$. For comparison, in Fig. 10, we show what the resulting cross sections would have been, (i) if only the $2\,^2\Sigma^+$ and $1\,^2\Pi$ states were allowed to interact, and (ii) if only the $1\,^2\Sigma^+$, $2\,^2\Sigma^+$ and $3\,^2\Sigma^+$ states were allowed to interact.[19] At lower velocities, both

Σ-Σ transitions go to zero exponentially while the Σ-Π cross section falls off very slowly. At higher energies, the Σ-Σ cross sections reach a maximum and then go to zero. On the other hand, the Σ-Π cross section does not possess a maximum, but continues to increase with increasing velocity. This defect results from the neglect of translational momentum of the electron (see Part I). This defect leads to an overemphasis of the Σ-Π cross section, resulting in too large a theoretical cross section for $K + Li^+$ with the error increasing with velocity. At the cross section maximum, this error leads to an apparent overestimate of the theoretical cross section, which is almost three times the experimental cross section. Similarly, the theoretical cross section for the endothermic process $Li + K^+$ is too small because amplitude on the $2\,^2\Sigma^+$ state is decreased by transitions to the $1\,^2\Pi$ state.

C. $Na + K^+$ and $K + Na^+$

The total cross sections for $Na + K^+$ and $K + Na^+$ represent a pair of cross sections which are intermediate between the nearly equivalent cross sections for $Li + Na^+$ and $Na + Li^+$ on the one hand and the rather dissimilar cross sections for $Li + K^+$ and $K + Li^+$ on the other hand. The cross sections for transitions to individual states are plotted in Fig. 11. As in $Li + Na^+$ and $Li + K^+$, the $Na + K^+$ total cross section is dominated by transitions from the $1\,^2\Sigma^+$ state to the $2\,^2\Sigma^+$ state. The $K + Na^+$ total cross section, on the other hand, represents a mixture of processes. At lower velocities the cross section is dominated by transitions

from the $2\,^2\Sigma^+$ state to the $1\,^2\Pi$. However, as the velocity increases, the $2\,^2\Sigma^+ \rightarrow 1\,^2\Sigma^+$ cross section quickly grows and soon dominates. At higher velocities, the $2\,^2\Sigma^+ \rightarrow 3\,^2\Sigma^+$ cross section also becomes important.

As for the $LiNa^+$ and LiK^+ an explanation of these results can be obtained from simple considerations of the potential energy curves for the NaK^+ molecule (see Fig. 2c). We see that the $2\,^2\Sigma^+$ curve is closer to the $1\,^2\Sigma^+$ curve ($\Delta E(\infty) = 0.030\,h = 0.82$ eV) than to the $3\,^2\Sigma^+$ curve ($\Delta E(\infty) = 0.048\,h = 1.31$ eV). Thus, the two-state $1\,^2\Sigma^+ \rightarrow 2\,^2\Sigma^+$ transition process will be quite important. It is essentially the only process available for the $Na + K^+$ collision. Since the energy defect is larger than in $LiNa^+$, the cross section for this process is smaller than for $LiNa^+$. For an electron starting in the $2\,^2\Sigma^+$ state, transitions can occur (i) to the $1\,^2\Sigma^+$ state through Σ-Σ coupling at large R or (ii) to the $1\,^2\Pi$ state through rotational coupling due to the curve crossing of the $2\,^2\Sigma^+$ and $1\,^2\Pi$ state at $R = 5.8\,a_0$. At higher energies, the electron can also transfer directly to the $3\,^2\Sigma^+$ state. Due to the small energy difference between the Na 3p and K 4p atomic states, strong coupling will occur between the $3\,^2\Sigma^+$ and $4\,^2\Sigma^+$ states and between $1\,^2\Pi$ and $2\,^2\Pi$ states. However, no oscillations occur between these pairs of states since the transition region is only crossed once. We see that oscillations in the total cross sections are caused by oscillations in the $1\,^2\Sigma^+ \rightarrow 2\,^2\Sigma^+$ cross section.

Aquilanti et al.[23] obtained experimental cross sections for $Na(3s) + K^+ \rightarrow Na(3p) + K^+$ and $Na(3s) + K^+ \rightarrow Na^+ + K(4p)$. The magnitudes

of these cross sections are so small that they are less than the error in our calculations due to effects at small impact parameters. However, our calculations predict that the cross section for forming Na(3p) should be larger than for forming K(4p) which is opposite from what they observe.

The experimental results of Perel and Daley[16,17] indicate that the cross sections for $Na + K^+$ and $K + Na^+$ meet at 3×10^7 cm/sec. The two cross sections, however, should have a continuously increasing difference since

$$\sigma_{Na + K^+ \rightarrow Na^+ + K} \approx \sigma_{1\,^2\Sigma^+ \rightarrow 2\,^2\Sigma^+} \tag{6}$$

while

$$\sigma_{K + Na^+ \rightarrow K^+ + Na} \approx \sigma_{2\,^2\Sigma^+ \rightarrow 1\,^2\Sigma^+} + \sigma_{2\,^2\Sigma^+ \rightarrow 1\,^2\pi} + \sigma_{2\,^2\Sigma^+ \rightarrow 3\,^2\Sigma^+} \tag{7}$$

(see Fig. 11), but

$$\sigma_{1\,^2\Sigma^+ \rightarrow 2\,^2\Sigma^+} = \sigma_{2\,^2\Sigma^+ \rightarrow 1\,^2\Sigma^+}$$

due to detailed balancing, so (7) should be greater than (6). Also, at low velocities, the $Na + K^+ \rightarrow Na^+ + K$ experimental cross section appears to go to a constant rather than decreasing exponentially to zero as it should. On the other hand, the splitting between the endothermic ($Na + K^+$) and exothermic ($K + Na^+$) cross sections is overestimated theoretically due to the neglect of translational momentum of the electron. This defect overestimates the Σ-Π transition probability, giving rise, in particular, to a $K + Na^+ \rightarrow K^+ + Na$ theoretical cross section which should be too large. Therefore, the actual charge transfer cross sections for $Na + K^+$ and $K + Na^+$ are probably somewhere between the theoretical and experimental results.

CONCLUSION

We have used the molecular wavefunction approach to calculate the charge transfer cross sections for alkali atoms colliding with alkali ions. We obtained cross sections which were in fairly good agreement with experiment. In the molecular wavefunction approach, coupling between states occurs either through the radial change of one state into another ($M_{ij} = \langle \psi_i | \frac{\partial}{\partial R} | \psi_j \rangle$) or through the rotational change of one state into another ($N_{ij} = \langle \psi_i | \frac{1}{R} \frac{\partial}{\partial \theta} | \psi_j \rangle$). However, transitions only occur between those states which are close in energy. Using the simple ideas of the coupling process, therefore, one need only examine the potential energy curves for each system to understand and even predict the resulting cross sections.

For the endothermic collisions (i.e., $Li + Na^+$, $Li + K^+$, $Na + K^+$), the electron is initially on the $1\,^2\Sigma^+$ state. Since the $2\,^2\Sigma^+$ state is the only state close in energy (ignoring small impact parameters), charge transfer occurs essentially through the two-state Σ-Σ coupling process. The cross section for this process rises exponentially with increasing velocity, reaches a maximum, and then goes to zero at high velocities. Oscillatory structure in the total cross section result from oscillations in this two-state process.

For the exothermic collisions (i.e., $Na + Li^+$, $K + Li^+$, $K + Na^+$), the electron is initially on the $2\,^2\Sigma^+$ state. In addition to the small energy difference with the $1\,^2\Sigma^+$ state, however, the $2\,^2\Sigma^+$ state also crosses the $1\,^2\Pi$ state. Therefore, charge transfer can occur either through Σ-Σ coupling to the ground state or through rotational coupling to the

Π state. In addition, a small energy difference can also occur between the $2\,^2\Sigma^+$ and $3\,^2\Sigma^+$ states, such as in $K + Li^+$, leading to charge transfer coupling between these two states. The relative importance of each of these processes depends on the energy difference and the velocity. At very low velocities, the Σ-Π transition dominates. The magnitude of the cross section is determined mostly by the internuclear distance of the crossing point. For small energy defects between the Σ states, such as for $Na + Li^+$, $2\,^2\Sigma^+ \rightarrow 1\,^2\Sigma^+$ transitions begin to dominate as the velocity increases. The larger cross section results from the larger internuclear distance of the transition region. For large energy defects, such as $K + Li^+$, the growth of the $2\,^2\Sigma^+ \rightarrow 1\,^2\Sigma^+$ as well as $2\,^2\Sigma^+ \rightarrow 1\,^2\Sigma^+$ cross sections occurs at much higher energies so that the Σ-Π transition remains a significant part of the total charge transfer cross section. The oscillatory structure in the total cross section as well as the cross section maximum result from the presence of these characteristics in the Σ-Σ transitions. The rotational coupling process appears to overestimate the charge transfer cross section as does the Σ-Σ coupling to a lesser extent due to neglect of the translational energy of the electron. However, the general shape of the charge transfer cross section is correct. In particular, the position of the maximum as well as the detailed oscillatory structure is in excellent agreement, both in the amplitude and in the phase of oscillations.

In conclusion, the molecular wavefunction approach can provide quite accurate total cross sections while at the same time providing a simple picture of the coupling processes. These results should be useful in making qualitative predictions of the electronic transitions which can occur in a variety of scattering systems.

FOOTNOTES

1. D. R. Bates, H. S. Massey, and A. L. Stewart, Proc. Roy. Soc. (London), A216, 437 (1953).
2. M. Born and J. R. Oppenheimer, Ann. Physik. 84, 457 (1927).
3. R. K. Colegrave and D. B. L. Stephens, J. Phys. B., 1, 856 (1968).
4. J. M. Peck, T. A. Green, J. Perel, and H. H. Michels, Phys. Rev. Lett. 26, 1419 (1968).
5. C. Bottcher and M. Oppenheimer, J. Phys. B. 5, 492 (1972).
6. C. F. Melius and W. A. Goddard III, Chem. Phys. Lett. 15, 524, (1972).
7. D. R. Bates and D. A. Williams, Proc. Phys. Soc. 83, 425 (1964).
8. W. L. McMillan, Phys. Rev. A4, 69 (1971).
9. R. McCarroll and R. D. Piacentini, J. Phys. B4, 1026 (1971).
10. D. W. Jepsen and J. O. Hirschfelder, J. Chem. Phys. 32, 1323 (1960).
11. C. F. Melius and W. A. Goddard (to be published).
12. See (a) C. F. Melius, W. A. Goddard III, and L. R. Kahn, J. Chem. Phys. 56, 3342 (1972); (b) C. F. Melius and W. A. Goddard III, to be published, (c) L. R. Kahn and W. A. Goddard III, J. Chem. Phys. 56, 2685 (1972).
13. Both ΔE and M_{12} were varied for small R ($<3.5\ a_0$) without significantly affecting the total cross section.

14. For the potential energy curves plotted, an extra s, p and d Gaussian was added to each center in order to describe the next Rydberg level states of each atom.

15. See, for example, A. Russek, Phys. Rev. A4, 1918 (1971).

16. (a) H. L. Daley and J. Perel, VIth ICPEAC, MIT, Cambridge (The MIT Press, Cambridge, Massachusetts, 1969), p. 1051; (b) J. Perel and H. L. Daley, Phys. Rev. A4, 162 (1971); (c) J. Perel and H. L. Daley, Bull. Am. Phys. Soc. 13, 1656 (1968) (unpublished cross section), (d) J. Perel and A. Y. Yahiku, Vth ICPEAC, Leningrad (Publishing House Nauka, Leningrad, 1967), p. 400; (e) H. L. Daley and J. Perel, Bull. Am. Phys. Soc. 17, 88 (1972)(unpublished cross section).

17. J. Perel, private communication.

18. V. Aquilanti, G. Liuti, F. Vecchio-Cattivi, and G. G. Volpi, VIIth ICPEAC, Amsterdam (North-Holland Publ. Co., Amsterdam, 1971), p. 600.

19. R. E. Olson [Phys. Rev. A., to be published] estimated the charge transfer cross section for $K + Na^+$ as the sum of the $2\,^2\Sigma^+ \rightarrow 1\,^2\Sigma^+$ and $2\,^2\Sigma^+ \rightarrow 3\,^2\Sigma^+$ cross sections, ignoring $2\,^2\Sigma^+ \rightarrow 1\,^2\Pi$ coupling.

Fig. 1. The potential energy curves for (a) $LiNa^+$, (b) LiK^+, (c) NaK^+, (d) Li_2^+, (e) Na_2^+, and (f) K_2^+ [atomic unites ($\hbar = 1$, $e = 1$, $m_e = 1$) are used; 1 hartree = 27.211 eV, 1 Bohr = 0.52917 Å].

Fig. 2. The coupling terms $Mij = \langle \Psi_i \mid \partial/\partial R \mid \Psi_j \rangle$ between the various molecular states for (a) $LiNa^+$, (b) LiK^+, and (c) NaK^+.

Fig. 3. The coupling terms $R\,Nij = \langle \Psi_i \mid \partial/\partial \Theta \mid \Psi_j \rangle$ between the various molecular states for (a) $LiNa^+$, (b) LiK^+, and (c) NaK^+.

Fig. 4. The total charge transfer cross sections for $Li + Na^+ \rightarrow Li^+ + Na$, $Na + Li^+ \rightarrow Na^+ + Li$, $Li + K^+ \rightarrow Li^+ + K$, $K + Li^+ \rightarrow K^+ + Li$, $Na + K^+ \rightarrow Na^+ + K$, and $K + Na^+ \rightarrow K^+ + Na$ (1 a.u. velocity = 2.18×10^8 cm/sec; $\pi a_0^2 = 0.879 \times 10^{-16}$ cm^2).

Fig. 5. Comparison of the theoretical and experimental cross sections for $Li + Na^+ \rightarrow Li^+ + Na$ and $Na + Li^+ \rightarrow Na^+ + Li$ [—— theoretical; --- experimental (Perel and Daley, Ref. 16)].

Fig. 6. Comparison of the theoretical and experimental cross sections for $Li + K^+ \rightarrow Li^+ + K$ and $K + Li^+ \rightarrow K^+ + Li$ [—— theoretical; --- experimental (Perel and Daley, Ref. 16)].

Fig. 7. Comparison of the theoretical and experimental cross sections for $Na + K^+ \rightarrow Na^+ + K$ and $K + Na^+ \rightarrow K^+ + Na$ [—— theoretical, --- experimental (Perel and Daley, Ref. 16)].

Fig. 8. Theoretical cross sections to individual states for (a) $Li + Na^+$ and (b) $Na + Li^+$.

Fig. 9. Theoretical cross sections to individual states for (a) $Li + K^+$ and (b) $K + Li^+$.

Fig. 10. Theoretical cross sections to individual states for (a) $Na + K^+$ and (b) $K + Na^+$.

Fig. 11. Theoretical cross sections to individual states for $K + Li^+$ in the three state ($1\,^2\Sigma^+$, $2\,^2\Sigma^+$, $3\,^2\Sigma^+$) approximation (——) and the two-state ($2\,^2\Sigma^+$, $1\,^2\Pi$) approximation.

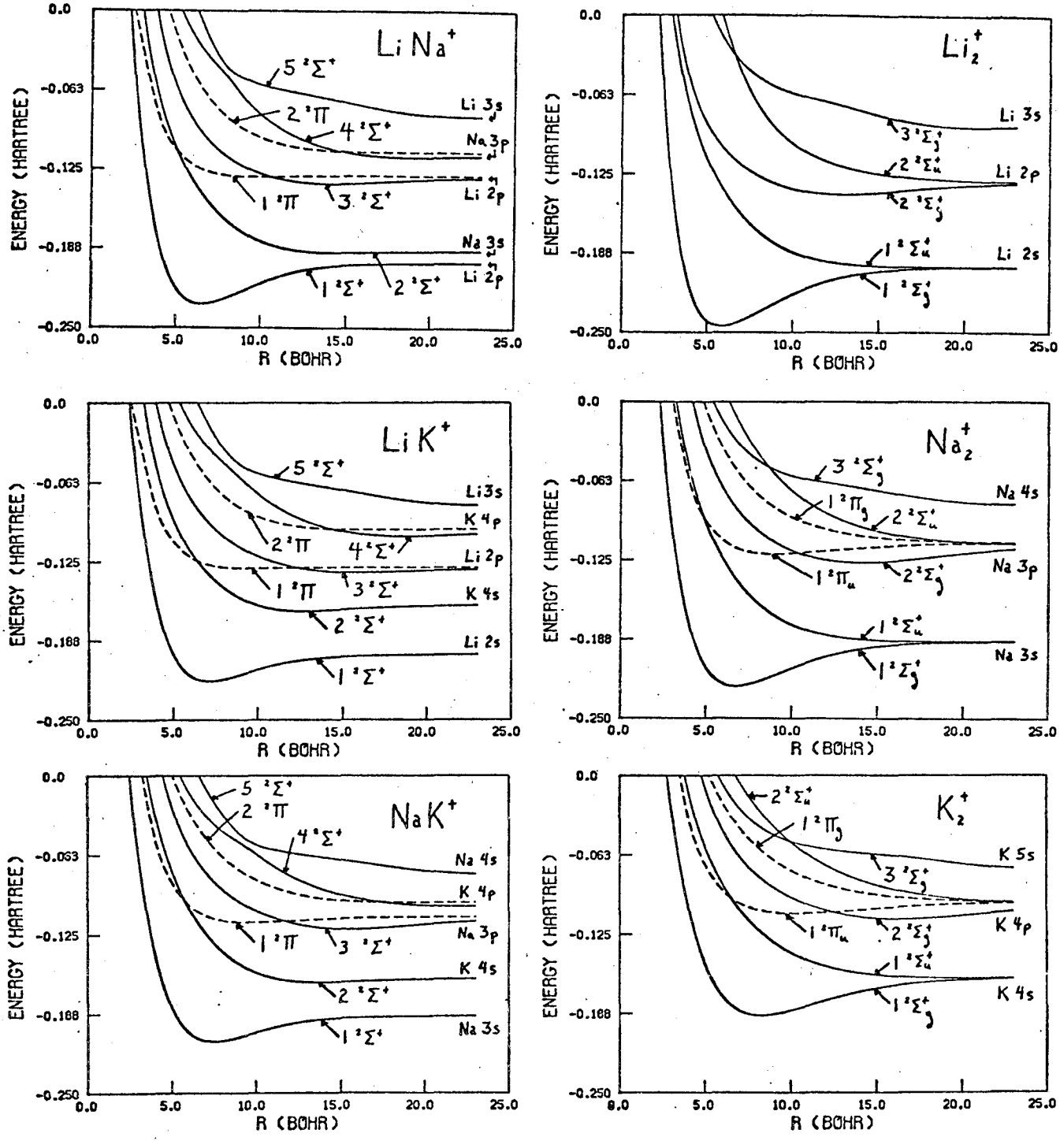
LiNa+
5 ²Σ+
2 ²Π
4 ²Σ+
1 ²Π
3 ²Σ+
1 ²Σ+
2 ²Σ+
Li 3s
Na 3p
Li 2p
Na 3s
Li 2p
Li2+
3 ²Σg+
2 ²Σu+
2 ²Σg+
1 ²Σu+
1 ²Σg+
Li 3s
Li 2p
Li 2s
LiK+
5 ²Σ+
2 ²Π
4 ²Σ+
1 ²Π
3 ²Σ+
2 ²Σ+
1 ²Σ+
Li3s
K 4p
Li 2p
K 4s
Li 2s
Na2+
3 ²Σg+
1 ²Πg
2 ²Σu+
1 ²Πu
2 ²Σg+
1 ²Σu+
1 ²Σg+
Na 4s
Na 3p
Na 3s
NaK+
5 ²Σ+
2 ²Π
4 ²Σ+
1 ²Π
3 ²Σ+
2 ²Σ+
1 ²Σ+
Na 4s
K 4p
Na 3p
K 4s
Na 3s
K2+
2 ²Σu+
1 ²Πg
3 ²Σg+
1 ²Πu
2 ²Σg+
1 ²Σu+
1 ²Σg+
K 5s
K 4p
K 4s
ENERGY (HARTREE)
0.0
-0.063
-0.125
-0.188
-0.250
R (BOHR)
0.0
5.0
10.0
15.0
20.0
25.0

Fig. 1

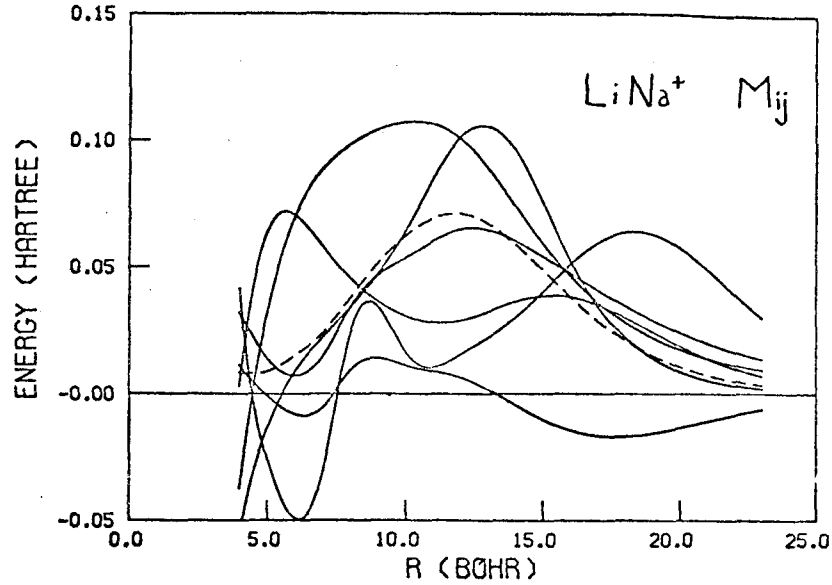
LiNa+ Mij
ENERGY (HARTREE)
0.15
0.10
0.05
-0.00
-0.05
0.0
5.0
10.0
15.0
20.0
25.0
R (BOHR)

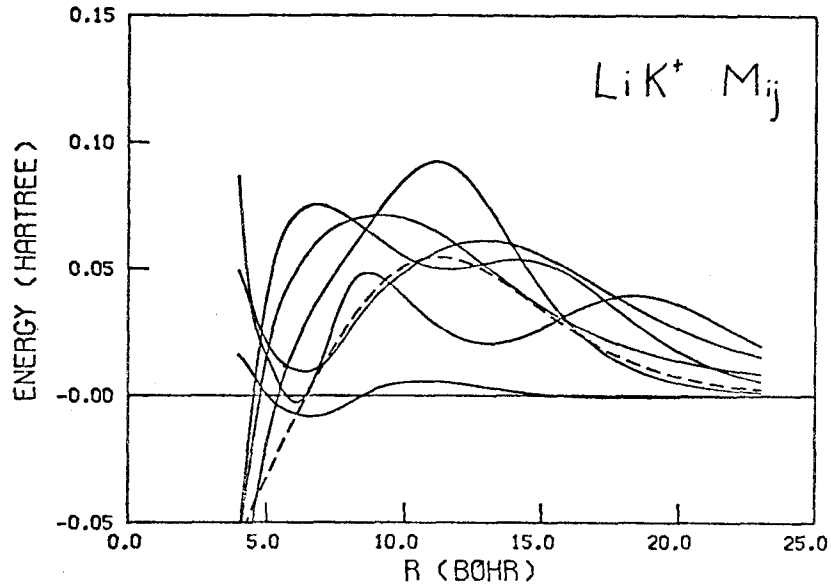
LiK+ Mij
ENERGY (HARTREE)
0.15
0.10
0.05
-0.00
-0.05
0.0
5.0
10.0
15.0
20.0
25.0
R (BOHR)

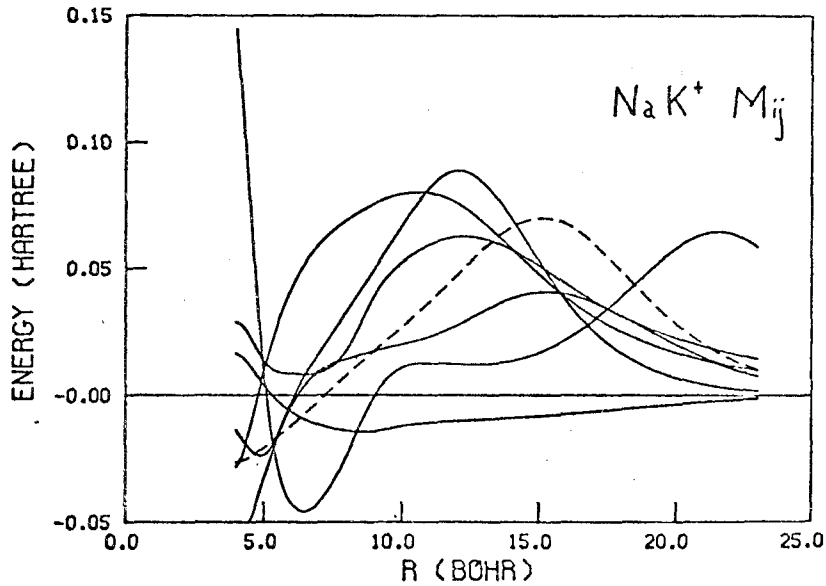
NaK+ Mij
ENERGY (HARTREE)
0.15
0.10
0.05
-0.00
-0.05
0.0
5.0
10.0
15.0
20.0
25.0
R (BOHR)

Fig. 2

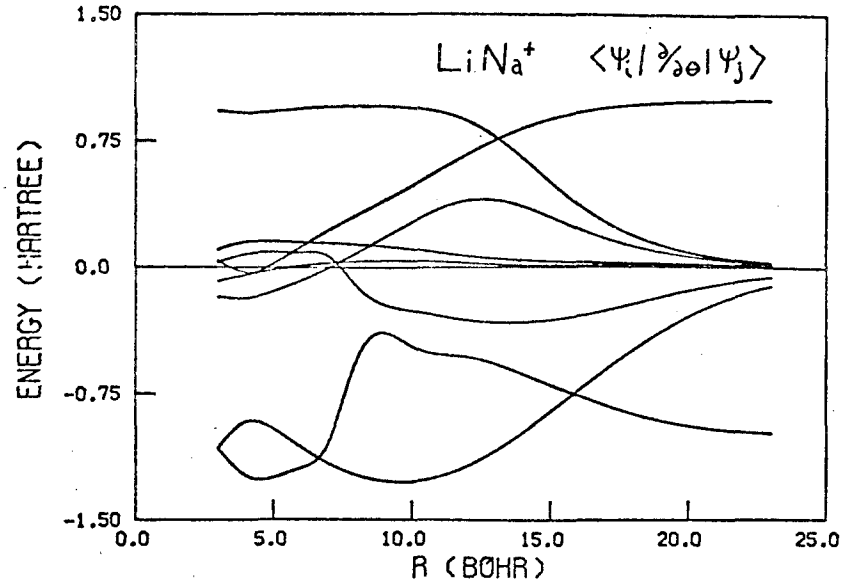
LiNa+ ⟨Ψi|∂/∂θ|Ψj⟩
ENERGY (HARTREE)
1.50
0.75
0.0
-0.75
-1.50
0.0
5.0
10.0
15.0
20.0
25.0
R (BOHR)

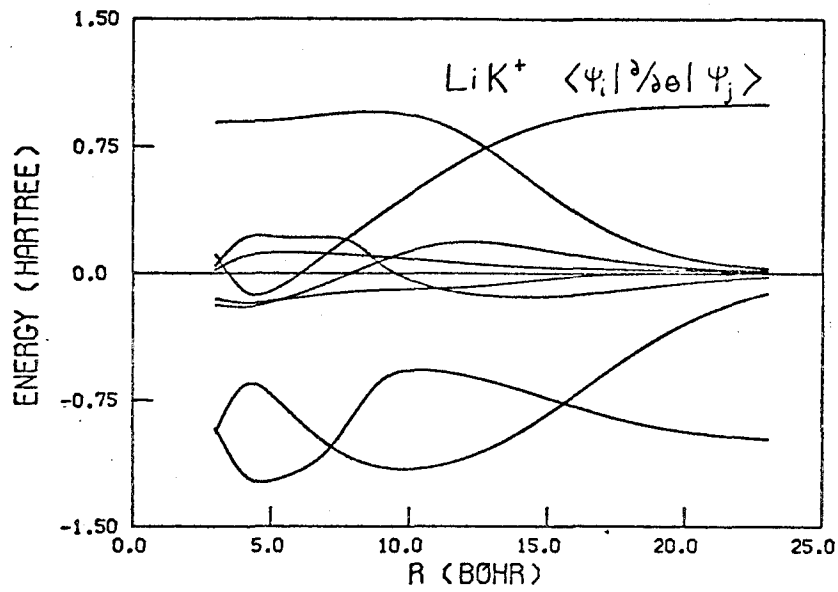
LiK+ ⟨Ψi|∂/∂θ|Ψj⟩
ENERGY (HARTREE)
1.50
0.75
0.0
-0.75
-1.50
0.0
5.0
10.0
15.0
20.0
25.0
R (BOHR)

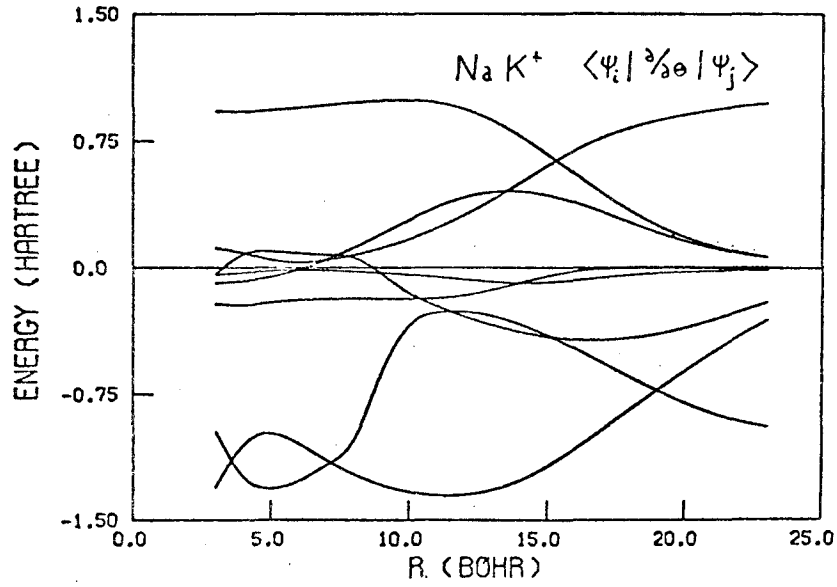
NaK+ ⟨Ψi|∂/∂θ|Ψj⟩
ENERGY (HARTREE)
1.50
0.75
0.0
-0.75
-1.50
0.0
5.0
10.0
15.0
20.0
25.0
R (BOHR)

Fig. 3

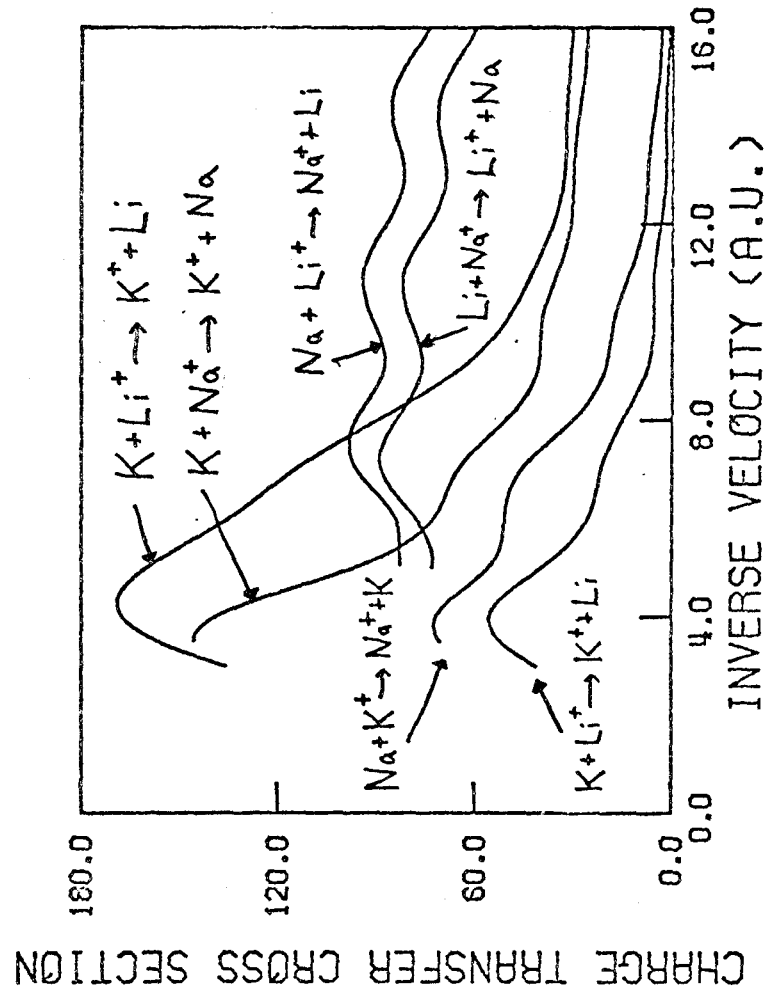
CHARGE TRANSFER CROSS SECTION
180.0
120.0
60.0
0.0
0.0
4.0
8.0
12.0
16.0
INVERSE VELOCITY (A.U.)
K+Li+→ K++Li
K+Na+→ K++Na
Na+Li+→ Na++Li
Li+Na+→ Li++Na
Na+K+→ Na++K
K+Li+→ K++Li

Fig. 4

Fig. 5

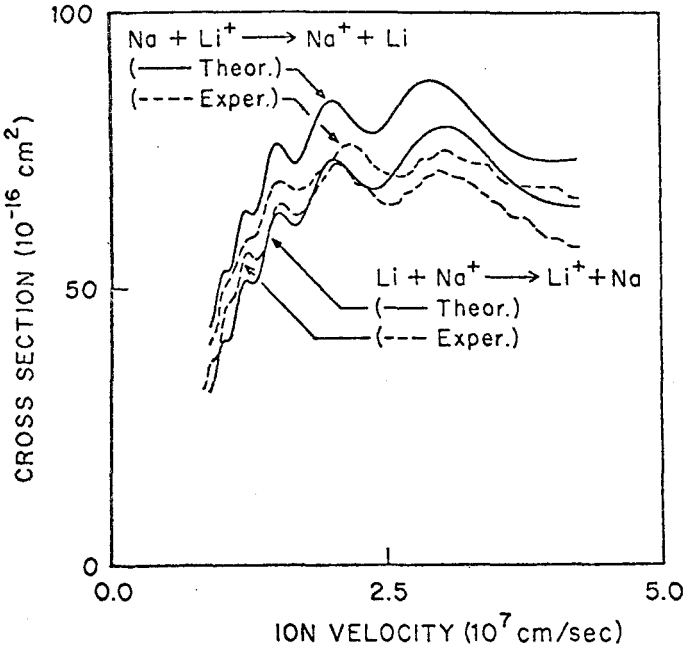

Fig. 6

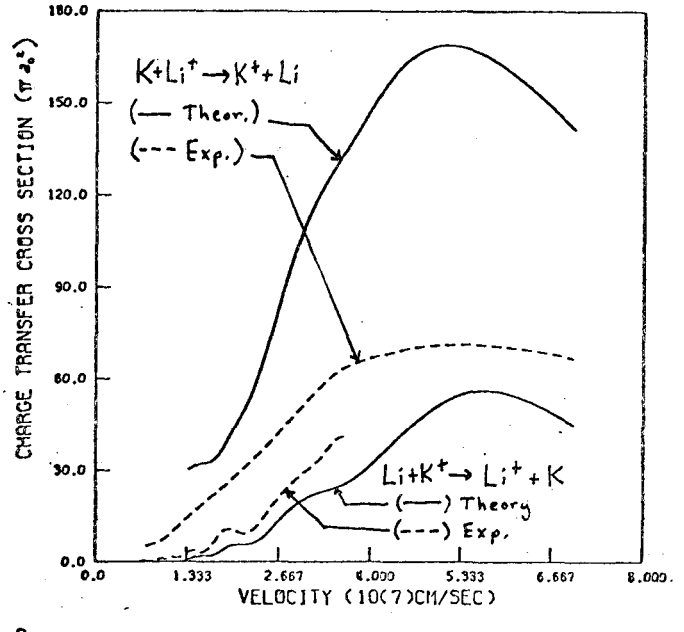

Fig. 7

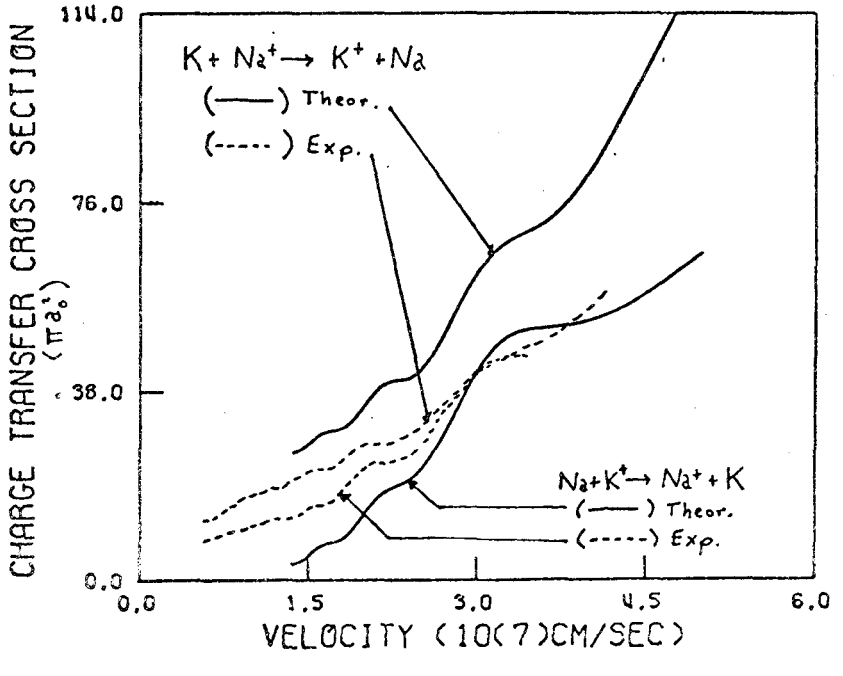

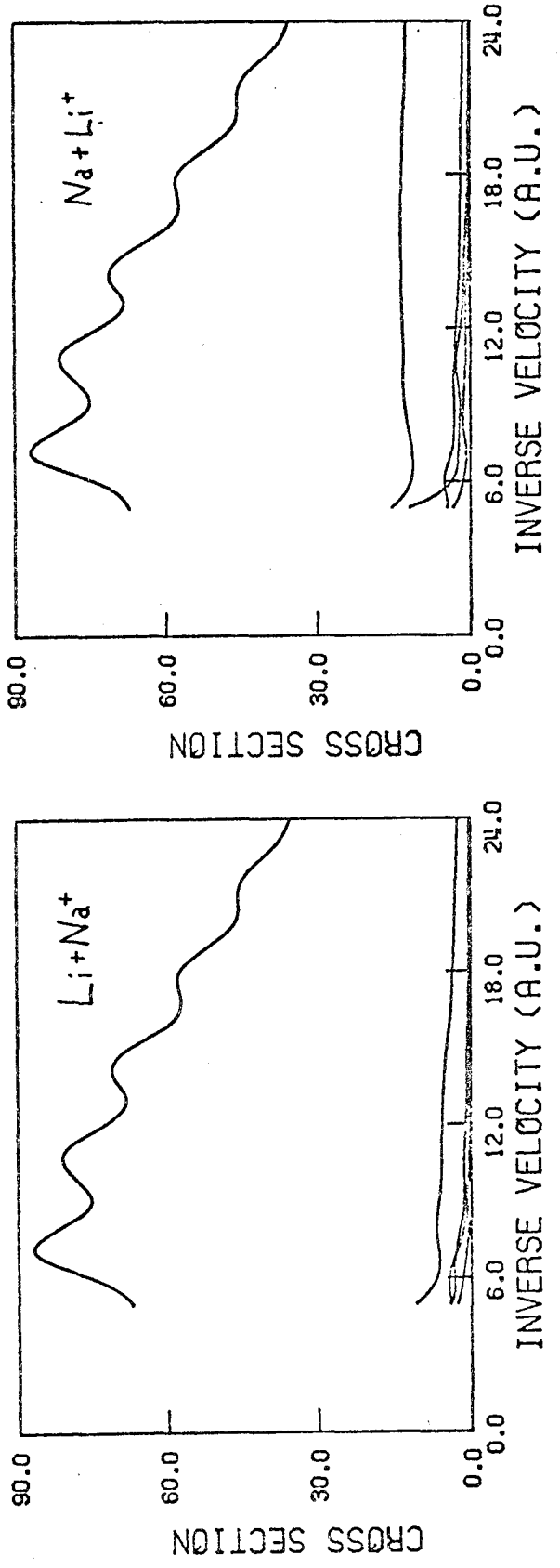
Na + Li+
Li + Na+
CROSS SECTION
INVERSE VELOCITY (A.U.)
90.0
60.0
30.0
0.0
6.0
12.0
18.0
24.0

Fig. 8

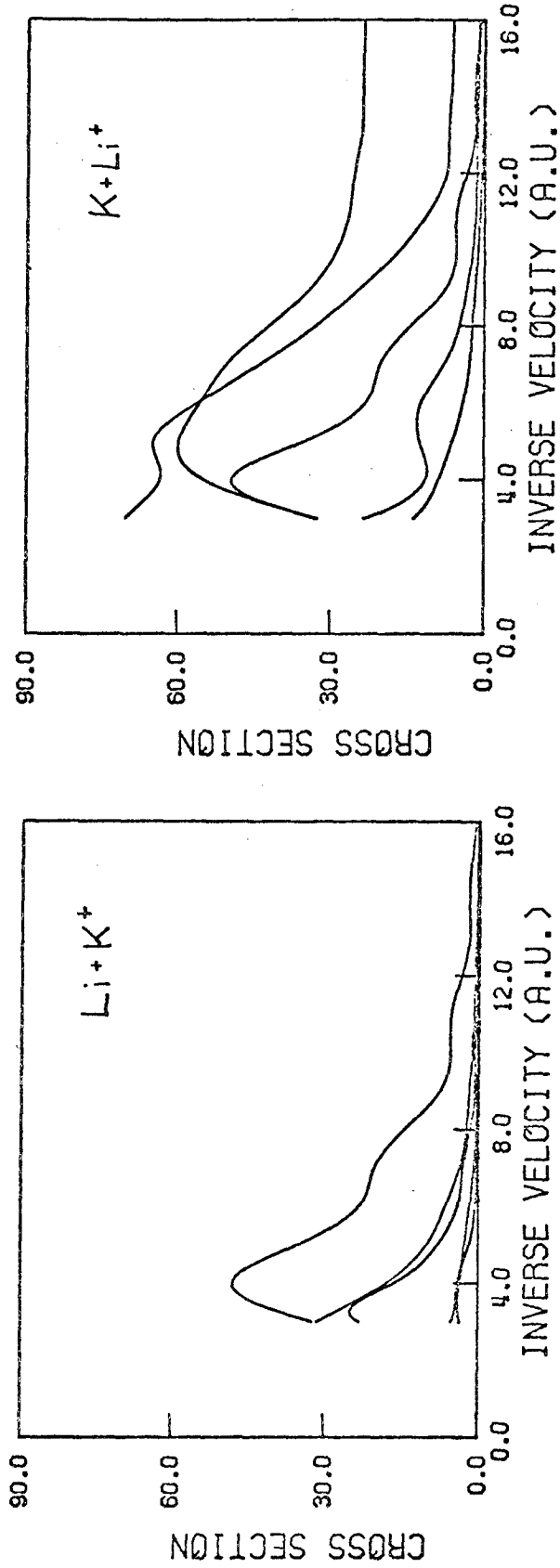
K+Li+
Li+K+
CROSS SECTION
INVERSE VELOCITY (A.U.)
0.0
30.0
60.0
90.0
4.0
8.0
12.0
16.0

Fig. 9

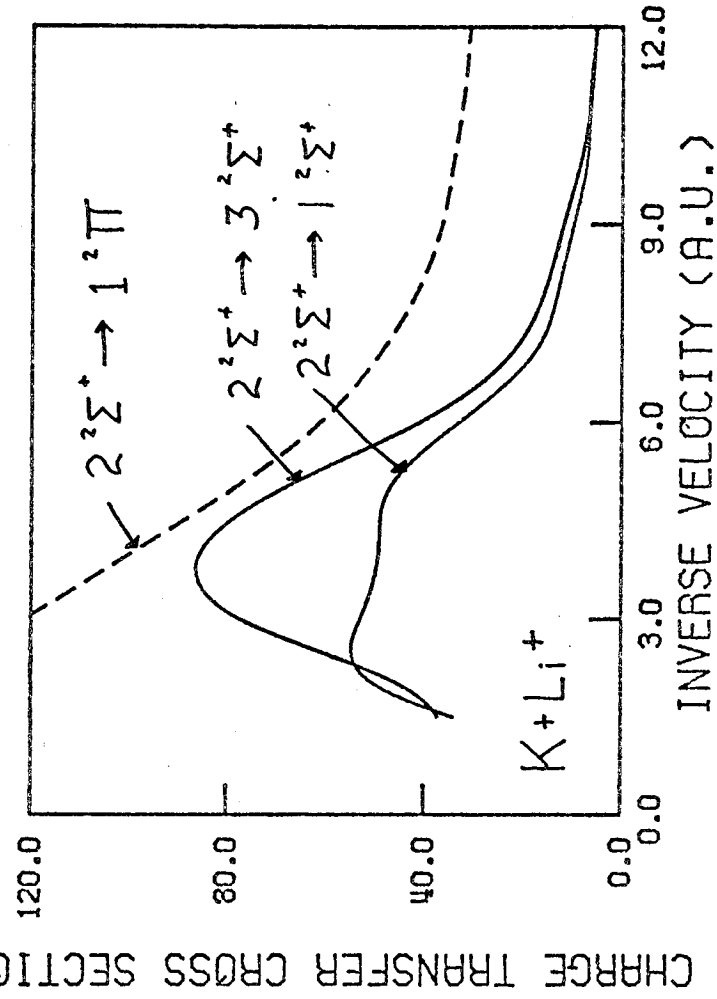
CHARGE TRANSFER CROSS SECTION
120.0
80.0
40.0
0.0
0.0
3.0
6.0
9.0
12.0
INVERSE VELOCITY (A.U.)
$2^2\Sigma^+ \rightarrow 1^2\Pi$
$2^2\Sigma^+ \rightarrow 3^2\Sigma^+$
$2^2\Sigma^+ \rightarrow 1^2\Sigma^+$
$K+Li^+$

Fig. 10

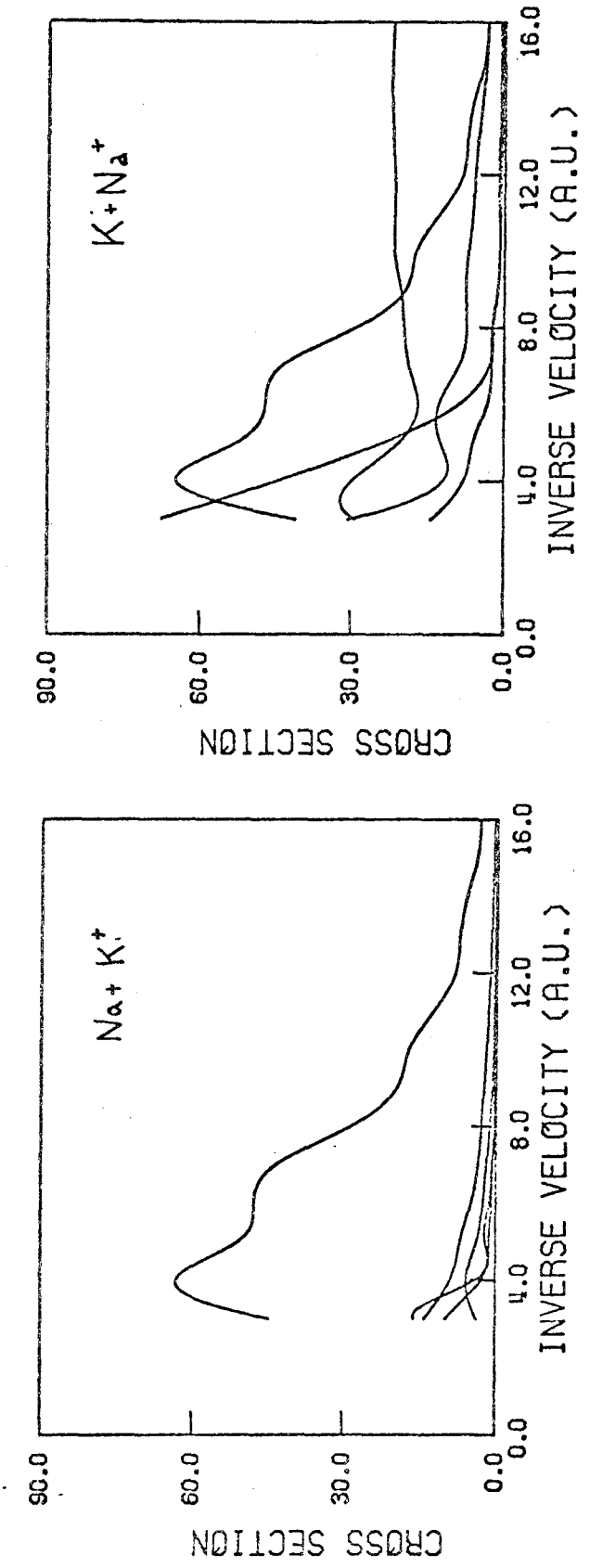
K+ Na+
Na+ K+
CROSS SECTION
INVERSE VELOCITY (A.U.)
0.0
30.0
60.0
90.0
4.0
8.0
12.0
16.0

Fig. 11

PART II

The Effective Potential Method in Molecular Quantum Mechanics

PART II-A

The Use of Ab-Initio Effective Potentials in Molecular Calculations

I. INTRODUCTION

For many years chemists and physicists have realized that many of the chemical and physical properties of atoms are determined by only the outer few (valence) electrons. Indeed, the concept of the periodic table derives from this idea. Thus in describing the nature of the chemical bond, one needs only focus his attention upon a few electrons for each atom, and, in a chemical sense, molecules involving Ra are no more complicated than those involving Mg. Unfortunately, in quantum mechanical considerations, the electrons are indistinguishable and all must be considered. Treating Ra is therefore considerably more complicated than treating Mg. However, it was clear to early workers that Ra and Mg could be described as simple two-electron problems by merely replacing the Rn and Ne cores, respectively, with an appropriate effective potential (EP) [1-2].

As was realized by these workers, the EP could not be just some simple electrostatic potential due to the core electrons. Rather, it must also incorporate the effects of the Pauli exclusion principle, leading to additional repulsive terms in the EP's. There are not unique solutions to this problem. As a result, a number of approaches have been suggested and used. Some approaches are empirical and adjust the EP to match some experimental data [1-3]. Other approaches are theoretically based and adjust the EP to match the results of ab initio calculations [4-10].

In this paper we present a theoretically based method which has evolved from an approach previously applied by Goddard, Kahn, and Melius [7-10] to some simple systems. The method has been formulated to yield ab intio quality wavefunctions for the valence electrons while remaining computationally simple and straightforward.

II. THE AB INITIO EFFECTIVE POTENTIAL

In the Hartree-Fock approximation to, say, the Na atom, the wavefunction has the form

$$\mathcal{A}\,[\Phi_{core}\phi_v \chi]\ , \tag{1}$$

where Φ_{core} is a product of (ten) spatial orbitals very similar to the orbitals of Na^+ and ϕ_v is the valence orbital (the one removed is going to Na^+). [χ is an appropriate product of spin functions.] The low-lying states of Na are also given by (1) but with nearly the same Φ_{core} so that only ϕ_v changes. To obtain the HF wavefunction we solve for the orbitals of (1) self-consistently leading to variational equations of the form

$$H^{HF}\phi_i = \epsilon_i\phi_i \tag{2}$$

where the one-electron HF Hamiltonian is given by

$$H^{HF} = -\tfrac{1}{2}\nabla^2 - \frac{Z_\alpha}{r_\alpha} + J_\alpha - \tfrac{1}{2}\hat{K}_\alpha \tag{3}$$

where $-\frac{1}{2}\nabla^2$ is the kinetic energy term, $-Z_\alpha/r_\alpha$ is the nuclear attraction potential. The quantities J_α and K_α depend upon which orbital is being solved for. For the valence orbital J_α is equivalent to the classical Coulomb potential due to a charge density corresponding to the Φ_{core}. The exchange operator $\hat{K}_\alpha$ is an integral operator resulting from the antisymmetric form of the wavefunction (i.e., from the Pauli Principle).

Ignoring slight changes in the core orbitals, the valence orbitals for the excited states of Na satisfy the same Eqn. (3). Similarly for a Na bonded to something else, we might expect that the core orbitals could be replaced by the effective potential

$$\hat{U}_\alpha^{HF} = J_\alpha - \hat{K}_\alpha \tag{4}$$

just as for the atomic states. The J_α in (4) can be expressed as a function of r. If U_α^{HF} could also be expressed as a function of r

$$U_\alpha^{EP}(r)$$

we could merely replace the core on each atom with $U_\alpha^{EP}(r)$ and consider only the valence electrons in all further considerations. In this case the potential in (3) would become

$$V_\alpha^{EP}(r_\alpha) = -\frac{Z_\alpha}{r_\alpha} + U_\alpha^{EP}(r_\alpha) \tag{5a}$$

so that (3) becomes

$$h = -\tfrac{1}{2}\nabla^2 + V_\alpha^{EP}(r_\alpha) \quad . \tag{5b}$$

Thus the HF theory provides a basic foundation for the use of EP's.

However (4) does not allow us to forget about the core orbitals since $\hat{K}_\alpha$ is an integral operator and upon operating on a function ϕ_v leads to terms involving integrals over products of ϕ_v with core orbitals. Thus to eliminate the core orbitals and obtain effective potentials of the form (5) we need to somehow approximate the effect of the exchange integral $\hat{K}_\alpha$. There are many ways of doing this leading to a number of types of EP's.

Even without using the EP approximations the wavefunction in (1) is an approximate one and hence the excitations energies from (2) will not be exactly the experimental values. These errors due to the approximate form of the wavefunction are referred to as correlation errors. [For a system with one valence electron these correlation errors are generally not large. (For Na the 3s and 3p ionization potentials are calculated to be and whereas the experimental values are and , thus the effect of correlation error upon these IP's is eV.] However they do lead to small errors in the predicted IP even if no EP approximation is made in (4).

A. Empirically Adjusted Potentials

The first work on effective potentials was by Hellmann [1] and Gombaś [2], who used a simple, repulsive potential of the form

$$U(r) = \frac{A}{r} \exp(-2Kr) \tag{6}$$

with A and K determined empirically so that the first few excitation energies [of (5)] match the experimental values. Since their work, more general forms of the potential in (6) have been used and fit to more of the experimental excitation energies [3].

Since the spectrum of states using (6) is fitted to the experimental spectrum, the potential (6) in some sense corrects for differences in correlation energies in the various states. Inclusion of correlation (i.e., superposition of configuration) involving ϕ_v invalidates the use of (2) and hence of the use of (5) to solve for the excited states of even a one-valence-electron system. Thus determining a generalized form of (6) to fit the excitation energies of the atom does not imply that the wavefunctions and hence the other properties are as well described. The use of several such potentials in a molecule could lead to large errors in describing molecular binding energies (and a fortiori other properties) despite good atomic excitation energies.

B. Theoretically based potentials

A different approach to EP's was suggested by Phillips and Kleinman [4] who modified the HF equations (4) (for a one-valence-electron system) into the form

$$(-\tfrac{1}{2}\nabla^2 - \frac{Z}{r} + \hat{U}^{HF} + \hat{U}^{PK})\chi_v = \epsilon_r \chi_v \tag{7a}$$

where χ_v differs from the HF valence orbital ϕ_v in that components of the core orbital are subtracted from ϕ_v in order to obtain a smooth valence orbital (i.e., no large oscillations in the core region like ϕ_v). With this transformation the total potential

$$V = -\frac{Z}{r} + \hat{U}^{HF} + \hat{U}^{PK} \tag{7b}$$

is relatively weak. This stimulated a great deal of theoretical analysis on the electronic properties of solids since using (7b) the presence of atoms could be considered as a perturbation to the free electron gas. Phillips and Kleinman showed that (7) leads to the same energy ϵ_v as (4) if $\hat{U}^{PK}$ has the form

$$\hat{U}^{PK} = \sum_c (\epsilon_v - \epsilon_c) |\phi_c\rangle \langle\phi_c| \tag{8}$$

In this viewpoint of the EP, V^{PK} (called the pseudopotential) is a repulsive potential which plays the role of enforcing the Pauli principle, preventing χ_v from collapsing into the core. The $\hat{V}^{PK}$ was generalized by Weeks and Rice [5, 12] in order to properly account for the off-diagonal Lagrange multipliers necessarily present in the HF equations for open shell systems. (A detailed discussion of these methods and others have been presented by Hazi, Weeks, and Rice [5] and by Kahn and Goddard [9]).

Although (7) and (4) are equivalent for the first state, ϵ_v, they are <u>not</u> equivalent in general for the excited states. In addition, there is not a unique (7) but rather an infinite number of possible choices (corresponding to all the ways of mixing core character ϕ_c into ϕ_v to form χ_v

$$\chi_v = [\phi_v - \lambda\phi_c]/(1 + \lambda^2). \tag{9}$$

Furthermore, the effective potential in (8) is still an integral operator and hence is not as convenient as a local potential such as (6). To obtain an EP that is a function of r we let $\hat{V}$ operate on $\chi_v(r)$ and then divide by $\chi_v(r)$. [If χ_v has a node, this approach leads to a difficulty since the resulting potential has a singularity, forcing all the excited state orbitals to also have a node at that point.] In any case this approach leads to an infinite number of such local potentials, each with its own spectra of excited states.

C. The G1 Ab Initio Effective Potential and the MKE Effective Potential

Goddard included dominant correlation terms missing in the HF method by using a wavefunction corresponding to a self-consistent form of a generalization of the valence bond type wavefunctions. With this approach the orbitals are given by a set of equations similar to (4)

$$H^{G1}\phi_i = \epsilon_i\phi_i \tag{10}$$

where H^{G1} is similar to H^{HF} but contains a more complicated exchange term (integral operators) than $\hat{K}_\alpha$. A major difference is that this method (called the G1 method [13] or GVB method [14]) leads to G1 valence orbitals that are not orthogonal to the core orbitals. In addition these orbitals are smooth in the core region and are uniquely determined. This suggested using the G1 ab initio method on the atoms to determine the unique (smooth) orbital ϕ_v and then to choose the effective potential (called the G1 atomic EP or GAEP [7, 9])

$$V^{G1}(r) = \frac{(\epsilon_i + \frac{1}{2}\nabla^2)\phi_v}{\phi_v} \quad . \tag{11}$$

This approach was applied by Kahn, Melius, and Goddard [8, 9, 10] to the

ground and excited states of several small diatomic and triatomic molecules and was found to provide good quality wavefunctions as well as energies.

While the G1 valence orbital ϕ_v^{G1} is unique, a combination of HF orbitals χ_v can be found that is similar to ϕ_v^{G1}. Surratt and Goddard [15] found that if λ in (9) is determined to minimize the kinetic energy of χ_v, the resulting orbital χ_v^{MKE} is very close to the G1 orbital. The resulting minimum kinetic energy effective potentials (MKE EP's) are therefore similar to the G1 EO's. Arbarenkov, Sham, and Horne [36] has previously suggested that the MKE EP would be a reasonable choice for defining a unique EP. Both of these potentials have been used for calculations on solids [16, 17] where the electronic wavefunctions are expressed in momentum space. Since the potentials are weak, and the orbitals are smooth, only a small number of plane wave states are needed to describe the wavefunctions, thereby reducing the computational effort.

D. The Coreless Hartree-Fock Effective Potential

In carrying out molecular calculations we expand each valence orbital in terms of a set of basis functions $\{\chi_\mu\}$ (e.g., experimental or Gaussian functions) of appropriate shape centered on the various atoms. In this case the differential Eqn. (2) becomes a matrix equation

$$\underset{\sim}{H}\underset{\sim}{C}_i = \epsilon_i \underset{\sim}{C}_i \tag{12a}$$

where

$$H_{\mu\nu} = \langle \mu | \mathcal{H}^{HF} | \nu \rangle \quad . \tag{12b}$$

The cost of the calculation depends crucially on how many basis functions must be included and we wish to keep the size of this set to a minimum without sacrificing accuracy.

For example, consider the Na atom. With Gaussian basis functions it requires about) functions to obtain a good description of the 1s HF orbital. The 2s HF orbital is orthogonal to the 1s orbital and requires the functions for the 10 plus 2 addition functions. The 3s HF orbital is orthogonal to the 1s and 2s orbitals and requires the) functions for the 1s and 2s plus 2 additional functions. By using instead the G1 or MKE description the valence orbital is relatively smooth in the core region and requires much fewer functions (only about) for a good description. Even though these G1 and MKE orbitals are relatively smooth they do have a cusp at the nucleus and possess some wiggles. To describe such cusps and wiggles requires basis functions in the core region. In order to reduce the basis set requirements to a minimum we would like to suppress all unnecessary cusps and wiggles in the core region. This suggests starting with the HF valence orbital and mixing with it core orbitals

$$\overline{\chi}_v = \chi_v - \sum_c C_c \chi_c \qquad (13)$$

with the requirement of minimizing the number of basis functions needed to describe χ_v. Since each HF orbital satisfies the cusp condition at the nucleus

$$\left(\frac{1}{\chi_v}\frac{d}{dr}\chi_v\right)_{r=0} = -\frac{Z}{\ell+1}$$

a cusp ($\frac{d}{dr}\chi_v \neq 0$) is avoided only if $\chi_v(0) = 0$. Thus we want the coefficients in (13) to be such that $\overline{\chi}_v(0) = 0$. One might then define the other conditions in the coefficients so that higher order derivatives would also be zero at r = 0. However we found that for K requiring the first derivatives to be zero led to a function that is slightly negative for small

r, changes sign at small r and then becomes large and positive. This character near r = 0 would tend to increase the size of the basis set.

We have instead formulated a different criteria that places conditions on the overall shape or $\bar{\chi}_v$ rather than upon properties at one point. Namely we will choose the coefficients in (13) so as to obtain a best fit of $\bar{\chi}_v$ to a $\mu = 3$ Slater orbital [19]

$$r^2 e^{-\zeta r}$$

(the ζ parameter is chosen so as to give the largest overlap with $\bar{\chi}_v$). This leads to a $\bar{\chi}_v$ that is smoothly decreasing in the core region, the desired property for reducing the size of the basis. Since this new orbital has had the core character removed, we will denote it as the coreless Hartree-Fock orbital (CHF). As indicated in Fig. 1, χ_v^{CHF} goes to ;zero at the origin as r^2 but has no other nodes in it. The corresponding EP can be obtained, then, by inverting the orbital

$$V^{CHF}(r) = \frac{(\epsilon_v + \frac{1}{2}\nabla^2)\chi_v^{CHF}}{\chi_v^{CHF}} \qquad (14)$$

The resulting CHF EP's as well as MKE EP's for various systems are presented in Sec. VI.

The advantage of this smooth Hartree-Fock orbital is obvious. Since the new orbital does not contain any core character, no tight basis functions (i. e., basis functions with high exponents) are used in the molecular calculations. In particular, one can use Gaussian basis functions. Gaussian basis functions are advantageous because the one- and two-electron integrals can be evaluated analytically, thereby greatly reducing the computational time. These same properties of the Gaussian basis functions can also be used to evaluate the effective potential integrals analytically (see Sec. IV).

The usual difficulty with Gaussian basis functions has been their poor description of the sharp cusp character of the orbital near the origin. Since Gaussians are flat at the origin, many tight Gaussian basis functions have been required to adequately describe the steep slope (with the integral time growing as the number of basis functions to the fourth power). On the other hand, using the smooth CHF orbital, the orbital is flat at the origin and no difficulty arises. We have therefore simplified the computation by requiring the evaluation of only valence type basis functions. As an example, we compare in Table I the basis sets required for the HF and CHF descriptions of the K 4s valence orbital (Table I [20]). We see that while both orbitals need the diffuse basis functions, the CHF orbital does not require any of the tight core basis functions used by the HF orbital.

III. The General Form of the Effective Potential

Empirical methods of generating EP's have generally concentrated on fitting the energy spectrum of the atom. However we are not just interested in the energy but rather want to obtain many other properties for molecular systems. Thus we want the EP to be such that the whole wavefunction is accurately described, not just the energy [21]. Indeed even to obtain good potential energy curves it is necessary that the various atomic orbitals have the right shape so that the interatomic overlaps (and other quantities related to bonding) behave properly with R. This suggests that the EP be chosen so that its eigenfunctions (not just its eigenvalues) are as close as possible to the eigenfunctions obtained with ab initio potentials.

In the self-consistent field approach such as HF (Eqn. 4) or G1 (Eqn. 10), each orbital (singly occupied) is an eigenfunction of a one-electron Hamiltonian which includes the effect of all the other orbitals

(and includes exchange or non-local terms). That is, for each ϕ_i (e.g., χ_v^{MKE}, ϕ_v^{G1}, χ_v^{CHF}),

$$H_i\phi_i = \epsilon_i\phi_i \tag{15a}$$

$$H_i \equiv -\tfrac{1}{2}\nabla^2 + \hat{V}_i \tag{15b}$$

where $\hat{V}_i$ (e.g. $\hat{V}_i^{MKE}$, $\hat{V}_i^{G1}$, $\hat{V}_i^{CHF}$) is a non-local potential operator depending on the other orbitals [22]. Replacing $\hat{V}_i$ by a local operator V(r)

$$V_i(r) = \frac{1}{\phi_i}\hat{V}_i\phi_i = \frac{(\epsilon_i + \frac{1}{2}\nabla^2)\phi_i}{\phi_i} \tag{16}$$

we obtain an effective potential which is equivalent to the non-local potential for that particular orbital. Solving for the eigenfunction of $V_i(r)$ then leads back to the original ϕ_i.

Let us now consider another electronic state of the system. Again, each orbital ϕ_i' is obtained from a one-electron Hamilton

$$H_i'\phi_i' = \epsilon_i'\phi_i' \tag{17a}$$

$$H_i' \equiv -\tfrac{1}{2}\nabla^2 + \hat{V}_i' \tag{17b}$$

for which one could obtain a new effective potential

$$V_i'(r) = \frac{(\epsilon_i' - (-\frac{1}{2}\nabla^2))\phi_i'}{\phi_i'} \tag{18}$$

In general, the V_i' obtained here is not equal to the corresponding V_i of another state for the molecular system. In some cases, however, when V_i for orbital ϕ_i is used in place of V_i' in Eqn. 17a, the new $\phi_i'^{EP}$ and $\epsilon_i'^{EP}$ will be very similar to the original ϕ_i' and ϵ_i' [23].

To understand when this will happen, we need to consider the non-local potential operators $\hat{V}_i$ and $\hat{V}_i'$. Since $\hat{V}_i$ is non-local, it depends on all the other orbitals of the system. We will consider only systems for which the other orbital (i.e., the core orbitals) would not readjust significantly from one state to another and we will take these core orbitals from (say) the ground state. Converting the non-local potentials $\hat{V}_i$ and $\hat{V}_i'$ to local potentials as in (16), we see that the potential depends (through the exchange operator) on the orbital to be solved for the valence orbital. Thus the two localized potentials will be similar, only if the two (valence) orbitals are similar in the core region.

Now the two orbitals cannot have the same description everywhere since they must be orthogonal to each other [24]. But the exchange operator weights only that part of the valence orbital which is near the core, by nature of the integration involving the core orbital. Therefore, as long as the excited state orbital has the same orbital description in the core region as the valence orbital [25], one would expect the local potential for one orbital to be similar to the local potential for the other.

As an example, let us consider the Li atom, with three electrons. In particular, we will consider the Gl representation for which each of the orbitals is uniquely defined. The excited states of the Li atom represent the excitation of the outer or valence electron, while the two inner electrons remain essentially the same as in the ground state. Therefore, the requirement that all the electrons except one be taken as frozen

is satisfied. However, in order to replace the core by an effective potential, we also require that for each excited state the valence orbital has the same description in the region of the core. To see when this is the case, we have plotted in Fig. (2) the valence orbitals for several of the low-lying states of the Li atom. We see that the 2^2P orbital is very different from the 2^2S orbital in the region of the core and thus we would not expect the effective potentials for these two states to be similar. On the other hand, the 3^2S orbital has essentially the same behavior as the 2^2S orbital in the core region [26] (within a scaling factor) as do the higher ^2S orbitals. Thus, for this case, we would expect the effective potentials to be similar. Likewise, all the ^2P states can be represented by the same effective potential, and so on for all the other angular momentum states. Therefore, we expect that the core orbitals can be replaced by an effective potential of the form

$$V_{eff} = \sum_{\ell=0}^{\infty}{}' V_\ell(r) |\ell m\rangle\langle \ell m| . \tag{19}$$

But where there is a different potential for each angular momentum one potential is sufficient for describing the various (bound) excited states of the same angular momentum.

The $V_s(r)$, $V_p(r)$, and $V_d(r)$ from the Li atom (excluding Z_n/r) are shown in Fig. 3. While V_s is quite different from V_p and V_d, we see that V_p and V_d are quite similar. This results from the p and d orbitals having similar character in the core region (zero amplitude at the origin while the s orbital contains core character. The higher angular momentum orbitals should be very similar to the d orbital in the core region, yielding V_ℓ's essentially equivalent to V_d. From such considerations we expect

that for angular momenta ℓ greater than that involved in the core λ ($\lambda = 0$ for Li, $\gamma = 1$ for Na) the V_ℓ should be approximately equal

$$V_\ell \approx V_{\lambda+1} \quad \text{for} \quad \ell > \lambda \quad .$$

In this case (19) becomes

$$V_{eff} = V_{\lambda+1}(r) + \sum_{\ell=0}^{\lambda} \Delta V_\ell(r) |\ell m\rangle\langle \ell m| \tag{20}$$

where $\Delta V_\ell = V_\ell - V_{\lambda+1}$.

In general, to replace cores of atoms containing at most s and p orbitals, one would expect V_s to differ from V_p and both should differ from V_d. However, we would expect that $V_\ell \approx V_d$ for $\ell > 2$ as L would equal 2. For atoms whose cores also contain d orbitals, L would equal 3.

We have so far considered the electron moving in a spherically symmetric potential of the atom, obtaining an effective potential which is valid for the spherically symmetric atomic case. We must now consider whether the potential is still valid for an electron moving in a molecular system. To proceed, we can expand the electronic orbital in terms of the spherical harmonics of the atom and use the potential as defined in (20). However, for the potential to be accurate, the radial part of the orbital for each angular term must have the same character near the core as did the corresponding atomic radial function. For most molecules, this is indeed the case. That is, near the atom the wavefunction can be expressed quite well as a linear combination of the lower lying states of that atom [27].

The effective potential will not be accurate however, when the electron is localized in a small region near the atom (for example, by getting a highly charged ion in close proximity with the atom). The reason is that the local effective potential obtained in (16) represents the actual non-local potential only in a global sense (averaging over the region of the core) not piecewise. Also, the effective potential will not be correct when the cores (which are taken to being frozen) are greatly perturbed. These are not serious problems though, if care is taken when applying effective potentials to molecular systems. In general, therefore, we find that effective potentials defined as in Eqn. 20 can be used in a wide range of molecular wavefunctions yielding results that should be in close agreement with the ab initio results.

IV. Analytic Form of the Effective Potential

In order for effective potentials to be utilized advantageously in SCF calculations, the integrals involving these potentials must be evaluated efficiently. Therefore, the effective potentials must have a simple form, yet have sufficient flexibility to reproduce the effect of the replaced electrons. It was shown in Section III that effective potentials can correctly represent the effect of the core electrons in molecular systems if they

have the form

$$V_{eff} = \sum_{\ell=0}^{\infty} V_\ell(r) |\ell m\rangle \langle \ell m| \qquad (17')$$

where V_ℓ is a function only of r [i.e., V_{eff} is a local potential not depending explicitly (as an integral function) on the core orbitals]. We further showed that for some $\ell = L_{max}$, V_{eff} could be put in the form

$$V_{eff} = V_{L_{max}}(r) + \sum_{\ell=0}^{L_{max}-1} \Delta V_\ell(r) |\ell m\rangle \langle \ell m| \qquad (18')$$

where $\Delta V_\ell = V_\ell - V_{L_{max}}$. We therefore wish to find a simple form for V_{eff} as defined in Eqn. 18.

In evaluating the integrals, we will take the basis function to be Gaussian. The advantage of Gaussians in evaluating the other integrals can also be used in evaluating the effective pctential integrals. As previously mentioned, by judiciously defining the effective potential, the major drawback of Gaussians (i.e., the need for many primitives) has been eliminated.

To understand what form the EP should take, we need to consider what type of integrals must be evaluated. Since the V_ℓ are only a function of r, the angular integration can be carried out directly, yielding the following types of radial equations:

$$\int_0^\infty U(r) r^n e^{-\rho r^2} r^2 \, dr \qquad (19a)$$

$$\int_0^\infty U(r) r^n e^{-\rho r^2} M_\ell(ar) \, r^2 \, dr \qquad (19b)$$

$$\int_0^\infty U(r)\, r^n\, e^{-\rho r^2}\, M_{\ell_1}(ar)\, M_{\ell_2}(br)\, r^2\, dr \tag{19c}$$

where U(r) represents $V_\ell(r)$ or $\Delta V_\ell(r)$ of V_{eff} and the M_ℓ's are modified spherical Bessel functions. To evaluate these integrals, one could integrate the integrals numerically. However, this procedure has been found to be too time consuming, thereby defeating the purpose of using effective potentials. Instead, we evaluate each of the integrals analytically. Therefore, we need to express U(r) as some analytic function such that the integrals in Eqn. 10 can be easily expressed analytically. One sees immediately that if we let

$$U(r) = \sum_k c_k\, r^{n_k}\, e^{-\zeta_k r^2}, \tag{20}$$

then the form of the integral is the same as if the U(r) were not present. That is, the integrals are essentially no more difficult to evaluate than the overlap [$U(r) \equiv 1$] and the nuclear potential [$U(r) \equiv Z/r$] integrals. These integrals can be readily expressed in analytic form [28].

We therefore need to develop a method for expressing the V_ℓ in the form defined by Eqn. 20. We must first establish what shape the potentials will have so that we will know what type of terms to include.

Any function of r can be expressed as in Eqn. 20 given a sufficient number of terms. To make the evaluation of effective potentials efficient, one would hope that only a few terms would be required to express the effective potentials accurately. The requirement of accuracy will be discussed in the Section V when methods of obtaining effective potentials are presented. It will be shown that, indeed, only a few terms are needed.

To see what type of terms these will be, we consider a typical potential. In particular, we will consider the V_s potential of the Li atom. First, we consider the EP obtained from the Gl Li 2^2S orbital (which has essentially the same behavior as the MKE HF orbital).

A plot of this potential, as obtained from Eqn. 14 is shown in Fig. 4a. The long-range nature of this potential is just $-1/r$. That is, an electron at a large distance from the Li nucleus sees an effective nuclear charge Z_{eff} of +1.0. Therefore, one of the terms in Eqn. 20 will have $c_k = -1.0$ with $n_k = -1$ and $\ell_k = 0.0$. Since this term is common to all V_ℓ, we can factor it out and have it replace the old nuclear charge term $-Z_n/r$ ($Z_n = 3.0$ for Li

To determine what other type of terms are required, let us multiply the effective potential by r, generating the negative of what we call the effective charge. Subtracting off the long range effective charge (which ($Z_{eff}(\infty) = 1.0$), we obtain a function which is plotted in Fig. 4b. At the nucleus, the function has the value of $-(Z_n - Z_{eff})$. We will denote this difference between the nuclear charge and the effective nuclear charge as the core charge ($Z_{core} = Z_n - Z_{eff}$).

Z_{core} represents, in general, the number of electrons which we are replacing. We see from Fig. 4b that the function is localized in the region of the core orbitals. It rises smoothly from a value of $-Z_{core}$ at the origin to a maximum around Bohr and then falls of quickly to zero. The positive region of the potential represents the repulsive character of the effective potential, keeping the valence orbital of Li from collapsing into the core.

From Fig. 4b, we see that terms of the type in Eqn. 20 can readily reproduce the behavior of this function. The exponential part allows the function to be localized in the region of the core. It is sufficient to let $n_k = -1$ or 0. The sum of the coefficients with $n_k = -1$ will equal $-Z_{core}$ while the sum of the coefficients with $n_k = 0$ will equal the slope of the function at the origin. To express $\Delta V_\ell(r)$ in the form of Eqn. 20 the Z_{core} behavior of the function is cancelled out so that only terms with $n_k = 0$ are needed.

Let us now consider the new V_s effective potential for the Li atom resulting from the coreless Hartree-Fock orbital (CHF). The V_s can be obtained, for example, by inverting the orbital as in Eqn. 14. This new potential is plotted in Fig. 4c. Since this new orbital has zero amplitude at the origin (and, thus, no core character), the effective potential must approach plus infinity as r^{-2}. (It is the repulsive singularity which prevents the lowest solution of the potential from collapsing into the core.) Thus, we need to include terms in Eqn. 20 with $n_k = -2$. [Note that no singularity exists in the effective potential integral since the r^{-2} factor is cancelled by the r^2 factor of the volume element.]

In conclusion, therefore, we see that in order to express any arbitrary EP in the form given in Eqn. 20 we need consider only terms with $n_k = 0, -1,$ or -2. Methods to determine values of the variables c_k and ζ_k for each term will be discussed next.

V. Methods for Obtaining Effective Potentials

In order to use effective potentials, we need a method for obtaining an analytic form for the EP which correctly represents the effect of the non-local potential due to the core electrons. It was shown that the EP should be of the form given in Eqn. 18 where $V_{L_{max}}$ and V_ℓ are expressed in the general form of Eqn. 20. We therefore need to develop a method for determining the c_k's, n_k's and ζ_k's so that V(r) will correctly represent the appropriate potential.

One method would be to obtain the potential V(r) by inverting the orbital, as defined in Eqn. 14. One can then "least squares" fit the potential to the form given in Eqn. 20, optimizing the exponents and the coefficients. By adding a sufficient number of terms, one can obtain a fit to whatever degree of accuracy is desired.

While this approach is straightforward, several problems arise. For instance, how accurate does the fit need to be (that is, how many terms are needed)? This problem is made more complex when one realizes that the orbital used in the inversion (see Eqn. 14) is not exact but usually is an approximation expressed in some basis set. Therefore, the potential to which we would fit is itself only an approximation. Furthermore, the potential for one state of the system (e.g. Li $2\,^2S$) is only an approximation for another state of the system (e.g., Li $3\,^2S$).

Additional problems can arise in this method due to the nature of the orbital used in Eqn. 14. The orbital must be nodeless to prevent singularities from arising in the potential (other than at the origin). Also, effective potentials can only be obtained for those systems which support a bound state so that an orbital exists which can be inverted. Thus, for example, one could not obtain a complete EP to replace the F atom since F^- ^3S, $^{1,3}P$, etc. states do not exist.

To circumvent these problems, a new method has been developed for obtaining effective potentials. The result is to obtain V_{eff} directly from what is known about the ab initio non-local potential operator to be replaced.

In general, the orbital which is used in Eqn. 14 has been obtained from diagonalization of a one-electron Hamiltonian defined over a set of basis functions. That is, our knowledge of the non-local potential is contained in a set of matrix elements of the potential defined over a given basis set. In order to define the effective potential, one may require that the local potential as given in Eqn. 20 reproduce the same matrix elements as those obtained from the original non-local potential. That is, we define V_{eff} such that

$$\langle i | V_{eff} | j \rangle = \langle i | \hat{V} | j \rangle . \tag{21}$$

However, since a local operator is not equivalent to a non-local operator, (21) cannot be an identity for all i and j. Thus, (21) must be satisfied in a least-squares sense. We choose the c_k's, n_k's, and ζ's of Eqn. 20 to minimize the quantity

$$I = \sum_{i,j} w_{ij} \left(\langle \chi_i | V_{eff} | \chi_j \rangle - \langle \chi_i | \hat{V} | \chi_j \rangle \right)^2 \qquad (22)$$

where the $\langle \chi_i | \hat{V} | \chi_j \rangle$'s are matrix elements of the non-local potential and w_{ij} is a weighting factor for each matrix element.

We see from this formulation that it is not necessary to evaluate $V_{eff}(r)$ as a function of r (as is implied from Eqn. 14). Indeed, the non-local potential itself does not exist pointwise as a function of r. To fit the potential to the form given by Eqn. 14 is to assume more knowledge of the potential than in fact exists. Inversion of the orbital (Eqn. 14) can lead to oscillations in the potential which are not meaningful and, in particular, lead to the wrong limit of the potential at large r [29]. The meaningful quantity for the EP is its integrated value, weighted by the appropriate basis function. Therefore, we define the EP directly by Eqn. 21.

By defining the effective potential as in (21) then any new electronic orbital we obtain from an EP calculation will correctly see the effect of the core electrons as long as the orbital is expressed in the same basis set as that used in fitting the matrix elements.

The picture presented so far is an ideal one which will not, in general, be obeyed in practice. The new orbitals cannot always be expressed in the original basis set, and even if they could, not all the matrix elements can be fit exactly (since a non-local operator is not equivalent to a local operator). However, we have the freedom to choose those basis functions and therefore those matrix elements [by a judicious choice of w_{ij} in (22)] which will be most important in describing the new orbitals. Therefore, we can at least make those matrix elements agree. The extent to which we can reproduce the non-local matrix elements by the EP matrix elements will provide a test of confidence which we can apply to any calculations we would carry out based on that EP.

Fortunately, for most cases, this is not a serious problem, and the effective potential idea works very well. The reason is due to the difference in the spatial extent of the core orbitals which are replaced and the valence orbitals. In general, basis functions used to describe the valence-like orbitals are much more diffuse than the basis functions used to describe the core. *Therefore, if we define our effective potential* [using (21)] in terms of matrix elements representing valence-like basis functions, we will, in fact, obtain a useful and meaningful effective potential.

A method which makes direct use of this point is to choose the χ_j to be the valence orbital for some molecular system containing the frozen core. That is, we define V_{eff} to be

$$\langle \chi_i | V_{eff} | \phi_v \rangle \simeq \langle \chi_i | \hat{V} | \phi_v \rangle \tag{23a}$$

$$\simeq \langle \chi_i | E_v - T | \phi_v \rangle \tag{23b}$$

where the χ_i are chosen to span the space of the valence orbital An immediate connection is seen between Eqn. 23 and Eqn. 14. However, since the inverse of ϕ_v is not required, it is permissible for ϕ_v to have nodes in it. Also, we can include other valence orbitals in Eqn. 23 permitting one to obtain the best EP which will satisfy both Eqn. 14 and Eqn. 16. For systems which do not have bound states, one can still use Eqn. 21 defined over basis functions.

VI. The Resulting Effective Potentials for Various Systems

In this section, we present examples of ab initio effective potentials which have been obtained for various systems. The potentials were obtained using methods described in the previous section.

VI-A. Alkali Atoms

The alkali atoms (Li, Na, K, etc.) contain a single valence electron with a completely filled inner core of electrons (isoelectronic with the rare gases). The excited states of the atom represent a one-electron excitation of the valence orbital while the core orbitals remain essentially frozen. Therefore, the alkali atoms represent the ideal system for using effective potentials.

We present here results for two different effective potentials for

the alkali atoms: (1) the EP obtained from the minimum kinetic energy Hartree-Fock orbital (MKE) [or from the nearly equivalent Gl orbital (GAEP)] and (2) the EP obtained from the newly defined coreless Hartree-Fock orbital (CHF). Plots of these various orbitals for Li, Na, and K are shown in Fig. 5 and compared with the HF orbitals.

We see that the amplitude outside the core is essentially the same for the HF, MKE, and CHF orbitals. However, the HF orbital has large oscillations and significant amplitude in the core region. Likewise, the MKE orbital, though it is flat in the core region, still has wiggles in it and, for the s orbital, has a cusp at the origin. Therefore, both of these type orbitals require tight basis functions. On the other hand, the coreless HF orbital (CHF) is smooth, having no wiggles in it.

To evaluate the EP's, Eqn. (23) was used, ϕ_v representing the MKE or CHF orbital. The basis functions χ_i were taken to be the same basis functions that were used to express ϕ_v. Since the matrix elements for the most diffuse basis functions represent integration over the entire potential [30], we desire that these matrix elements be very accurate. Therefore, a weighting of the matrix elements proportional to the inverse of the orbital exponent was used. Since calculations using the CHF-EP will not use any tight core-like function, it is not necessary to use matrix elements from tight basis functions in the fit.

The resulting EP's are smoothly varying functions. Therefore, very few terms are needed to express the potential. It turns out that the EP's obtained from the fit do not, in general, possess the behavior near the origin that would be expected from inversion of the orbital (e.g.,

$-Z_N/r$ for the MKE orbital) since the orbital itself is not sufficiently accurate. However, this behavior near the origin is not important, since integration over the EP to obtain the matrix elements cancels out any errors.

After performing the least-squares fit of the matrix elements, we obtain effective potentials for the various atoms. The effective charges representing these potentials are shown in Fig. 6. [The actual function plotted is $-(Z_{eff}(r) - Z_{eff}(\infty))$ where $V_{eff} - Z_{eff}/r$]. The expansion terms for each of the EP's are given in Table II.

In general, we see that if the valence orbital has the same symmetry as one of the core orbitals, then the EP contains some repulsive character in the core region to prevent the valence orbital from collapsing into the core. For the CHF orbitals, the repulsive character is represented by the singularity at the origin. The MKE-EP's, on the other hand, are proportional to $-A/r$ $(A > 0)$ near the origin [31].

Using these EP's, we have determined a set of optimized (Gaussian) basis functions for each atom. We will devote our attention to CHF orbitals which were formulated in order to reduce the size of the basis set. The basis sets were chosen to provide an accuracy in the energy to within 10^{-4} Hartree ($\sim 3 \times 10^{-3}$ eV or $\sim 6 \times 10^{-2}$ Kcal). The resulting basis sets are given in Table III.

As one can see, the larger the atom, the fewer number of basis functions are needed. This is in direct contrast with the orthogonal HF orbitals for which the number of basis functions grow very quickly with the size of the atom.

Thus, the CHF effective potential provides a significant reduction in computation of the integrals while still providing ab initio quality.

VI-B. The Hydrogen Negative Ion

We next consider a quite different type of electronic system for which one can obtain an effective potential. This type of system contains a core which is not filled, though the orbitals can be taken as frozen. Such systems would include the halide ions. As an example, we consider the hydrogen negative ion.

When the hydrogen atom combines with other atoms to form molecules, one of the orbitals remains essentially a hydrogenic 1s orbital about the proton [32]. Therefore, one would expect that an effective potential could be used to replace this orbital. Since another electron can couple with the 1s electron to form a singlet or a triplet, two different effective potentials are needed. Expressing the EP in the form (18), we can, to a good approximation, take L_{max} equal to 1 since the core is only of S symmetry.

To obtain each of the V_ℓ's, we cannot use Eqn. 5, because only the ^1S valence orbital exists. No bound states for the ^3S, ^1P, and ^3P states exist. However, using the method of fitting matrix elements, one can use Eqn. 21 to obtain an effective potential which correctly represents

the non-local potential.

In obtaining the matrix fit, we give greater weight to the more diffuse basis functions (e. g. using a weight proportional to the inverse of the sum of the orbital exponents) since the more diffuse basis functions will be most important in describing an electron in the region of a hydrogen atom. In particular, we can transform the basis functions so that they represent eigenfunctions of the Hamiltonian (Eqn. 13a) as was done to obtain Eqn. 23a, and then weight only the lowest eigenfunctions.

We first consider the EP for H^- ^3S. For the ^3S state, the valence orbital can contain an arbitrary amount of 1s core character, since the two electrons are tripletly coupled. Therefore, we can define a MKE orbital or a CHF orbital, as well as the HF orbital, and obtain an effective potential for each of these potentials. The orbitals are shown in Fig. 7.

We first look at the effective potential obtained from the HF orbital. If we obtain the effective potential by inverting the orbital, we obtain a discontinuous singularity in the potential due to the node in the orbital [33]. Using the matrix element fitting method, however, we can obtain a different effective potential which has no singularities. The procedure is to transform the basis functions of Eqn. (21) to a space orthogonal to that of the H 1s orbital. That is, we work in the Hilbert space for which the pseudopotential (or the generalized Phillip-Kleinman potential) is zero. The resulting H^- ^3S EP (which is denoted HF-EP) is plotted in Fig. 7. This EP can be used in molecular calculations as long as the basis functions are taken to be orthogonal to the H 1s orbital.

It is inconveneint and time consuming, however, to require the basis functions to be orthogonal to a given space. We would prefer to include a repulsive term in the EP which represents the localization of the generalized Phillip-Kleinman potential. This leads us to either the MKE-EP or the CHF-EP. These potentials are also plotted in Fig. 7. We see that both these potentials contain a repulsive region which replaces the orthogonality constraint of the HF-EP.

In using these different potentials, we find that the MKE-EP can, in certain instances, lead to erroneous results. To see why this error occurs, we must understand what happens to the core solution in the effective potential framework. For the HF-EP, the core solution is projected away and no longer exists. For the MKE-EP and CHF-EP, the core solution exists but, due to the repulsive term in the potential, the energy for this orbital has been shifted above the energy of the valence orbital [34] (in general, the orbital energy becomes unbound).

When we carry out a molecular calculation, the new orbital may be expressed in terms of the energy states of the atomic effective potential. The degree of mixing of the states can be estimated from simple perturbation theory. For the CHF-EP, the core orbital's energy is raised essentially to infinity, so no mixing will occur between the EP orbital and the core orbital. For the MKE-EP, however, the core orbital's energy is raised just into the continuum. This presents little difficulty for the alkali atoms because there are still an infinite number of bound states lower than this core solution. For the H^- ^3S state, however, the 2s valence

orbital is itself unbound and lies very near in energy to the/core orbital energy shifted leading to strong mixing possibilities. The problem results from the fact that the local effective/ potential as mentioned in Sectior V, does not have meaning point wise, but rather, only after integration. The repulsive term in the EP will be correct only if it acts on basis functions which are more diffuse than the core. In general, this is satisfied even for H^- since the hydrogen will not attract another electron which is tripletly coupled. However, if we localize the electron in a small region of the potential (i. e. by putting a positive charge in close proximity to the H atom), then the entire EP is not sampled and the EP approximation breaks down. Therefore, the MKE-EP for H^- ^3S can lead to erroneous results.

We next consider the EP for H^- ^1S. The outer orbital is obtained using the GI method [35]. Since the outer orbital is unique and nodeless the orbital can be inverted to obtain an EP. This potential is shown in Fig. 8 [36]. On the other hand, one can use the matrix element fit to obtain a similar effective potential. This potential is also shown in Fig. 8. Both potentials reproduce the same valence orbital, indicating that information in obtaining effective potentials is limited by the finite basis sets.

The effective potentials for H^- ^1P and H^- ^3P are considered next. The EP's are obtained straightforwardly by the matrix element fitting method and are plotted in Fig. 9. Since the p orbitals are orthogonal to the core by symmetry, the singlet and triplet EP's represent $\hat{J} + \hat{K}$ and $\hat{J} - \hat{K}$, respectively, where $\hat{J}$ is the coulomb operator and $\hat{K}$ is the exchange

operator. By taking the sum and differences, we can therefore obtain a local representation for the exchange operator $\hat{K}$ (which is purely non-local) as well as for the local coulomb operator $\hat{J}$.

VI-C. The EP for the Fe Core

Proceeding as in the case for alkali atoms, one can obtain effective potentials to replace the filled core orbitals of other atoms. One treats the frozen core of the atom plus an electron (which is isoelectronic with the alkali atoms) in the same manner as was discussed for the alkali atoms. This method is straightforward and can provide effective potentials for the atom in close agreement with the ab initio results. The effective potential approximation, however, is not quite as accurate as was the case for the alkali atoms. To understand what difficulties begin to arise, we present an example from the transition metals, in particular, the Fe atom.

As mentioned in the previous section, the effective potential method works best when the valence orbital is much more diffuse than the core (that is, the valence orbital occupies a different Hilbert space). Now the Argon-like core of Fe contains no 3d orbitals, even though it contains 3s and 3p orbitals. Therefore, the Argon-like core is, in a sense, not filled. For K, this presents no difficulty because the 3d is much more diffuse than the core. Its orbital energy is above that of the Rydberg K 5s orbital. For Fe^{+7}, however, the 3d orbital is quite contracted, becoming very similar to the iron core in radial extent. Its orbital energy has dropped down below the valence 4s orbital. Therefore, the iron 3d orbitals are not separated from, but rather, have become a part of the iron core which is unfilled. Strong electron correlation exists between the 3p, 3s, and 3p orbitals and the 3d orbitals.

The difficulty does not prevent us from obtaining an effective potential for the Fe atom, but certain precautions must be taken. The Fe^{+8} core can still be taken as frozen and we can fit the matrix elements to obtain an effective potential. We find, however, that we cannot simultaneously fit the matrix elements for the valence-like basis functions and the Rydberg basis functions. For studying binding of Fe to other molecules we wish to obtain an effective potential which can be used to describe the valence orbitals of Fe and not the Rydberg orbitals. We choose the appropriate weighting factors in Eqn. 23. This allows us to obtain a valid effective potential for the iron atom which will correctly describe the 4s- 4p- and 3d-like orbitals of the Fe in a molecular system [37]. This effective potential for Fe is shown in Fig. 10.

For other transition elements, similar precautions must be used. Once the 3d shell is filled (as for Cu, Zn, Ga, ...)[38], one can consider these orbitals as part of the frozen core. In this case, one can proceed in the usual manner as for the alkali atoms (Sec. VI-A).

VI-D. Effective Potentials That Fit Experimental Data

The effective potential method has been developed in an effort to provide results which will agree with full electron ab initio calculations [39]. The basic approximation was only that the core orbitals remain frozen. There are times, however, when the ab initio calculations are not sufficiently accurate. The error results from the neglect of instantaneous electron correlation between the core orbitals and the valence

orbitals. Correcting this error in full electron calculations is exceedingly expensive, requiring the introduction of configuration interactions. However, when we introduce instantaneous electron correlation, we can no longer discuss an "independent particle interpretation." That is, no orbital exists from which one can obtain a unique effective potential. In addition, the electron correlation differs greatly, for different states, yielding different effective "cores."

On the other hand, effective potentials can be modified to include, to some extent, the average effect of electron correlation without introducing extra work. We can add arbitrary terms which can help bring the ab initio calculations into closer agreement with experiment. Considering the K atom as an example, we find that the error in the ionization energy due to electron correlation depends upon which eigenstate is considered (see Table III). The larger the interaction of the valence electron with the core, the larger is the error in the ionization energy. In general, we need a modified effective potential which is more attractive. Since the electron correlation takes place in the core region, we add to the ab initio effective potential an attractive term which extends over the core region. The coefficient is determined by matching the orbital energy to the experimental ionization energy. The exact form of this additional term is not important (as long as it is small) since only the integrated average is important.

In carrying out this process, we find that only one eigenvalue of a given symmetry can be matched with experiment. The difficulty arises because each orbital of a given symmetry has the same shape in the core region, even though the electron correlation is different for each state.

Since we are usually interested in the lowest state of each symmetry, it is a good approximation to match the lowest eigenvalues of each symmetry.

Another method for obtaining local effective potentials involves the direct fitting of some arbitrary analytic form of a potential to the experimental energies of the atomic spectra [3].

However, very little information is available since only the lowest (valence) state, representing one data point, samples the core region appreciably. The core character of the excited (Rydberg) state corresponds to the valence orbital which has been mixed in for orthogonality purposes. Thus, the higher lying energy states are already determined essentially from the strength (i.e., integrated value) of the effective potential. [For this reason, it has not mattered much what form has been chosen for the empirical (or model) potential, as long as the quantity $(Z_{eff}(r) - Z_{eff}(\infty)$ is limited to the core region. The averaged effective charge of the core appears as a parameter in the Rydberg series formula for the excited state energies.]

Since the empirical potentials are arbitrary in shape, the resulting empirical orbitals will not be equivalent to the ab initio orbitals, even within the general space defined by Eqn. (9). This can lead to possibly serious errors in multielectron effective potential calculations, where the two-electron energy depends on the shape of the valence orbitals. Also, the empirical potential can lead to an additional low lying corelike solution to the EP calculation (since the valence orbital is not necessarily nodeless) [3b]. This lower lying solution must be ignored, yet basis functions must be included to describe this state.

VII Conclusion

The purpose of effective potentials has been to simplify the computational efforts required in large polyatomic molecular calculations. Toward this end we have developed the ab initio effective potential method to provide reliable yet computationally efficient results. We define a new type of effective potential (CHF EP) derived from the newly defined coreless Hartree-Fock orbital (CHF). Since the CHF orbital does not contain any core character, no tight basis functions are necessary in the calculations. To further simplify the computational efforts, we express the effective potential in an analytic form which permits rapid evaluation of the potential integrals over Gaussian basis functions. To ensure a reliability in the EP calculations, we derive the local EP directly from the matrix elements of the actual ab initio non-local potential defined over a given set of basis functions. The extent of the fit between the EP elements and the non-local potential matrix elements provides a test of the reliability we can expect from the use of similar EP matrix elements in molecular calculations. Furthermore, by using the matrix fit method for defining EP's, we can obtain EP's for systems which have no bound states (e.g. Cl^-, ^3S, $^{1,3}P$). In fact, using the matrix fit, we can obtain EP's representing the potential an electron sees due to a molecular system, such as a CO ligand in a metal complex. The essential requirement is that the electronic molecular core (being replaced) can be taken as frozen.

Thus, using the methods developed in this paper, one should be able to use the effective potential method as a reliable tool for calculations of large molecular systems.

REFERENCES

[1] H. Hellmann, J. Chem. Phys. 3 (1935) 61.

[2] P. Gombás, Z. Physik 94 (1935) 473.

[3] See, for example, (a) I. V. Abarenkov and V. Heine, Phil. Mag. 12 (1965) 529; (b) A. Dalgarno, C. Bottcher, and G. A. Victor, Chem. Phys. Lett. 7 (1970) 265; (c) Gary Simons, J. Chem. Phys. 55 (1971) 756.

[4] J. C. Phillips and L. Kleinman, Phys. Rev. 116 (1959) 287.

[5] J. D. Weeks, A. Hazi, and S. A. Rice, Adv. Chem. Phys. 16 (1969) 283.

[6] L. Szasz and G. McGinn, J. Chem. Phys. 47 (1967) 3495.

[7] W. A. Goddard, Phys. Rev. 174 (1968) 659.

[8] L. R. Kahn and W. A. Goddard III, Chem. Phys. Lett. 2 (1968) 667.

[9] L. R. Kahn and W. A. Goddard III, J. Ch. Phys. 56 (1972) 2685.

[10] C. F. Melius, W. A. Goddard III, and L. R. Kahn, J. Chem. Phys. 56 (1972) 3342.

[11] When we discuss electrons, we are referring to the orbitals as obtained from an independent particle type wavefunction, such as obtained from the Hartree-Fock (HF) or Generalized Valence Bond (GVB) method (See Ref. 14). Each electron is described by an orbital which represents the state of an electron moving in the average field due to the other electrons. Since electrons are indistinguishable, it is actually the orbitals which are distinguished.

[12] J. D. Weeks and S. A. Rice, J. Chem. Phys. 49 (1968) 2741.

[13] W. A. Goddard III, Phys. Rev. 157 (1967) 81.

[14] W. A. Goddard III and R. C. Ladner, J. Am. Chem. Soc. 93, (1971) 6750.

[15] G. T. Surratt and W. A. Goddard III, unpublished results. (See G. T. Surratt, Masters Thesis, Caltech, August 1970.

[16] H. Harrison, Pseudopotentials in the Theory of Solids, W. A. Benjamin, Inc., New York, 1966.

[17] P. M. O'Keefe and W. A. Goddard III, Phys. Rev. 180 (1969) 747; Phys. Rev. Lett. 23 (1969) 300; W. A. Goddard III and P. M. O'Keefe, in Computational Methods in Bond Theory, p. 542 (P. M. Marcus, J. F. Jonok, and A. R. Williams, editors) (Plenum Press, New York, 1971).

[18] P. J. Hay, W. A. Goddard III, and T. H Dunning, unpublished results. The cores are replaced by adding the matrix elements $\langle \mu | 2J_{core} - K_{core} | \nu \rangle$ to the one-electron potential energy terms, $\langle \mu | \sum_a' (-Z_a/r_a) | \nu \rangle$.

[19] One should note that the new orbital is not equivalent to a Slater orbital since it is restricted to be a linear combination of the HF valence orbital and its core orbitals as in (9).

[20] The basis set used for the HF orbital of K is from A. J. H. Wachters, J. Chem. Phys. 52 (1969) 1033. The four tightest functions are not really necessary unless a good cusp description is required.

[21] That is, substituting the EP wavefunction into the ab initio calculations, we would expect the EP result to be close to the SCF result.

[22] In addition to the exchange operator, $\hat{V}_i$ also contains projection operators which depend on the overlap of the valence orbital with the core.

[23] If ϕ_i' represents an excited state of the system, then we require that $\phi_i'^{EP}$ be restricted to the space orthogonal to ϕ_i. For HF orbitals, special care must be taken. The orbitals ϕ_i and ϕ_i' are not unique (Eqn. 9). Therefore, the V_i and V_i' of Eqn. (14) and Eqn. 16 are not uniquely defined since they are also replacing the ion-local projection operators which project away the arbitrary amount of core character. However, by requiring ϕ_i' to be orthogonal to ϕ_i, then we can directly compare $\phi_i'^{EP}$ and ϕ_i.

[24] This orthogonality is not a part of the potential but rather represents a separate operator.

[25] The orbitals may differ by a normalization factor, since the Hamiltonian equation is homogeneous in ϕ_i.

[26] This should be expected since the 3'S state must mix in 2'S character in order to be orthogonal to the 2'S state.

[27] See, for example, C. F. Melius and W. A. Goddard, J. Chem. Phys. 56 (1972) 3348.

[28] The resulting integrals (Eqn. 19) can be expressed in terms of exponentials, error functions ($\int_0^x e^{-\sigma^2} d\sigma$) and Dawson's integral [$(e^{-x^2} \int_0 e^{\sigma^2} d\sigma)$]. See (a) C. F. Melius, Ph. D. Thesis, California Institute of Technology, and (b) C. F. Melius and W. A. Goddard (to be published).

[29] One can check for consistency in the potential by examining the changes in the potential due to changes in the basis set describing the orbital.

[30] The $-z(\infty)/r = -1/r$ term has been removed before fitting the matrix elements.

[31] The constant A obtained from the fit is not necessarily equal to Z_{NUC}. However, one can constrain A to be equal to Z_{NUC} during the fit.

[32] See, for example, Ref. 27 or R.J. Blint and W.A. Goddard, Ch. Phys. Lett.

[33] See, for example, the discussion of the effective potential for the Li 2 ^{2}S HF orbital in Ref. 9.

[34] In the Phillips-Kleinman formalism, the core orbital is taken to have the same energy as the valence orbital. However, when the potential becomes localized, this is no longer the case.

[35] W.A. Goddard, Phys. Rev. 172, 7 (1968).

[36] This potential differs somewhat from the potential obtained in Ref. 35 because of the different basis set used.

[37] The resulting Fe potential will correctly replace the HF core but will not include electron correlation with the core.

[38] The potential for Cu would not be appropriate if excitation of the 3d shell is important. Similarly the EP method is not appropriate for any other system where core excitation is important.

[39] By ab initio, we mean any method which treats the core electrons as an independent particle type wavefunction but allows electron correlation to be included between valence electrons.

Table I

Orbital Exponents (ζ_i) and Coefficients (C_i) to Describe the K4s HF and CHF Orbitals in a Gaussian Basis Set

HF[a]		CHF	
ζ_i	C_i	ζ_i	C_i
150591.	- .00001		
22629.6	-0.00004		
5223.16	-0.00019		
1498.06	-0.00076		
495.165	-0.00253		
180.792	-0.00681		
71.1940	-0.01337		
29.3723	-0.01081		
8.68863	0.05066		
3.46382	0.09076		
.811307	-0.14349		
.312555	-0.30129	.270275	-.21571
.035668	0.70102	.040528	+.59488
.016517	0.40765	.018283	+.51810

a) A.J.H. Wachters, J. Ch. Phys. 52, 1033, (1969).

Table II

Expansion Terms for the CHF Effective Potentials[a,b]

Potential	c_i	n_i	ζ_i
Li V_{S-D}	2.5378	-2	1.9088
	1.1097	0	.9470
	0.3527	0	.4905
	0.00894	0	.09825
Li V_{P-D}	-0.1261	0	1.0147
	-0.1901	0	13.1143
	-0.2393	0	3.0810
Li V_D	-1.0	-1	0.0
	0.4296	-1	11.0026
	-0.2426	-1	1.5083
	2.0262	0	4.3868
	2.5342	0	1.7530
	-0.03384	0	.7159
Na V_{S-D}	5.8539	-2	1.3940
	29.4418	0	28.4200
	1.5541	0	.6105
	.00667	0	.0762
Na V_{P-D}	51.5653	-2	3.9264
	-46.9069	-2	1.7704
	87.5679	0	2.8630
	16.1439	0	1.5166
	3.5816	0	.3031
Na V_D	-1.0	-1	0.0
	11.0039	-1	12.2245
	-11.0951	-1	1.3859
	9.3093	0	4.2010
	10.2369	0	1.7972
	-0.0220	0	.2280
K V_{S-D}	8.2055	-2	.3538
	0.5086	-2	.0846
	-0.7927	0	1.0910
K V_{P-D}	6.8315	-2	.4676
	0.2874	0	.1496
	1.1498	0	.4673
K V_D	-1.0	-1	0.0
	-4.4701	-1	.6990
	-0.2924	-1	.2042
	-0.1675	-2	.3325

[a] $V_\ell = \Sigma\, c_i\, r^{n_i} \exp[-\zeta_i r^2]$ [b] $V_S = V_{S-D} + V_D$; $V_{P-D} + V_D$.

Table III

Gaussian Basis Sets for CHF Orbitals

Orbital	Exponent ζ_i	Coefficient c_i	ΔE[a]
Li 2s	2.89379	-0.01833	.00004
	.61815	-0.10355	
	.07385	0.56443	
	.02817	0.51544	
Li 2p[b]	2.697	0.01105	.00002
	.535	0.05975	
	.147	0.23126	
	.0528	0.50862	
	.02014	0.36686	
Li 3d[b]	.07569	0.11767	.00006
	.02260	0.49639	
	.00830	0.52600	
Na 3s	1.22999	-0.03546	.00002
	.45196	-0.11338	
	.05780	0.67383	
	.02191	0.41526	
Na 3p	1.24376	-0.00772	.00003
	.10841	0.11749	
	.04619	0.47586	
	.01769	0.50738	
Na 3d[b]	.07677	0.10844	.00007
	.02245	0.51879	
	.00825	0.52922	
K 4s	.27028	-0.21571	.00005
	.04053	0.59488	
	.01828	0.51810	
K 4p	.44296	-0.02645	.00004
	.03888	0.50049	
	.01439	0.57413	
K 3d[b]	.10366	.10643	.00017
	.02485	.52483	
	.00849	.54588	

[a] ΔE equals the difference between the orbital energy for the given basis set and the orbital energy for an infinite basis set.

[b] The Li 2p, Li 3d, Na 3d, and K 3d HF orbitals are unique.

Fig. 1. A comparison of the HF, MKE and CHF orbitals of K 4s.

Fig. 2. A plot of the various G1 orbital wavefunctions for the valence electron of Li atom.

Fig. 3. The U_s, U_p, and U_d local potentials for Li atom using G1 orbitals.

Fig. 4. A plot of (a) the MKE Vs effective potential and (b) the resulting effective charge Z_{eff}^{MKE} ($Z_{eff} = r\,V_s$) for Li atom and (c) the corresponding Z_{eff}^{CHF} for the CHF V_s local potential of Li.

Fig. 5. The various HF, MKE, and CHF orbitals of Li, Na, and K (since Li 2p contains no p core orbitals, it is unique).

Fig. 6. The various effective potentials for (a) Li, (b) Na, and (c) K. The actual quantities plotted are $Z_{eff}(r) - Z_{eff}(\infty) = r\,V_\ell - 1.0$.

Fig. 7. The HF, MKE, and CHF effective potentials for the H^- ^3S system [the actual quantities plotted are $Z_{eff}(r)$ ($Z_{eff}(\infty) = 0$)].

Fig. 8. The effective charges for the H^- ^1S system obtained from inverting the orbital (Z_{eff}^{I}) and from the matrix fit method (Z_{eff}^{M}).

Fig. 9. The effective charges for the H^- ^1P and the H^- ^3P systems.

Fig. 10. The effective potentials which replace the Fe^{+8} core. [actual quantities plotted are $Z_{eff}(r) - Z_{eff}(\infty)$].

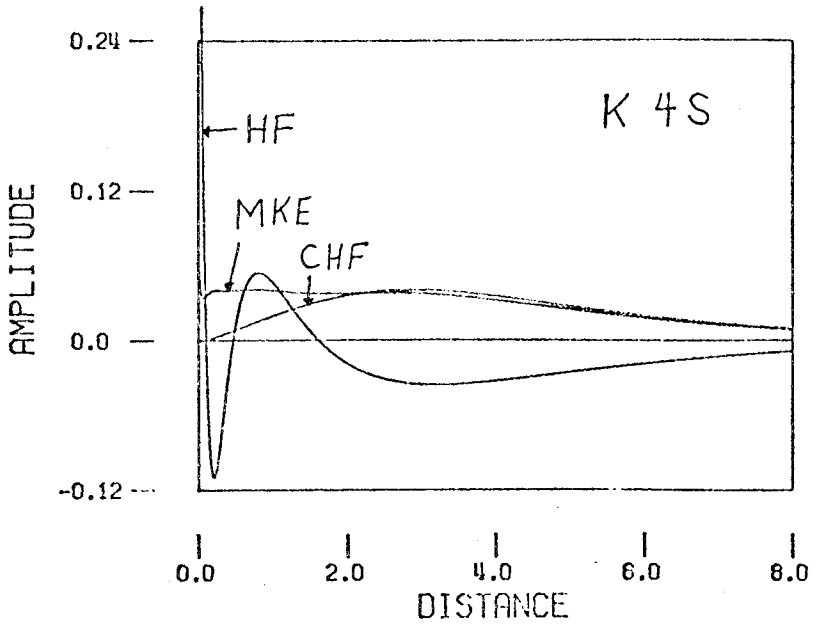

Fig. 1

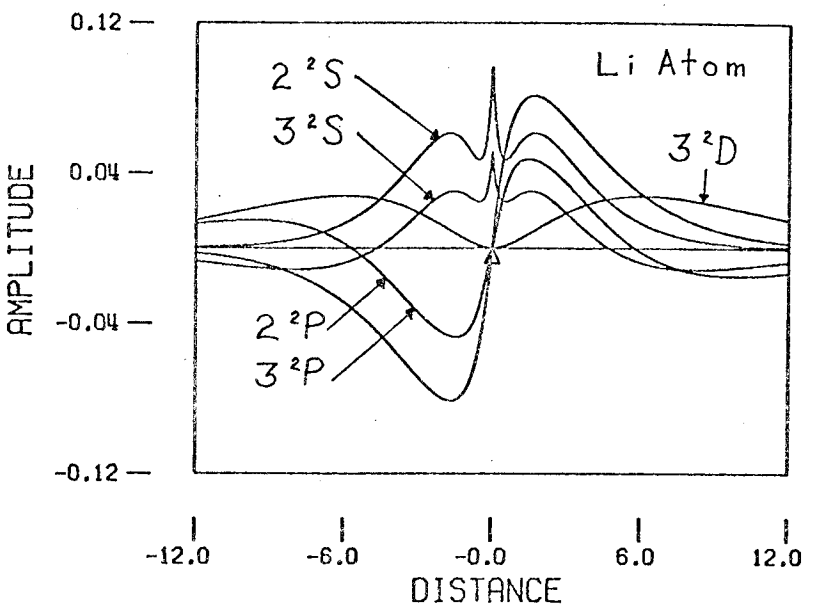

Fig. 2

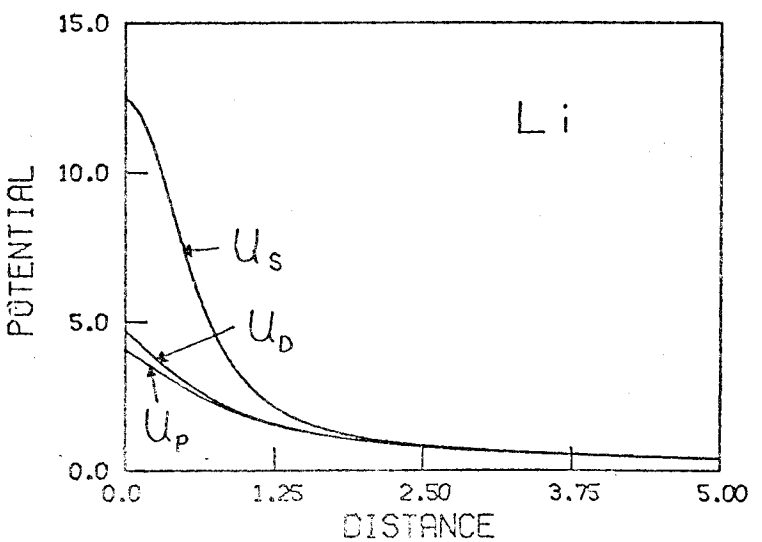

Fig. 3

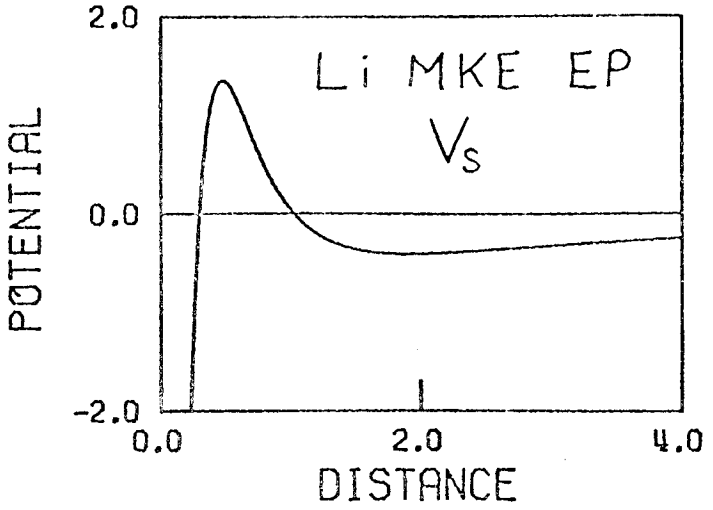
Li MKE EP
V_S
POTENTIAL
2.0
0.0
-2.0
0.0
2.0
4.0
DISTANCE

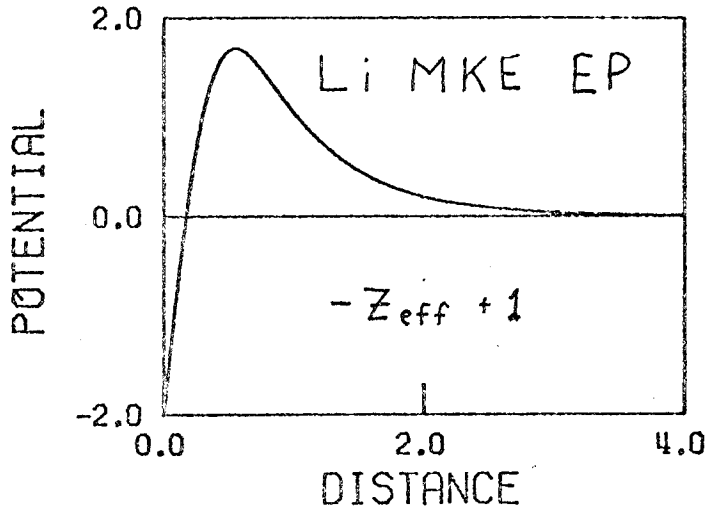
Li MKE EP
$-Z_{eff}+1$
POTENTIAL
2.0
0.0
-2.0
0.0
2.0
4.0
DISTANCE

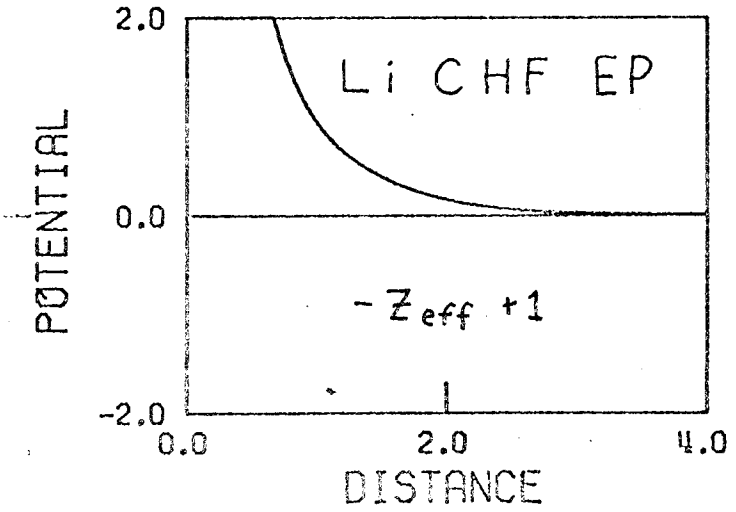
Li CHF EP
$-Z_{eff}+1$
POTENTIAL
2.0
0.0
-2.0
0.0
2.0
4.0
DISTANCE

Fig. 4

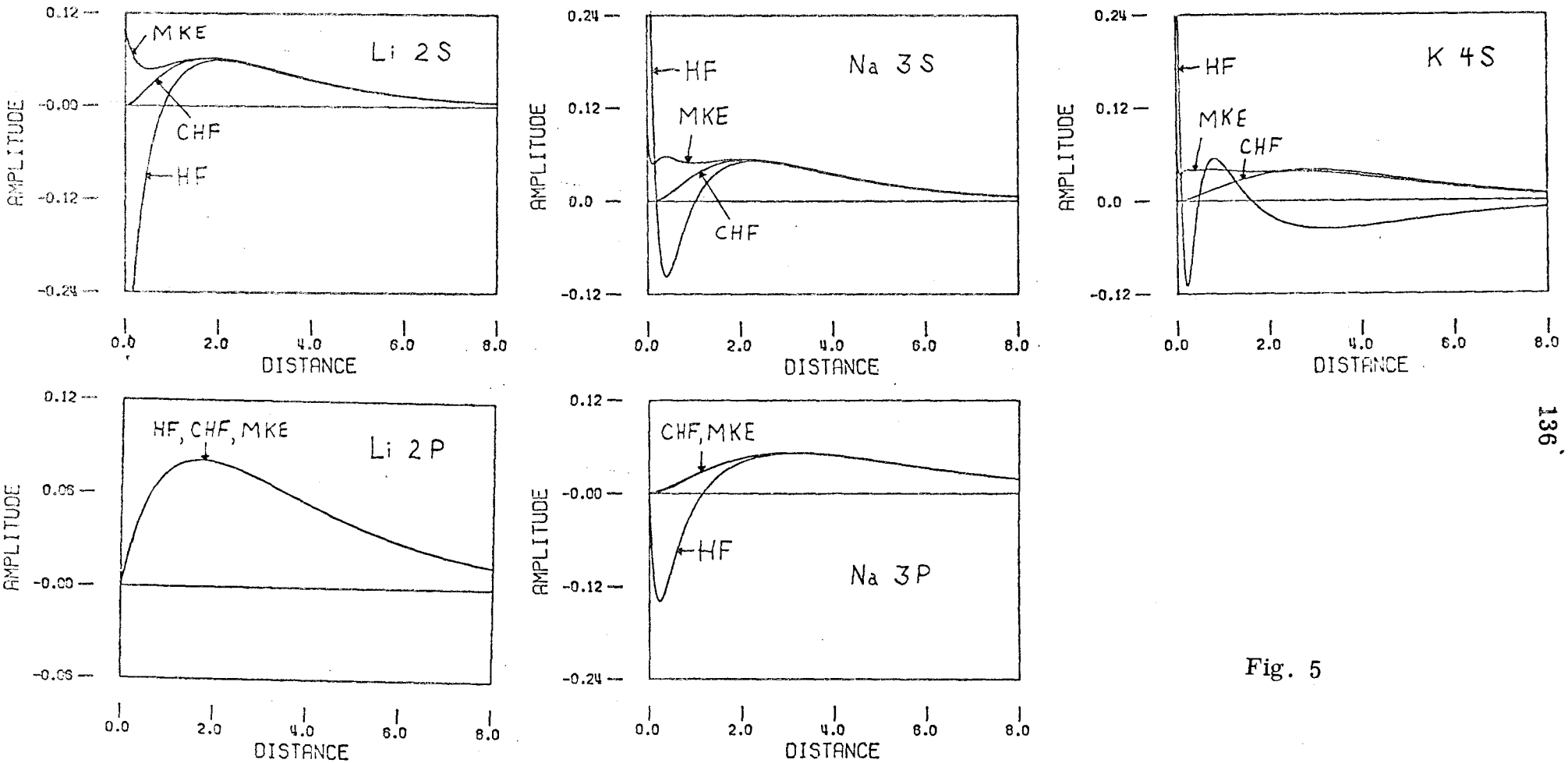
Li 2S
MKE
CHF
HF
Na 3S
HF
MKE
CHF
K 4S
HF
MKE
CHF
Li 2P
HF, CHF, MKE
Na 3P
CHF, MKE
HF
AMPLITUDE
DISTANCE
0.0
2.0
4.0
6.0
8.0

Fig. 5

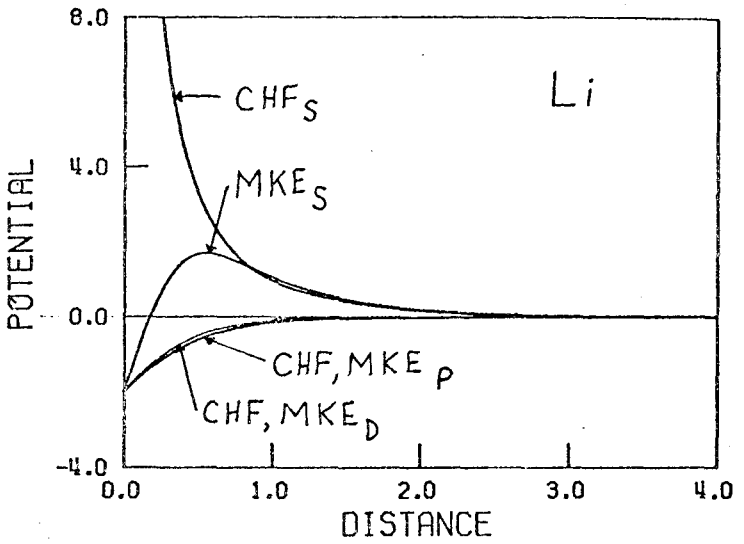
8.0
4.0
0.0
-4.0
POTENTIAL
CHF$_S$
Li
MKE$_S$
CHF, MKE$_P$
CHF, MKE$_D$
0.0
1.0
2.0
3.0
4.0
DISTANCE

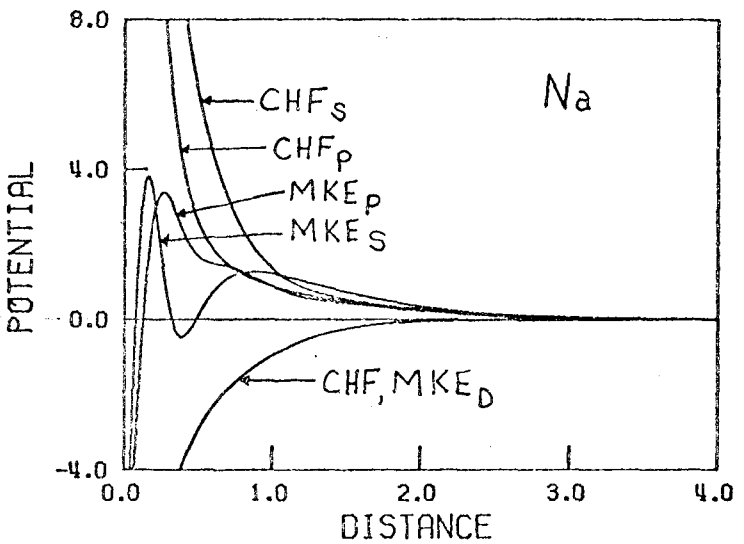
8.0
4.0
0.0
-4.0
POTENTIAL
CHF$_S$
Na
CHF$_P$
MKE$_P$
MKE$_S$
CHF, MKE$_D$
0.0
1.0
2.0
3.0
4.0
DISTANCE

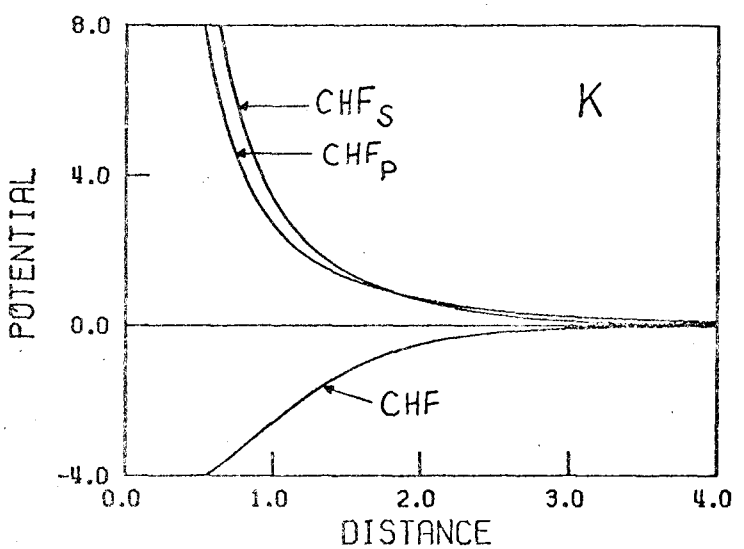
8.0
4.0
0.0
-4.0
POTENTIAL
CHF$_S$
K
CHF$_P$
CHF
0.0
1.0
2.0
3.0
4.0
DISTANCE

Fig. 6

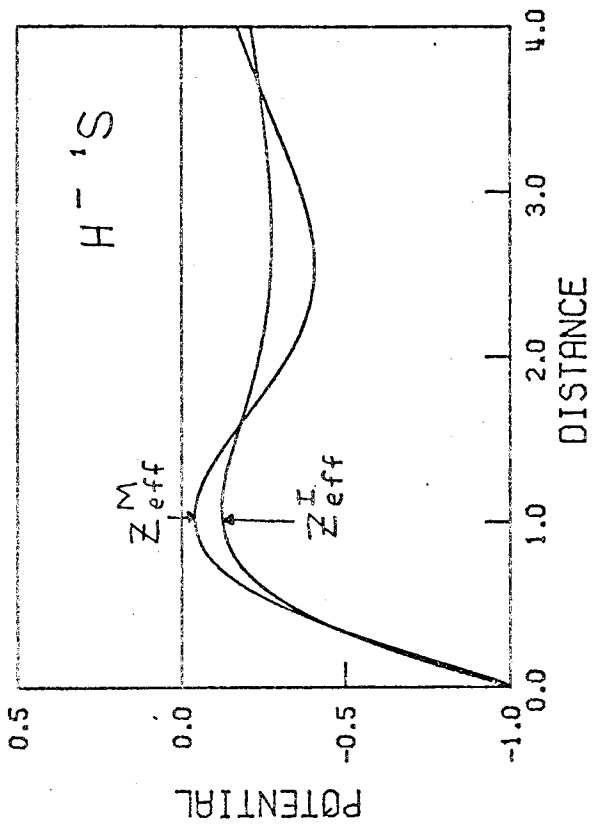

Fig. 8

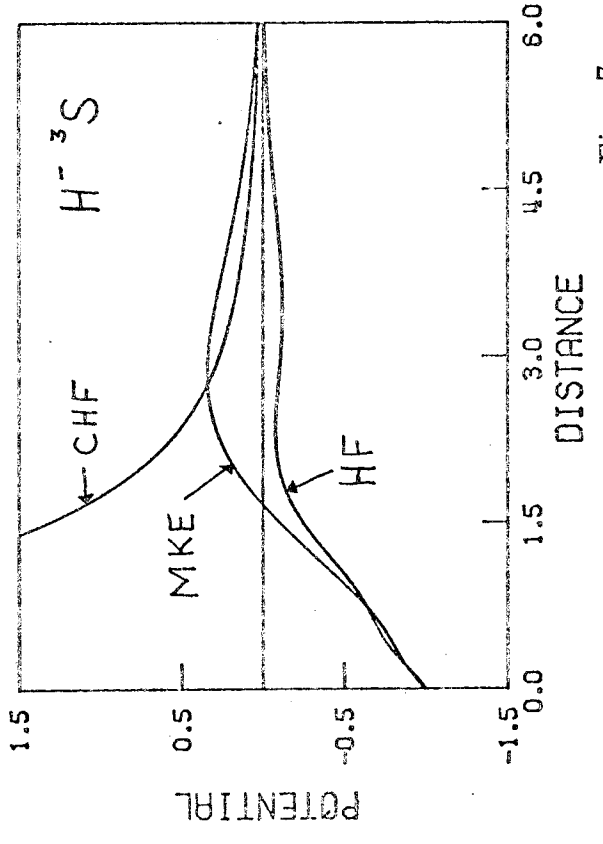

Fig. 7

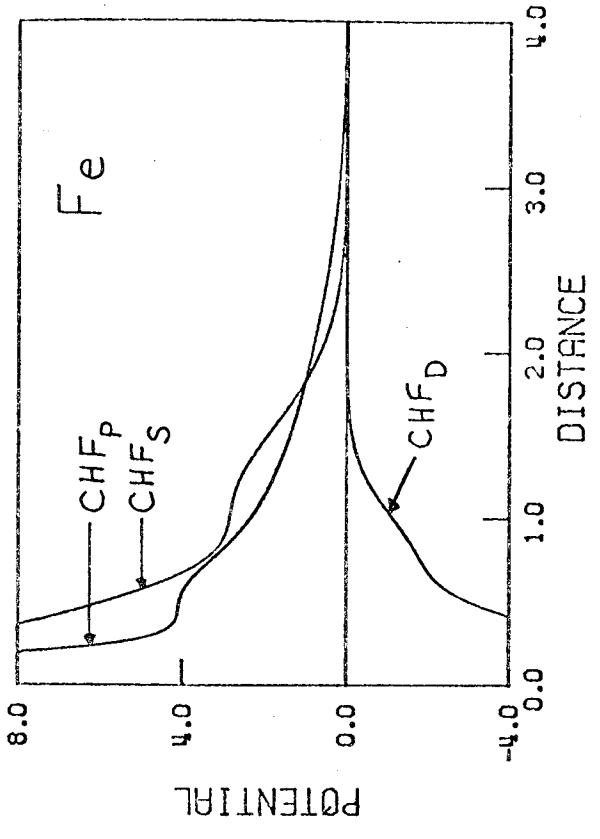

Fig. 10

Fig. 9

PART II

The Effective Potential Method in Molecular Quantum Mechanics

PART II-B

The Evaluation of Effective Potential Matrix Elements in a Gaussian Basis Set

EVALUATION OF THE EFFECTIVE POTENTIALS OVER A MULTICENTER GAUSSIAN BASIS SET

We wish to evaluate the effective potential matrix elements $\langle G_B | U_A | G_C \rangle$ where G_B is a Gaussian basis function located on center B

$$G_B = N\, x_B^{n_x}\, y_B^{n_y}\, z_B^{n_z}\, e^{-\zeta r_B^2} \tag{III-1}$$

and U_A is an angular dependent effective potential located on center A

$$U_A = U_{LMAX}(r_A) + \sum_{\ell=0}^{LMAX-1} \sum_{m=-\ell}^{\ell} \Delta U_\ell(r_A) | \ell m_{\Omega_A} \rangle \langle \ell m_{\Omega_A} | \tag{III-2}$$

where $U_{LMAX} + \Delta U_\ell$ are local (i.e., functions of r, not integral operators). Though we will only be concerned with s, p, and d basis functions, and LMAX $\leq$ 2, the formulas derived are general and can be easily extended to f, etc., basis functions and to larger LMAX.

Since the effective potential contains angular projection operators on center A, the integration will be done with respect to center A, using spherical coordinates. We must, therefore, expand the Gaussian basis functions onto center A. In our notation, we will use a small letter subscript i, i = 1, 2, 3, to represent the x, y, and z direction, respectively, and a capital letter subscript to label the center. When there is no ambiguity, the subscript for center A will be dropped. Thus,

$$r_{B_1} = x_B,\ r_{B_2} = y_B,\ \text{and}\ r_{B_3} = z_B.$$

A Gaussian s function on center B will be denoted by $G_B(s)$, a Gaussian p function on center B will be denoted by $G_B(r_{B_i})$, and a Gaussian d function on center B will be denoted by $G_B(r_{B_i} r_{B_j})$.

To transfer the angular factors of the Gaussian function on center B (i.e., r_{B_i}) to center A, we use the relationship

$$r_{B_i} = r_{A_i} - \overline{BA}_i \tag{III-3}$$

where

$$\overline{BA}_i = \overline{B}_i - \overline{A}_i = -\overline{AB}_i, \quad \overline{BA} = |\overline{B} - \overline{A}|.$$

To transfer the exponential term $e^{-\zeta r_B^2}$ to center A, we must rotate the A - coordinate system so that the new z'- axis points toward center B. In the prime coordinate system

$$r_B^2 = r_A^2 + \overline{BA}^2 - 2\overline{BA}\, r_A \cos\theta_{A'} \quad . \tag{III-4}$$

Having expressed the local potential integral $\langle G_B | U_A | G_C \rangle$ in terms of spherical coordinates on center A, we may now proceed to evaluate the integral. We divide the local potential into its LMAX parts, evaluating $\langle G_B | U_{LMAX} | G_C \rangle$ and each $\langle G_B | \Delta U_\ell \sum_m | \ell m \rangle \langle \ell m | G_C \rangle$ separately and then summing together.

$$\langle G_B | U_A | G_C \rangle = \langle G_B | U_{LMAX} | G_C \rangle + \sum_{\ell=0}^{LMAX-1} \langle G_B | \Delta U_\ell \sum_{m=-\ell}^{\ell} | \ell m \rangle \langle \ell m | G_C \rangle \tag{III-5}$$

Three types of integrals must be considered: (1) the one-center integral where centers A, B, and C are the same, (2) the two-center integral where centers A and C are the same but not equivalent to center B, and (3) the three-center integral where center A differs from both center B and center C but where B and C may be the same.

The one-center integrals are trivial and are considered later. The two-center integrals can be readily evaluated from the three-center integral by setting $\overline{CA}$ equal to zero. Of the three-center integrals, $\langle G_B | U_{LMAX} | G_C \rangle$ is related to the two-center integral, and as such is a simplification of the angular momentum dependent integral $\langle G_B | \Delta U_\ell \sum_m |\ell m\rangle\langle \ell m| \, | G_C \rangle$ with $\ell = 0$. We, therefore, derive a general analytic expression for the integral which contains the three-center angular projection operator, i.e.,

$$\langle G_B\,(r_{B_i} r_{B_j} \ldots) | \Delta U_\ell(r_A) \sum_{m=-\ell}^{\ell} |\ell m_{\Omega_A}\rangle\langle \ell m_{\Omega_A}| \, | G_C(r_{C_k} r_{C_\ell} \ldots)\rangle .$$

We first integrate over the angular coordinates, reducing the integrand to a function of r_A only. Due to the projection operator, the total integral consists of a sum over m terms of products of two angular integrations. We denote a generalized angular integration by

$$I\,ang_{D,\ell,m}(r_A) = \int_{\Omega_A} Z^{\sigma}_{\ell,m}(\Omega_A)\, G_D(r_{B_i}, r_{C_j} \ldots)\, d\Omega_A \qquad \text{(III-6)}$$

such that

$$\langle G_B | \Delta U_\ell \sum_m |\ell m\rangle\langle \ell m| \, | G_C \rangle =$$

$$\int_0^\infty r^2_A \, dr_A \, \Delta U_\ell (r_A) \sum_m \left(I_{ang_{B,\ell,m}}(r_A) \, I_{ang_{C,\ell,m}}(r_A) \right) \qquad \text{(III-7)}$$

To evaluate $I_{ang\,B,\ell,m}$, we first expand the Gaussian function located on center D onto center A. Using relations (III-3) and (III-4), we can express $I_{ang_{D,\ell,m}}$ as a sum of functions $ZG_{\ell m}(r_{A_i}, r_{A_j}, r_{A_k} \ldots)$ where

$$ZG_{\ell_m}(r_{A_i} r_{A_j} \ldots) = N(r_A) \int_{\Omega_A} Z_{\ell m}(\Omega_A) r_{A_i} r_{A_j} \ldots e^{-2\zeta_i \overline{BA}\, r_A \cos\theta_{A'}} \, d\Omega_A$$

(III-8)

and

$$N(r_A) = N_i \, e^{-\zeta_D r^2_A} \, e^{-\zeta_D \overline{DA}^2}$$

In transforming the Gaussian from center D to center A (see III-4), the A-coordinate system was rotated into the A′ coordinate system. Let the inverse rotation matrix be denoted by $\underset{\sim}{A}$. Each component of $\underset{\sim}{r}_A$ must be transformed into $\underset{\sim}{r}'_A$

$$\underset{\sim}{r}_A = \underset{\sim}{A} \, \underset{\sim}{r}'_A \qquad \text{(III-9)}$$

Since the angular momentum projection operators are fixed to the axis, they must also be rotated. For ℓ=0, there is no change ($Z_{00}(\Omega_A) = Z_{0\,0}(\Omega_A)$). For $\ell = 1$, the $Z^{\sigma}_{1,m}(\Omega_A)$'s transform like x_A, y_A, and z_A. Using Table A-I of App I,

we can express the projection operators in terms of the corresponding components of $\underset{\sim}{r}_A$. Defining a new $ZG'(r'_k\ r'_\ell \ldots)$ whose angular integration is carried out in the primed coordinate system

$$ZG'(r'_k\ r'_\ell \ldots) = \int_0^{2\pi} \int_0^{\pi} r'^{A_k}\, r'^{A_\ell} \ldots e^{2\zeta_i \overline{DA}\, r_A \cos\theta'_A}$$

$$d(\cos\theta_{A'})\, d\phi_{A'}, \qquad \text{(III-10)}$$

we can express the integral $ZG(r_i r_j \ldots)$ as a linear combination of the $ZG'(r'_k r'_\ell \ldots)$'s through the transformation $\underset{\sim}{A}$.

To evaluate $ZG'(r'_i r'_j \ldots)$, each r_i' is expressed in spherical coordinates and the exponential function of $\cos\theta_{A'}$ is expressed in terms of the modified spherical Bessel functions (see App. III)

$$e^{2\zeta_i \overline{DA}\, r_A \cos\theta_{A'}} = \sum_{\ell=0}^{\infty} (2\ell + 1)\, M_\ell\, (2\zeta_i\, \overline{DA}\, r_A) P_\ell(\cos\theta_{A'}). \qquad \text{(III-11)}$$

The $\phi_{A'}$ integration is carried out making use of the integrals in Table A-II. The θ dependent terms are expressed in terms of the Legendre polynomials (see App. I) and integrated with respect to $d(\cos\theta)$. The infinite sum resulting from (III-11) is reduced to a finite sum by making use of the orthogonality of the Legendre polynomials.

We will consider only s, p, and d functions ($\ell \leq 2$) and potentials with $LMAX \leq 2$; hence, we need only consider the integrals $ZG'(r'_i r'_j \ldots)$ containing at most four r'_i's. These integrals are listed in Table I. (The argument for M_ℓ is understood to be

$2\zeta_i \overline{DA}\, r_A$). As an example, the integration is carried out in detail for $ZG'(x'^2 z')$ in App. IV-a.

Having evaluated the $ZG'(r'_i r'_j \ldots)$ as a function of r_A, we can now express the $ZG(r_i r_j \ldots)$ in terms of these ZG'. Using (III-9) and taking advantage of the zero integrals of Table I, we obtain general expressions for $ZG(r_i r_j \ldots)$ which are listed in Table II. As an example, we carry out the transformation for $ZG(r_i r_j r_k)$ in App. IV-b.

Finally, we can express the $I_{ang_{D,\ell,m}}(r_A)$ in terms of the expressions for $ZG(r_i r_j r_k \ldots)$ by using the transformation in (III-3). These are listed in Table III, with the following notation being used. Terms of like powers of r and values of ℓ are collected together to form the general expression

$$I_{ang_D}(r_A) = N(r)\sqrt{4\pi}\,(2\ell+1) \sum_{n,\,\ell'} C_{n\ell'}\, r^n M_{\ell'} \qquad \text{(III-12)}$$

For the $\ell = 1$ projection operators, each expression had to be multiplied by $\frac{\sqrt{3}}{r}$ because of relationship between $Z^{\sigma}_{\ell,m}$ and r_i (see Table A-II). Since center D is equivalent to center B, we substitute $\frac{BA_i}{BA}$ for D_i (see App. II). In addition the symbol $Z_{1,m}$ is used such that

$$Z_{1,1} \equiv Z^{c}_{1,1} \qquad Z_{1,2} \equiv Z^{s}_{1,1} \qquad Z_{1,3} \equiv Z_{1,0}$$

An example for $\int z_{00}\, G_D(r_{B_i} r_{B_j} r_{C_k})\, d\Omega_A$ is given in App. IV-c.

Substituting III-12 into III-7, summing over m, and collecting terms of like powers of r_A^n and same M_{ℓ_1} and M_{ℓ_2}, we obtain as an integral over r_A the expression

$$\langle G_B | \Delta U_\ell \sum_m |\ell m\rangle\langle \ell m| | G_C\rangle = 4\pi\,(2\ell+1) \sum_{n,\ell_1,\ell_2} C_{n\ell_1\ell_2}$$

$$\cdot \int_0^\infty r_A^2\, dr_A\, \Delta U_\ell(r_A)\, N_B(r_A)\, N_C(r_A)\, r_A^n M_{\ell_1}(2\zeta_C \overline{CA}\, r_A)$$

$$\cdot M_{\ell_2}(2\zeta_B \overline{BA} r_A) \qquad \text{(III-13)}$$

where

$$N_B(r_A) = e^{-\zeta_B r_A^2}\, e^{-\zeta_B \overline{BA}^2}, \text{ etc.},$$

the ℓ, refers to center C, and the ℓ_2 refers to center B. As an example, the substitution of (III-12) into (III-7) is carried out in detail for $\langle G_B(r_{B_i}) | \Delta U_p | p\rangle\langle p | | G_C(r_{C_j}\rangle$ in App. IV-d.

We note from Table III that the modified spherical Bessel functions involved are M_0, M_1, M_2, M_3 and M_4. We can eliminate M_2, M_3 and M_4 by use of the recursion formula for Bessel functions (see A-III-4), thereby reducing the number of terms in III-13 to only those for which ℓ_1 and ℓ_2 equal zero and one.

Next, we consider the integral $\langle G_B(r_{B_i} r_{B_j} \ldots) | U_{LMAX}(r_A) | G_C(r_{C_k} r_{C_\ell} \ldots)\rangle$. Since there is no projection operator, we can combine the Gaussian exponentials on centers B and C to form a new Gaussian exponential on center D (see App. V), thereby obtaining the integral $\langle U_{LMAX}(r_A) | G_D(r_{B_i} r_{B_j} \ldots r_{C_k} r_{C_\ell} \ldots)\rangle$. Since $U_{LMAX}(r_A)$ is spherically symmetric, only that part of G_D which is spherically symmetric about center A will contribute to the integral. We can, therefore, write the integral in an equivalent form $\langle U_{LMAX} | s\rangle\langle s | G_D\rangle$.

But this is just

$$\int_0^\infty r_A^2 \; dr_A \; \sqrt{4\pi} \; U_{LMAX}(r_A) \, N_B(r_A) \, N_C(r_A) \, I_{ang_{D,0,0}}(r_A)$$

where $I_{ang_{D,0,0}}$ has already been defined in (III-6) and evaluated (see Table III). Thus, we have

$$\langle G_B | U_{LMAX} | G_C \rangle = 4\pi \sum_{n,\ell} C_{n,\ell} \int_0^\infty r_A^2 \; dr_A \; U_{LMAX}(r_A)$$

$$N_B(r_A) \, N_C(r_A) \; r_A^n \, M_\ell \left(2(\zeta_B + \zeta_C)\, \overline{DA}\, r_A\right) \qquad \text{(III-14)}$$

After integrating (III-13) and (III-14) over the radial coordinate, the integrals are summed together (see III-5) to obtain the total value for the three-center local potential integral $\langle G_B | U_A | G_C \rangle$.

To evaluate the two-center integral $\langle G_A(r_{A_i} \ldots) | U_A | G_B(r_j \ldots) \rangle$, we may use the same expressions obtained for $\langle G_B | U_{LMAX} | G_C \rangle$ in (III-14), letting $\overline{CA} = 0$, replacing U_{LMAX} by the correct local potential. Rewriting the local potential in (III-2) in its original form

$$U_A = \sum_{\ell=0}^{\infty} U_\ell \sum_{m=-\ell}^{\ell} |\ell m\rangle\langle \ell m| \qquad \text{(III-2}'\text{)}$$

where for $\ell < LMAX$, we must have

$$U_\ell \equiv U_{LMAX} + \Delta U_\ell$$

to ensure consistency in the integral evaluation. The projection operator on center A operating on a Gaussian s or p function on center A

will leave only one non-zero term in III-2′. Considering the Gaussian s function, for example, we can let $U_\ell = U_s$ for all ℓ, thus treating $\langle G_A(s)|U_A|G_B\rangle$ as a three-center integral of the type expressed in (III-14) except that U_{LMAX} is replaced by U_s. Similarly, for $\langle G_A(r_{A_i})|U_A|G_B\rangle$. U_{LMAX} is replaced by U_p. The integral $\langle G_A(r_{A_i} r_{A_j})|U_A|G_B(r_{B_k}\ldots)\rangle$ must be treated somewhat differently since $G_A(r_{A_i} r_{A_j})$ is not necessarily of pure d symmetry. Using U_A as in (III-2), we evaluate $\langle G_A(r_{A_i} r_{A_j})|U_{LMAX}|G_B\rangle$ as in (III-14) (assuming LMAX $\leq$ 2) with $\overline{CA} = 0$ and find that

$$\langle G_A(r_{A_i} r_{A_j})\Big|\sum_{\ell=0}^{LMAX-1} \Delta U_\ell |\ell m\rangle\langle \ell m|\Big|G_B\rangle =$$

$$\sqrt{4\pi}\ \frac{\delta_{ij}}{3}\langle G_A(s)\, r^2|\Delta U_s|G_B\rangle \qquad \text{(III-15)}$$

which is evaluated just like $\langle G_A(s)|U_A|G_B\rangle$ considered above with U_s replaced by $r^2\Delta U_s$. The sum of these two terms represents the total integral for $\langle G_A(r_i r_j)|U_A|G_B\rangle$.

For the one center integrals, we express U_A in the form (III-2′), the projection operators reducing the infinite sum to one term, or as in the case of $G_A(r_i^2)$, two terms, the resulting radial integration being

$$\langle G_A|U_A|G_A\rangle = \sum_n C_n \int_0^\infty r_A^2\ dr_A\ r_A^n\, e^{-(\zeta_{A_1}+\zeta_{A_2})\, r_A^2}\, U_\ell(r_A) \qquad \text{(III-16)}$$

We note that when $\langle G_B|U_{LMAX}|G_C\rangle$ has G_D centered on A, the integral reduces to a sum of one-center type integrals.

Table I: The Function $ZG'(r'_i r'_j \ldots)$

$ZG'(s) = N\sqrt{4\pi}\ M_0$

$ZG'(z') = N\sqrt{4\pi}\ rM_1$, all other $ZG'(r'_i) = 0$

$ZG'(x'^2) = ZG'(y'^2) = N\sqrt{4\pi}\ \frac{r^2}{3}(M_0 - M_2)$

$ZG'(z'^2) = N\sqrt{4\pi}\ \frac{r^2}{3}(M_0 + 2M_2)$, all other $ZG'(r'_i r'_j) = 0$

$ZG'(x'^2 z') = ZG'(y'^2 z') = N\sqrt{4\pi}\ \frac{r^3}{5}(M_1 - M_3)$

$ZG'(z'^3) = N\sqrt{4\pi}\ \frac{r^3}{5}(3M_1 + 2M_3)$, all other $ZG'(r'_i r'_j r'_k) = 0$

$ZG'(x'^4) = ZG'(y'^4) = N\sqrt{4\pi}\ \frac{r^4}{105}(9M_4 - 30M_2 + 21M_0)$

$ZG'(x'^2 z'^2) = ZG'(y'^2 z'^2) = N\sqrt{4\pi}\ \frac{r^4}{105}(-12M_4 + 5M_2 + 7M_0)$

$ZG'(x'^2 y'^2) = N\sqrt{4\pi}\ \frac{r^4}{105}(3M_4 - 10M_2 + 7M_0)$

$ZG'(z'^4) = N\sqrt{4\pi}\ \frac{r^4}{105}(24M_4 + 60M_2 + 21M_0)$

All other $ZG'(r'_i r'_j r'_k r'_\ell) = 0$

Table II: The Function $ZG(r_i r_j \ldots)$

$$ZG(s) = N\sqrt{4\pi}\ [M_0]$$

$$ZG(r_i) = N\sqrt{4\pi}\ r\ [D_i M_1]$$

$$ZG(r_i r_j) = N\sqrt{4\pi}\ r^2 \left[\left(D_i D_j - \frac{\delta_{ij}}{3}\right) M_2 + \frac{\delta_{ij}}{3} M_0\right]$$

$$ZG(r_i r_j r_k) = N\sqrt{4\pi}\ r^3 \left[\left(D_i D_j D_k - \left(D_i \frac{\delta_{jk}}{5} + D_j \frac{\delta_{ik}}{5} + D_k \frac{\delta_{ij}}{5}\right)\right) M_3 + \left(D_i \frac{\delta_{jk}}{5} + D_j \frac{\delta_{ik}}{5} + D_k \frac{\delta_{ij}}{5}\right) M_1\right]$$

$$ZG(r_i r_j r_k r_\ell) = N\sqrt{4\pi}\ r^4 \left[A \frac{1}{15} M_0 + \left(B - \frac{2}{21} A\right) M_2 + \left(C - B + \frac{1}{35} A\right) M_4\right]$$

where $A = \delta_{k\ell}\delta_{ij} + \delta_{j\ell}\delta_{ik} + \delta_{jk}\delta_{i\ell}$

$$B = \frac{\delta_{ij}}{7} D_k D_\ell + \frac{\delta_{ik}}{7} D_j D_\ell + \frac{\delta_{i\ell}}{7} D_j D_k + \frac{\delta_{jk}}{7} D_i D_\ell + \frac{\delta_{j\ell}}{7} D_i D_k + \frac{\delta_{k\ell}}{7} D_i D_j$$

$$C = D_i D_j D_k D_\ell$$

Table III: The Function $I_{ang\ D,\ \ell,\ m}$

$$\int Z_{00} G_D(s) d\Omega_A = N\sqrt{4\pi}\ [C_{00} M_0\ ]; \qquad C_{00} = 1$$

$$\int Z_{00} G_D(r_{B_i}) d\Omega_A = N\sqrt{4\pi}\ [C_{00} M_1 + C_{11} r M_1\ ];$$

$$C_{00} = -BA_i \qquad C_{11} = D_i$$

$$\int Z_{00} G_D(r_{B_i} r_{C_j}) d\Omega_A = N\sqrt{4\pi}\ [C_{00} M_0 + C_{20} r^2 M_0 + C_{11} r M_1 + C_{22} r^2 M_2\ ];$$

$$C_{00} = BA_i CA_j \qquad C_{20} = \frac{\delta_{ij}}{3}$$

$$C_{11} = BA_i D_j + CA_j D_i \qquad C_{22} = D_i D_j - C_{20}$$

$$\int Z_{00} G_D(r_{B_i} r_{B_j} r_{C_k}) d\Omega_A = N\sqrt{4\pi}\ [C_{00} M_0 + C_{20} r^2 M_0 + C_{11} r M_1 + C_{31} r^3 M_1$$

$$+ C_{22} r^2 M_2 + C_{33} r^3 M_3\ ]$$

$$C_{00} = -BA_i BA_j CA_k \qquad C_{11} = BA_i BA_j D_k + BA_i CA_k D_j + BA_j CA_k D_i$$

$$C_{20} = -\left(BA_i \frac{\delta_{jk}}{3} + BA_j \frac{\delta_{ik}}{3} + CA_k \frac{\delta_{ij}}{3}\right)$$

$$C_{22} = -(BA_i D_j D_k + BA_j D_i D_k + CA_k D_i D_j + C_{20})$$

$$C_{33} = D_i D_j D_k - C_{31}$$

$$\int Z_{00} G_D(r_{B_i} r_{B_j} r_{C_k} r_{C_\ell}) d\Omega = N\sqrt{4\pi}\ [C_{00} M_0 + C_{11} r M_1 + C_{20} r^2 M_0 + C_{22} r^2 M_2$$

$$+ C_{31} r^3 M_1 + C_{33} r^3 M_3 + C_{40} r^4 M_0 + C_{42} r^4 M_2 + C_{44} r^4 M_4\ ]$$

$$C_{00} = BA_i BA_j CA_k CA_\ell$$

TABLE III-Continued

$$C_{11} = -(BA_iBA_jCA_kD_\ell + BA_iBA_jCA_\ell D_k + BA_iCA_kCA_\ell D_j + BA_jCA_kCA_\ell D_i)$$

$$C_{20} = (BA_iBA_j \frac{\delta_{k\ell}}{3} + BA_iCA_k \frac{\delta_{j\ell}}{3} + BA_iCA_\ell \frac{\delta_{jk}}{3} + BA_jCA_k \frac{\delta_{i\ell}}{3} + BA_jCA_\ell \frac{\delta_{ik}}{3} + CA_kCA_\ell \frac{\delta_{ij}}{3})$$

$$C_{22} = (BA_iBA_jD_kD_\ell + BA_iCA_kD_jD_\ell + BA_iCA_\ell D_jD_k + BA_jCA_kD_iD_\ell + BA_jCA_\ell D_iD_k + CA_kCA_\ell D_iD_j) - C_{20}$$

$$C_{31} = -(BA_iD_j \frac{\delta_{k\ell}}{5} + BA_iD_k \frac{\delta_{j\ell}}{5} + BA_iD_\ell \frac{\delta_{jk}}{5} + BA_jD_i \frac{\delta_{k\ell}}{5} + BA_jD_k \frac{\delta_{i\ell}}{5} + BA_jD_\ell \frac{\delta_{ik}}{5} + CA_kD_i \frac{\delta_{j\ell}}{5} + CA_kD_j \frac{\delta_{i\ell}}{5} + CA_kD_\ell \frac{\delta_{ij}}{5} + CA_\ell D_i \frac{\delta_{jk}}{5} + CA_\ell D_j \frac{\delta_{ik}}{5} + CA_\ell D_k \frac{\delta_{ij}}{5})$$

$$C_{33} = -(BA_iD_jD_kD_\ell + BA_jD_iD_kD_\ell + CA_kD_iD_jD_\ell + CA_\ell D_iD_jD_k) - C_{31}$$

$$C_{40}' = \delta_{k\ell}\delta_{ij} + \delta_{j\ell}\delta_{ik} + \delta_{i\ell}\delta_{jk}$$

$$C_{42}' = (D_kD_\ell \frac{\delta_{ij}}{7} + D_jD_\ell \frac{\delta_{ik}}{7} + D_iD_\ell \frac{\delta_{jk}}{7} + D_jD_k \frac{\delta_{i\ell}}{7} + D_iD_k \frac{\delta_{j\ell}}{7} + D_iD_j \frac{\delta_{k\ell}}{7})$$

$$C_{44}' = D_iD_jD_kD_\ell$$

$$C_{40} = C_{40}'/15$$

$$C_{42} = C_{42}' - \frac{2}{21} C_{40}'$$

$$C_{44} = C_{44}' - C_{42}' + C_{40}'/35$$

Table III- Continued

$$\int Z_1, {}_m G_B(s)d\Omega = N\sqrt{12\pi}\ [C_{0\,1}M_1]; \qquad C_{0\,1} = \frac{BAm}{BA}$$

$$\int Z_1, {}_m G_B(r_{B_i})d\Omega_A = N\sqrt{12\pi}\ [C_{0\,1}M_1 + C_{10}\,rM_0 + C_{12}rM_2];$$

$$C_{0\,1} = \frac{-BA_i BA_m}{BA},\ C_{10} = \frac{\delta im}{3},\ C_{12} = -(C_{0\,1}/BA + C_{10})$$

$$\int Z_1, {}_m G_B(r_{B_i} r_{B_j})d\Omega_A = N\sqrt{12\pi}\ [C_{0\,1}M_1 + C_{10}\,rM_0 + C_{12}rM_2 + C_{21}r^2M_1 +$$

$$C_{23}r^2M_3];$$

$$C_{0\,1} = BA_i BA_j\ \frac{BAm}{BA}$$

$$C_{10} = -(BA_i \frac{\delta jm}{3} + BA_j \frac{\delta im}{3})$$

$$C_{12} = -(2\,BA_i BA_j\ \frac{BA\,m}{BA^2}) - C_{10}$$

$$C_{21} = (\frac{BA_i}{BA}\ \frac{\delta jm}{5} + \frac{BA_j}{BA}\ \frac{\delta im}{5} + \frac{BAm}{BA}\ \frac{\delta ij}{5})$$

$$C_{23} = \frac{BA_i BA_j BA_m}{BA^3} - C_{21}$$

Having carried out the angular integration, each local potential integral is found to be expressed in terms of only three radial integrations (see equations (III-13), (III-14), and (III-16));

$$\sum_{n'} C_{n'} \int_0^\infty r^2 dr\, e^{-(\zeta_i + \zeta_j)r^2} r^{n'} U(r) \qquad \text{(III-17a)}$$

$$\sum_{n',\ell} C_{n'\ell} \int_0^\infty r^2 dr\, e^{-(\zeta_i + \zeta_j)r^2} r^{n'} U(r)\, M_\ell(ar) \qquad \text{(III-17b)}$$

$$\sum_{n',\ell_1,\ell_2} C_{n'\ell_1\ell_2} \int_0^\infty r^2 dr\, e^{-(\zeta_i + \zeta_j)r^2} r^{n'} U(r)\, M_{\ell_1}(ar)\, M_{\ell_2}(br) \qquad \text{(III-17c)}$$

where U(r) represents $U_\ell(r)$ or $\Delta U_\ell(r)$. One could evaluate each of these integrals by numerical integration. However, this method is very time consuming and defeats the purpose of using local potentials. Instead, the U(r) is expressed in terms of some analytic functions which would permit each of the integrals (i), (ii), and (iii) of (III-17) to be evaluated analytically. At the same time, the analytic functions must contain enough freedom to adequately and simply describe the local potential. We find that a potential of the form

$$U(r) = \sum_k c_k r^{n_k} e^{-\zeta_k r^2} \qquad n_k \geq -2 \qquad \text{(III-18)}$$

satisfies these conditions. This form of the potential adds no complications to the evaluation of the integral since (1) the exponential part can be incorporated into the exponential already present, and

(2) the power of r is added to the power of r already present. Letting r^n represent the product of the n dependence ($n = 2 + n' + n_k$) and letting $\zeta = \zeta_i + \zeta_j + \zeta_k$, we have (after a change of variables) the following three types of integrals to evaluate

$$A_n(\zeta) = \frac{1}{\zeta^{(n+1)/2}} \int_0^\infty e^{-r^2} r^n \, dr \tag{III-19a}$$

$$I_{n,\ell}(\zeta, \frac{a}{\sqrt{\zeta}}) = \frac{1}{\zeta^{(n+1)/2}} \int_0^\infty e^{-r^2} r^n M_\ell(\frac{a}{\sqrt{\zeta}} r) dr \tag{III-19b}$$

$$J_{n,\ell_1,\ell_2}(\zeta, \frac{a}{\sqrt{\zeta}}, \frac{b}{\sqrt{\zeta}}) = \frac{1}{\zeta^{(n+1)/2}} \int_0^\infty e^{-r^2} r^n M_{\ell_1}(\frac{a}{\sqrt{\zeta}} r)$$

$$\cdot M_{\ell_2}(\frac{b}{\sqrt{\zeta}} r) \, dr \tag{III-19c}$$

where $n \geq 0$ and $\ell(\ell_1, \ell_2) = 0, 1$.

The first type of integral is well known

$$A_n(\zeta) = \frac{1}{\zeta^{(n+1)/2}} \int_0^\infty e^{-r^2} r^n \, dr = \frac{\Gamma(\frac{n+1}{2})}{2\zeta^{(n+1)/2}} \tag{III-20}$$

The second type of integral must be evaluated by two different means. For $n \geq \ell + 1$, M_ℓ may be expressed in terms of the sinh and cosh functions, each term integrated separately and then added together. Expressing the sinh and cosh in terms of exponentials and defining

$$VP_n(x) = \int_0^\infty r^{n-1} (e^{-(r-x)^2} + e^{-(r+x)^2}) dr$$

$$VM_n(x) = \int_0^\infty r^{n-1} (e^{-(r-x)^2} - e^{-(r+x)^2}) dr \tag{III-21}$$

$$V_n(x) = VP_n(x) - \frac{1}{2x}\, VM_{n-1}(x),$$

we have that

$$\begin{aligned} I_{n,0}(\zeta,\ a') &= \frac{1}{2} e^{+\frac{a'^2}{4}} \quad \frac{1}{a' \zeta^{(n+1)/2}}\ VM_n(\tfrac{a'}{2}) \\ I_{n,1}(\zeta,\ a') &= \frac{1}{2} e^{+\frac{a'^2}{4}} \quad \frac{1}{a' \zeta^{(n+1)/2}}\ V_n(\tfrac{a'}{2}) \end{aligned} \qquad \text{(III-22)}$$

The functions $VM_n(x)$ and $V_n(x)$ have the following recursion relations

$$\begin{aligned} VM_{n+2}(x) &= x\, V_{n+1}(x) + \frac{n+1}{2}\, VM_n(x) \\ V_{n+3}(x) &= (x^2 + \frac{n}{2})\, V_{n+1} + \frac{n+1}{2}\, VM_n(x) \end{aligned} \qquad \text{(III-23)}$$

Therefore, we need only integrate the two sets of integrals $\{VM_1,\ V_2\}$ and $\{VM_2,\ V_3\}$ from which all the other VM_n and V_n can be evaluated from the recussion relations. The integrations are straight forward (see App. VIa), the results given in Table IV.

For $n=\ell$, $M_\ell(a'r)$ cannot be decomposed into a sum of functions involving $e^{a'r}$ and $e^{-a'r}$ since the integral of each term taken separately would diverge. To evaluate $I_{0,0}$ and $I_{1,1}$, therefore, M_ℓ is expressed in terms of its integral representation (see App. III), the order of integration is reversed, and the r integration is carried out first (see App. VI-b). Putting the integral in the form of (III-22), an expression is obtained for VM_0 and V_1 (See Table IV).

Table IV

$$VM_0(x) = 2\sqrt{\pi}\, D_0(x) \qquad V_1(x) = \sqrt{\pi}\left(1 - \frac{D_0(x)}{x}\right)$$

$$VM_1(x) = 2\ E_0(x) \qquad V_2(x) = \left(x - \frac{1}{2x}\right)2\ E_0(x) + e^{-x^2}$$

$$VM_2(x) = \sqrt{\pi}\ x \qquad V_3(x) = \sqrt{\pi}\ x^2$$

$$VM_{n+2}(x) = x\, V_{n+1}(x) + \frac{n+1}{2} VM_n(x) \qquad V_{n+3}(x) = \left(x^2 + \frac{n}{2}\right) V_{n+1}(x) + \left(\frac{n+1}{2}\right) x VM_n(x)$$

where

$$D_0(x) = e^{-x^2} \int_0^x e^{\sigma^2} d\sigma \qquad E_0(x) = \int_0^x e^{-\sigma^2} d\sigma$$

For the third type of integral, the same procedure is followed as for the two center integrals. For $n \geq \ell_1 + \ell_2 + 2$, M_{ℓ_1} and M_{ℓ_2} may be expressed in terms of the sinh and cosh functions, with each term being integrated separately. The final expression can be expressed in terms of the functions defined in (III-21). Modifying the definitions of (III-21) so that $VP'(x) = e^{-x^2} VP(x)$, etc, we have

$$J_{n,0,0}(\zeta,a',b') = \frac{1}{\zeta^{(n+1)/2}} \frac{1}{4a'b'} \left[VP'_{n-1}\left(\frac{a'+b'}{2}\right) - VP'_{n-1}\left(\frac{b'-a'}{2}\right)\right]$$

$$J_{n,0,1}(\zeta,a',b') = \frac{1}{\zeta^{(n+1)/2}} \frac{1}{4a'b'} \left[\left(VM'_{n-1}\left(\frac{a'+b'}{2}\right) - VM_{n-1}\left(\frac{b'-a'}{2}\right)\right) - \frac{1}{b'}\left(VP'_{n-2}\left(\frac{a'+b'}{2}\right) - VP'_{n-2}\left(\frac{b'-a'}{2}\right)\right)\right]$$

$$J_{n,1,0}(\zeta,a',b') = \frac{1}{\zeta^{(n+1)/2}} \frac{1}{4a'b'} \left[\left(VM'_{n-1}\left(\frac{a'+b'}{2}\right) + VM'_{n-1}\left(\frac{b'-a'}{2}\right)\right) - \frac{1}{a'}\left(VP'_{n-2}\left(\frac{a'+b'}{2}\right) - VP'_{n-2}\left(\frac{b'-a'}{2}\right)\right)\right]$$

$$J_{n,1,1}(\zeta,a',b') = \frac{1}{\zeta^{(n+1)/2}} \frac{1}{4a'b'} \left[\left(VP'_{n-1}\left(\frac{a'+b'}{2}\right) + VP'_{n-1}\left(\frac{b'-a'}{2}\right)\right) - \frac{1}{a'}\left(VM'_{n-2}\left(\frac{a'+b'}{2}\right) - VM'_{n-2}\left(\frac{b'-a'}{2}\right)\right)\right.$$

$$\left. - \frac{1}{b'}\left(VM'_{n-2}\left(\frac{a'+b'}{2}\right) + VM'_{n-2}\left(\frac{b'-a'}{2}\right)\right) + \frac{1}{a'b'}\left(VP'_{n-3}\left(\frac{a'+b'}{2}\right) - VP'_{n-3}\left(\frac{b'-a'}{2}\right)\right)\right] \qquad \text{(III-24)}$$

For $n < \ell_1 + \ell_2 + 2$, each of the M_ℓ's must be expressed in their integral representation and the order of the integration switched. The actual integration is carried out in App. VIII, resulting in the general expression

$$J_{n,\ell_1,\ell_2}(\zeta,a',b') = \frac{1}{\zeta^{(n+1)/2}} \frac{1}{2\ell_1+\ell_2+1} \sum_{i_1=0}^{\ell_1} \sum_{i_2=0}^{\ell_2} (-)^{i_1+i_2} \binom{\ell_1}{i_1}\binom{\ell_2}{i_2}$$

$$a'^{(\ell_1-2i_1-1)} b'^{(\ell_2-2i_2-1)} \qquad \text{(III-25)}$$

$$\sum_{j_1=0}^{2i_1} \sum_{j_2=0}^{2i_2} \binom{2i_1}{j_1} (-)^{j_2} \binom{2i_2}{j_2} \frac{1}{j_1+j_2+1} \sum_{j=0}^{k} \left(F^{+}(k,j,i_1+i_2,j_1+j_2,\ell,a',b')\right.$$

$$\left. - F^{-}(k,j,i_1+i_2,j_1+j_2,\ell,a',b')\right)$$

where for $n + \ell_1 + \ell_2 = 2k$

$$F^{\pm}_{k,j,i,j',\ell}(a',b') = \Gamma(j+\tfrac{1}{2}) e^{\frac{(b'\pm a')^2}{4}} f^{\pm}_{j',\ell}(a',b') D_{2(k-j)+2i-j+\ell}$$

$$\left(\frac{b'\pm a'}{2}\right)$$

while for $n + \ell_1 + \ell_2 = 2k + 1$

$$F^{\pm}_{k,j,i,j',\ell}(a',b') = e^{\frac{(b'\pm a')^2}{4}} f^{\pm}_{j',\ell}(a',b') \left\{2\binom{2k+1}{2j} DE_{j,2k-j+1+2i}\right.$$

$$\left. -j'+\ell \left(\frac{b'\pm a'}{2}\right) + \binom{2k+1}{2j+1} \sum_{\lambda=0}^{j} \frac{j!}{(j-\lambda)!} D_{2k-j-\lambda+2i-j'+\ell}\left(\frac{b'\pm a'}{2}\right)\right\}$$

Care must be taken in evaluating J_{n,ℓ_1,ℓ_2} by means of equation (III-25) since considerable accuracy is lost when $a' \ll b'$ or $b' \ll a'$. To avoid this problem, a power series expansion is used for $M_{\ell_1}(a')$ (see App. III) when a' is small (similarly for $M_{\ell_2}(b')$ if b' is small)

$$J_{n,\ell_1,\ell_2,}(\zeta,a',b') = \frac{1}{\zeta^{(n+1)/2}} \frac{a'^{\ell_1}}{(2\ell_1+1)!!} \sum C_k \int_0^{\infty} e^{-r^2} r^{n+\ell_1+2k} M_{\ell_2}(b'r)dr$$

(III-26)

$$= \frac{a'^{\ell_1}}{(2\ell_1+1)!!} \sum C_k \, I_{n+\ell_1+2k,\, \ell_2}(\zeta, b')$$

where $C_0 = 1$ and $CK = \frac{\frac{1}{2}a'^2}{k(2\ell_2+2k+1)} \; C_{k-1}$

The $I_{n+\ell_1+2k,\, \ell_2}$ are readily evaluated from equation (III-22) using (III-25).

Though the program originally contained the general expressions for $J_{n,\, \ell_1 \ell_2}$ in (III-24) and (III-25), a restriction has since been made requiring $n + \ell_1 + \ell_2$ to be an even number. In particular, n_k of (III-18) must equal -2 or 0. This restriction on n_k does not limit the accuracy of (III-18), while significantly simplifying the analytic expressions for $J_{n,\, \ell_1,\, \ell_2}$. Instead of (III-24), we have, for example,

$$J_{2,0,0}(\zeta, a', b') = N \sinh(z)$$

$$J_{3,0,1}(\zeta, a', b') = N\left[\left(\frac{b'}{2} - \frac{1}{b'}\right) \sinh(z) + \frac{a'}{2} \cosh(z)\right] \qquad \text{(III-27)}$$

where $z = \frac{1}{2} a'b'$ and $N = \frac{1}{\zeta^{(n+1)/2}} \; \frac{\sqrt{\pi}}{4z} \; e^{\frac{a'^2 + b'^2}{4}}$

For (III-25) all terms containing D_k are collected together and written explicitly. Terms containing $DE_{i,\, j}$ do not exist. Therefore, the evaluation of the $J_{n,\, \ell_1,\, \ell_2}$ integrals, which is the most time consuming part of the potential integral evaluation, is greatly reduced.

Appendix I: Spherical Harmonics and Legendre Polynomials

$Z^{\sigma}_{\ell,m}(\Omega_A)$ is defined as a real spherical harmonic on center A:

$$Z^{c}_{\ell,m} = \frac{1}{\sqrt{2}}\left(Y_{\ell,m} + Y^{*}_{\ell,-m}\right)$$
$$Z^{s}_{\ell,m} = \frac{-i}{\sqrt{2}}\left(Y_{\ell,m} - Y^{*}_{\ell,-m}\right) \qquad \text{(AI-1)}$$

The first few real spherical harmonics are defined in Table A-I

Table A-I

$$Z_{00} = \sqrt{\frac{1}{4\pi}}$$

$$Z^{c}_{1,1} = \sqrt{\frac{3}{4\pi}}\ \frac{x}{r} \qquad Z^{s}_{1,1} = \sqrt{\frac{3}{4\pi}}\ \frac{y}{r} \qquad Z_{1,0} = \sqrt{\frac{3}{4\pi}}\ \frac{z}{r}$$

$$Z^{c}_{2,2} = \sqrt{\frac{5}{4\pi}}\ \frac{\sqrt{3}}{2}\ \frac{(x^2-y^2)}{r^2} \qquad Z^{s}_{2,2} = \sqrt{\frac{5}{4\pi}}\ \sqrt{3}\ \frac{xy}{r^2}$$

$$Z^{c}_{2,1} = \sqrt{\frac{5}{4\pi}}\ \sqrt{3}\ \frac{xz}{r^2} \qquad Z^{s}_{2,1} = \sqrt{\frac{5}{4\pi}}\ \sqrt{3}\ \frac{yz}{r^2}$$

$$Z_{2,0} = \sqrt{\frac{5}{4\pi}}\ \frac{1}{2}\ \frac{(3z^2-r^2)}{r^2}$$

where $x = r\sin\theta\cos\phi$, $y = r\sin\theta\sin\phi$, and $z = r\cos\theta$. Useful angular integrals are given in Table A-II.

Table A-II

$$\int_0^{2\pi}\cos\phi\, d\phi = \int_0^{2\pi}\sin\phi\, d\phi = \int_0^{2\pi}\cos\phi\sin\phi\, d\phi = \int_0^{2\pi}\sin^2\phi\cos\phi =$$

$$\int_0^{2\pi}\sin\phi\cos^2\phi\, d\phi = 0$$

$$\int_0^{2\pi} \cos^2\phi \, d\phi = \int_0^{2\pi} \sin^2\phi \, d\phi = \pi$$

$$\int_0^{2\pi} \cos^4\phi \, d\phi = \int_0^{2\pi} \sin^4\phi \, d\phi = \frac{3}{4}\pi \qquad \int_0^{2\pi} \cos^2\phi \sin^2\phi = \frac{1}{4}\pi$$

The first few Legendre polynomials are given in Table A-III

Table A-III

$$P_0(x) = 1 \qquad P_1(x) = x \qquad P_2(x) = \frac{1}{2}(3x^2-1) \qquad P_3(x) = \frac{1}{2}(5x^3-3x)$$

$$P_4(x) = \frac{1}{8}(35x^4 - 30x^2 + 3)$$

(where $x = \cos\theta$). The orthogonality relationship for the Legendre Polynomials is given by

$$\int_{-1}^{1} P_\ell(x) \, P_{\ell'}(x) \, dx = \frac{2}{(2\ell+1)} \, \delta_{\ell\ell'} \qquad \text{(AI-2)}$$

Useful relationships between the trigonometric functions and the Legendre polynomials are given in Table A-IV.

Table A-IV

$$\cos\theta = P_1$$

$$\sin^2\theta = \frac{2}{3} P_0 - \frac{2}{3} P_2 \qquad \cos^2\theta = \frac{1}{3} P_0 + \frac{2}{3} P_2$$

$$\sin^2\theta \cos\theta = \frac{2}{5} P_1 - \frac{2}{5} P_3 \qquad \cos^3\theta = \frac{3}{5} P_1 + \frac{2}{5} P_3$$

$$\cos^4\theta = \frac{8}{35} P_4 + \frac{4}{7} P_2 + \frac{1}{5} P_0 \qquad \cos^2\theta \sin^2\theta = \frac{8}{35} P_4 + \frac{2}{21} P_2 + \frac{2}{15} P_0$$

$$\sin^4\theta = \frac{8}{35} P_4 - \frac{16}{21} P_2 + \frac{8}{15} P_0$$

Appendix II: Rotation of Coordinate Systems

Let $\underset{\sim}{A}$ be the matrix that transforms the $\underset{\sim}{x}'$ coordinate system into the $\underset{\sim}{x}$ coordinate system, i.e.

$$\underset{\sim}{x} = \underset{\sim}{A}\ \underset{\sim}{x}' \tag{A-II-1}$$

where $\cos\Theta_x = \dfrac{\overline{DA}_x}{\sqrt{\overline{DA}_x^2 + \overline{DA}_y^2}}$ and $\cos\Theta_z = \dfrac{\overline{DA}_z}{\overline{DA}}$. Then

$$\underset{\sim}{A} = \begin{pmatrix} \dfrac{\overline{DA}_x\,\overline{DA}_z}{\overline{DA}\sqrt{\overline{DA}_x^2 + \overline{DA}_y^2}} & \dfrac{-\overline{DA}_y}{\sqrt{\overline{DA}_x^2 + \overline{DA}_y^2}} & \dfrac{\overline{DA}_x}{\overline{DA}} \\ \dfrac{\overline{DA}_y\,\overline{DA}_z}{\overline{DA}\sqrt{\overline{DA}_x^2 + \overline{DA}_y^2}} & \dfrac{\overline{DA}_x}{\sqrt{\overline{DA}_x^2 + \overline{DA}_y^2}} & \dfrac{\overline{DA}_y}{\overline{DA}} \\ \dfrac{-\sqrt{\overline{DA}_x^2 + \overline{DA}_y^2}}{\overline{DA}} & 0 & \dfrac{\overline{DA}_z}{\overline{DA}} \end{pmatrix} \tag{A-II-2}$$

Since the transformation involves rotation of both the basis function and the projection operator, the integral involves products of the elements of the transformation matrix. The following relationships are used in App. IV-b.

$$A_{k3} = \frac{\overline{DA}_k}{\overline{DA}} \equiv D_k \tag{A-II-3}$$

From the unitarity property of $\underset{\sim}{A}$

$$\sum A_{ik}\,A_{jk} = \delta_{ij} \tag{A-II-4}$$

(taking A as real), so that

$$2A_{i3}A_{j3} - A_{i1}A_{j1} - A_{i2}A_{j2} = 3D_iD_j - \delta_{ij} \qquad \text{(A-II-5)}$$

Appendix III: Modified Spherical Bessel Functions of the First Kind

$$M_\ell(\xi) = i^\ell j_\ell(-i\xi) \tag{A-III-1}$$

where j_ℓ is the spherical Bessel function (see Abramowitz and Stegun p. 443).

$$j_\ell(z) = z^\ell \left(-\frac{1}{z}\frac{d}{dz}\right)^\ell \left(\frac{\sin z}{z}\right) \tag{A-III-2}$$

We have

$$M_0(\xi) = \frac{\sinh(\xi)}{\xi}$$

$$M_1(\xi) = \frac{\cosh(\xi)}{\xi} - \frac{\sinh(\xi)}{\xi^2} \tag{A-III-3}$$

From the recursion relationship for Bessel functions

$$M_{\ell-1}(\xi) - M_{\ell+1}(\xi) = (2\ell+1)\, M_\ell(\xi)/\xi \tag{A-III-4}$$

For small values of the argument, a power series expansion may be made:

$$M_\ell(\xi) = \frac{\xi^\ell}{(2\ell+1)!!} \sum_{k=0}^{\infty} \frac{(\frac{1}{2}\xi^2)^k}{k!(2\ell+2k+1)!!} \tag{A-III-5}$$

The integral representation of the modified spherical Bessel function is

$$M_\ell(\xi) = \frac{\xi^\ell}{2^{\ell+1}\ell!} \int_{-1}^{1} \cosh(\xi u)\,(1-u^2)^\ell\, du \tag{A-III-6}$$

The exponential of the cosine function can be represented in terms of modified spherical Bessel functions by the relation

$$e^{a\cos\theta} = \sum_{\ell=0}^{\infty} (2\ell+1)\, M_{\ell}(a)\, P_{\ell}(\cos\theta) \qquad \text{(A-III-7)}$$

Appendix IV: Detailed Evaluation of the Local Potential Integral

Part A: Evaluation of $ZG'(x'^2z')$

$$ZG'(x'^2z') = \frac{N}{\sqrt{4\pi}} \int_{\Omega_{A'}} x'^2z' \, e^{2\zeta_i \overline{BA} r \cos\theta_{A'}} \, d(\cos\theta_{A'}) d\phi_{A'}$$

Using(A-III-7)

$$ZG'(x'^2z') = \frac{N}{\sqrt{4\pi}} \int_0^{2\pi} \int_{-1}^{1} (r \sin\theta_{A'} \cos\phi_{A'})^2 (r \cos\theta_{A'}) \{ \sum_{\ell=0}^{\infty} (2\ell+1) M_\ell$$

$$(2\zeta_i \overline{BA} r) P_\ell(\cos\theta_{A'}) \} \, d(\cos\theta_{A'}) \, d\phi_{A'}$$

From Table A-II and Table A-IV and integrating over $\phi_{A'}$,

$$ZG'(x'^2z') = N \frac{\sqrt{\pi}}{4} r^3 \int_{-1}^{1} (\frac{2}{5} P_1(x) - \frac{2}{5} P_3(x))(\sum_{\ell=0}^{\infty} (2\ell+1) M_\ell(2\zeta_i \overline{BA} r) P_\ell(x)) dx$$

Finally, using A-I-2 we have

$$ZG'(x'^2z') = N\sqrt{4\pi} \frac{r^3}{5} [M_1(2\zeta_i \overline{BA} r) - M_3(2\zeta_i \overline{BA} r)]$$

Part B: Transformation of $ZG'(r'_\ell r'_m r'_n)_{\Omega_{A'}}$ to $ZG(r_i r_j r_k)_{\Omega_A}$

We wish to express $ZG'(r_i r_j r_k)_{\Omega_A}$ in terms of the $ZG'(r'_\ell r'_m r'_n)_{\Omega_A}$'s. Since only $ZG'(x'^2z')$, $ZG'(y'^2z')$ and $ZG'(z'^3)$ are non-zero, we need only consider the coefficients involving these terms. Considering all permutations of the indices, we can see that

$$r_i r_j r_k = (A_{i1}A_{j1}A_{k3} + A_{i1}A_{j3}A_{k1} + A_{i3}A_{j1}A_{k1})x'^2z'$$

$$+ (A_{i2}A_{j2}A_{k3} + A_{i2}A_{j3}A_{k2} + A_{i3}A_{j2}A_{k2})y'^2z'$$

$$+ (A_{i3}A_{j3}A_{k3}) z'^3 + \text{other terms}$$

Since $ZG'(x'^2z')$ and $ZG(y'^2z')$ are equal (see Table I), we can combine the first two expressions together obtaining

$$ZG(r_i r_j r_k) = N\sqrt{4\pi}\ [((A_{i1}A_{j1} + A_{i2}A_{j2})A_{k3} + (A_{i1}A_{k1} + A_{i2}A_{k2})A_{j3} + (A_{j1}A_{k1} + A_{j2}A_{k2})A_{i3})\frac{r^3}{5}(M_1 - M_3) + A_{k3}A_{j3}A_{i3}\ \frac{r^3}{5}\ (3M_1 + 2M_3)]$$

Using (A-II-3) and (A-II-5), we obtain

$$ZG(r_i r_j r_k) = N\sqrt{4\pi}\ (C_{31}\, r^3 M_1\, (2\zeta_i \overline{BA}r) + C_{33}\, r^3 M_3\, (2\zeta_i \overline{BA}r))$$

where

$$C_{31} = (\frac{\delta_{ij}}{5} D_k + \frac{\delta_{jk}}{5} D_i + \frac{\delta_{ik}}{5} D_j)$$

$$C_{33} = D_i D_j D_k - C31$$

Part C: Expressing $(Z_{oo}{}_A | G(r_{B_i} r_{B_j} r_{C_k}))$ in terms of the modified spherical Bessel functions.

Transforming $r_{B_i} r_{B_j} r_{C_k}$ to center A, we obtain (using (III-3))

$$r_{B_i} r_{B_j} r_{C_k} = r_i r_j r_k - B_i r_j r_k - B_j r_i r_k - C_k r_i r_j + B_i B_j r_k + B_i C_k r_j + B_j C_k r_i - B_i B_j C_k$$

Therefore,

$$(Z_{oo}{}_A | G_D(r_{B_i} r_{B_j} r_{C_k})) = ZG(r_i r_j r_k) - (B_i\, ZG(r_j r_k) + B_j\, ZG(r_i r_k) C_k\, ZG(r_i r_j)) + (B_i B_j ZG(r_k) + B_i C_k\, ZG(r_j) + B_j C_k\, ZG(r_i)) - B_i B_j C_k\, ZG(s))$$

Finally, using Table II, we obtain the appropriate expression in Table IV.

Part D: Evaluation of $\langle G_B(r_{B_i}) | \Delta U_p | p \rangle \langle p | | G_C(r_{C_j}) \rangle$

From (III-7) we have

$$\langle G_B(r_{B_i}) | \Delta U_p | p \rangle \langle p | | G_C(r_{C_j}) \rangle = \int_0^\infty r_A^2 \, dr_A \, \Delta U_p(r_A) \sum_m (I\,ang_{B,l,m} \; I\,ang_{C,l,m})$$

Using Table III, we see that

$$I\,ang_{B,l,m} = \sqrt{12\pi}\; N_B(r_A)\left[C_{01B}^{m} M_1(\beta) + C_{10B}^{m} r M_0(\beta) + C_{12B}^{m} r M_2(\beta)\right]$$

where

$$C_{01B}^{m} = -\frac{BA_i BA_m}{BA} \qquad C_{10B}^{m} = \frac{\delta_{im}}{3} \qquad C_{12B}^{m} = -(C_{01B}^{m}/BA + C_{10B}^{m})$$

and $I\,ang_{C,l,m} = \sqrt{12\pi}\; N_C(r_A)\left[C_{01C}^{m} M_1(\alpha) + C_{10C}^{m} r M_0(\alpha) + C_{12C}^{m} r M_2(\alpha)\right]$

where $C_{01C}^{m} = -\frac{CA_i CA_m}{CA}$ $\quad C_{10C}^{m} = \frac{\delta_{im}}{3}$ $\quad C_{12C}^{m} = -(C_{01C}^{m}/CA + C_{10C}^{m})$

and where $\alpha = 2\zeta_C \overline{CA}\, r_A$ and $\beta = 2\zeta_B \overline{BA}\, r_A$

Thus,

$$\sum_{m} I\ ang_{B,l,m}\ I\ ang_{C,l,m} = 12\pi\ N_B(r)N_C(r)\ [\ C_{200}\, r^2 M_0(\alpha)M_0(\beta) + C_{101}\, rM_0(\alpha)M_2(\beta) + C_{110}\, rM_1(\alpha)M_0(\beta) + C_{011}M_1(\alpha)M_1(\beta) + C_{202}\, r^2 M_0(\alpha)M_2(\beta) + C_{220}\, r^2 M_2(\alpha)M_0(\beta) + C_{112}\, rM_1(\alpha)M_2(\beta) + C_{121}\, rM_2(\alpha)M_1(\beta) + C_{222}\, r^2 M_2(\alpha)M_2(\beta)]$$

where $C_{200} = \sum_{m=1}^{3} C_{10B}^{m}\, C_{10C}^{m} = \sum_{m=1}^{3} \frac{\delta_{im}}{3}\,\frac{\delta_{jm}}{3} = \frac{\delta_{ij}}{9}$

$$C_{101} = \sum_{m=1}^{3} C_{10C}^{m}\, C_{01B}^{m} = \sum_{m=1}^{3} -BA_i\,\frac{BA_m}{BA}\,\frac{\delta_{im}}{3} = -\frac{BA_i BA_j}{3BA}$$

$$C_{110} = \sum_{m=1}^{3} C_{01C}^{m}\, C_{10B}^{m} = \sum_{m=1}^{3} -CA_j\,\frac{CA_m}{CA}\,\frac{\delta_{im}}{3} = -\frac{CA_i CA_j}{3CA}$$

$$C_{011} = \sum_{m=1}^{3} C_{01C}^{m}\, C_{01B}^{m} = \sum_{m=1}^{3} CA_j\,\frac{CA_m}{CA}\,\frac{BA_i BA_m}{BA} = BA_i CA_j\,\frac{\vec{CA}\cdot\vec{BA}}{|CA|\,|BA|}$$

From the relation $C_{12B}^{m} = -(C_{01B}^{m}/BA + C_{10B})$ and $C_{12C}^{m} = -(C_{01C}^{m}/CA + C_{10C}^{m})$ we obtain $C_{202} = -\frac{C_{101}}{BA} - C_{200}$, $C_{220} = -\frac{C_{110}}{CA} - C_{200}$, $C_{112} = -\frac{C_{011}}{BA} - C_{110}$, $C_{121} = -\frac{C_{011}}{CA} - C_{101}$, and $C_{222} = -\frac{C_{121}}{BA} - C_{220}$ or $-\frac{C_{112}}{CA} - C_{202}$.

Appendix V: Combining two Gaussian Exponentials on Center B and C to form a new Gaussian Exponential on Center D

$$e^{-\zeta_C(\vec{r}-\vec{C})^2} e^{-\zeta_B(\vec{r}-\vec{B})^2} = e^{-(\zeta_C+\zeta_B)r^2+2x(\zeta_C\vec{C}_x+\zeta_B\vec{B}_x) + 2y(\zeta_C\vec{C}_y+\zeta_B\vec{B}_y)}$$

$$+ 2z(\zeta_C\vec{C}_z+\zeta_B\vec{B}_z) - (\zeta_C\vec{C}^2+\zeta_B\vec{B}^2)$$

Let $\vec{D}_x = \frac{\zeta_C\vec{C}_x+\zeta_B\vec{B}_x}{\zeta_C+\zeta_B}$, $\vec{D}_y = \frac{\zeta_C\vec{C}_y+\zeta_B\vec{B}_y}{\zeta_C+\zeta_B}$ + $\vec{D}_z = \frac{\zeta_C\vec{C}_z+\zeta_B\vec{B}_z}{\zeta_C+\zeta_B}$

Then $e^{-\zeta_C(\vec{r}-\vec{C})^2}\ e^{-\zeta_B(\vec{r}-\vec{B})^2} = e^{-\frac{\zeta_C\zeta_B}{\zeta_C+\zeta_B}\overline{CB}^2}\ e^{-(\zeta_C+\zeta_B)(\vec{r}-\vec{D})^2}$

Thus, the product of two Gaussian exponentials is a Gaussian exponential on a new center times a constant.

Appendix VI(a): Evaluation $VP_m(x)$ and $VM_m(x)$

(i) $$VP_m(x) = \int_0^\infty dr \left[e^{-(r-x)^2} + e^{-(r+x)^2} \right] r^{m-1}\, dr$$

$$\underline{m = 2k+1}$$

$$VP_{2k+1}(x) = \sum_{j=0}^{k} \Gamma(j+\tfrac{1}{2}) \binom{2k}{2j} x^{2(k-j)}$$

$$VP_3(x) = \sqrt{\pi}\ (x^2 + \tfrac{1}{2})$$

$$\underline{m = 2k+2}$$

$$VP_{2k+2}(x) = 2\sum_{j=0}^{k} \binom{2k+1}{2j} x^{2k+1-2j} E_j(x) + \sum_{j=0}^{k} \binom{2k+1}{2j+1} e^{-x^2} \sum_{\lambda=0}^{j} \frac{j!}{(j-\lambda)!} x^{2(k-\lambda)}$$

$$VP_2(x) = 2x\, E_0(x) + e^{-x^2}$$

(ii) $$VM_m(x) = \int_0^\infty dr \left[e^{-(r-x)^2} - e^{-(r+x)^2} \right] r^{m-1}\, dr$$

$$\underline{m = 2k+1}$$

$$VM_{2k+1}(x) = 2\sum_{j=0}^{k} \binom{2k}{2j} x^{2(k-j)} E_j(x) + \sum_{j=0}^{k-1} \binom{2k}{2j+1} e^{-x^2} \sum_{\lambda=0}^{j} \frac{j!}{(j-\lambda)!} x^{2(k-\lambda)-1}$$

$$VM_1(x) = 2E_0(x)$$

$$\underline{m = 2k+2}$$

$$VM_{2k+2}(x) = \sum_{j=0}^{k} \Gamma(j+\tfrac{1}{2}) \binom{2k+1}{2j} x^{2(k-j)+1}$$

$$VM_2(x) = \sqrt{\pi}\ x$$

where $E_j(x) = \int_0^x \sigma^{2j} e^{-\sigma^2}\, d\sigma$ (see Appendix VIII-a), Γ = Gamma function,

and $\binom{i}{j}$ = Binomial Coefficient

Appendix VI-b: Special Cases $VM_0(x)$ and $V_1(x)$

$$I_{0,0}(\zeta, 2x) = \frac{1}{\sqrt{\zeta}} \int_0^\infty dr\, e^{-r^2} M_0(2xr)$$

From (A-III-6) $\qquad M_0(\xi) = \frac{1}{2} \int_{-1}^{1} \cosh(\xi u)\, du$

$$I_{0,0}(\zeta, 2x) = \frac{1}{\sqrt{\zeta}} \int_0^\infty dr\, e^{-r^2} \tfrac{1}{2} \int_{-1}^{1} \cosh(2xru)\, du$$

$$= \frac{1}{\sqrt{\zeta}} \tfrac{1}{2} \int_{-1}^{1} du \int_0^\infty dr\, e^{x^2u^2} \left[e^{-(r-x)^2} + e^{-(r+x)^2} \right]$$

$$= \frac{1}{\sqrt{\zeta}} \tfrac{1}{1} \int_{-1}^{1} du\, e^{x^2u^2} VP_1(xu)$$

From (App. VI-a) $\qquad VP_1(xu) = \sqrt{\pi}$

Let $D_j(x) = \dfrac{e^{-x^2}}{2} \int_{-x}^{x} e^{\sigma^2} \sigma^{2j}\, d\sigma$ (See App. VIII-b)

$$I_{0,0}(\zeta, 2x) = \tfrac{1}{2} e^{x^2} \frac{1}{(2x)\sqrt{\zeta}} \left[2\sqrt{\pi}\, D_0(x) \right]$$

Thus, $\qquad VM_0(x) = 2\sqrt{\pi}\, D_0(x)$

$$I_{1,1}(\zeta, 2x) = \frac{1}{\zeta} \int_0^\infty dr\, re^{-r^2} M_1(2xr)$$

$$M_1(\xi) = \frac{\xi}{4} \int_{-1}^{1} \cosh(\xi u)(1-u^2)\, du$$

$$I_{1,1}(\zeta, 2x) = \frac{1}{\zeta} \frac{x}{4} \int_{-1}^{1} du\, e^{x^2u^2} (1-u)\, VP_3(xu)$$

From (App. VI-a) $\qquad VP_3(xu) = \sqrt{\pi}\,(x^2u^2 + \tfrac{1}{2})$

$$I_{1,1}(\zeta, 2x) = \frac{1}{\zeta} \frac{x}{4} \frac{2\sqrt{\pi}}{x} e^{x^2} \left(\tfrac{1}{2} D_0(x) + D_1(x) - \frac{1}{2x^2} D_1(x) - \frac{1}{x^2} D_2(x) \right)$$

Using the recursion relations for $D_j(x)$ (See App. VIII-b)

$$I_{1,1}(\zeta, 2x) = \frac{1}{\zeta}\frac{1}{2}\frac{e^{x^2}}{2x}\left[2\sqrt{\pi}\,\frac{D_1(x)}{x}\right]$$

Thus,

$$V_1(x) = 2\sqrt{\pi}\,\frac{D_1(x)}{x} = \sqrt{\pi}\left(1-\frac{D_0(x)}{x}\right)$$

Appendix VII: Evaluation of the $J_{n\ell_1\ell_2}$ integral

$$J_{n,\ell_1,\ell_2}(\zeta, a', b') = \frac{1}{\zeta^{(n+1)/2}} \int_0^\infty e^{-r^2} M_{\ell_1}(a'r)\, M_{\ell_2}(b'r)\, r^n\, dr$$

$$= \frac{1}{\zeta^{(n+1)/2}} \frac{a'^{\ell_1} b'^{\ell_2}}{2^{\ell_1+\ell_2+2}\, \ell_1!\, \ell_2!} \int_{-1}^{1} du\, (1-u^2)^{\ell_1} \int_{-1}^{1} dv\, (1-v^2)^{\ell_2} \qquad \text{A-VII-1}$$

$$* \int_0^\infty e^{-r^2} \cosh(a'ur) \cosh(b'vr)\, r^{n+\ell_1+\ell_2}\, dr$$

Substituting the relation

$\cosh(a'ur)\cosh(b'vr) = \frac{1}{2}[\cosh((a'u + b'v)r) + \cosh((a'u - b'v)r)]$ into (A-VII-1) and noting that the integral is even in v for both terms, we may change v to -v in the second term which is equivalent to the first so that

$$J_{n,\ell_1,\ell_2}(\zeta, a', b') = \frac{1}{\zeta^{(n+1)/2}} \frac{a'^{\ell_1} b'^{\ell_2}}{2^{\ell_1+\ell_2+2}\, \ell_1!\, \ell_2!} \int_{-1}^{1} dv (1-v^2)^{\ell_2} \int_{-1}^{1} dv (1-v^2)^{\ell_2}$$

$$\int_0^\infty e^{-r^2} \cosh((a'u+b'v)r) r^{n+\ell_1+\ell_2} dr$$

$$= \frac{1}{\zeta^{(n+1)/2}} \frac{a'^{\ell_1} b'^{\ell_2}}{2^{\ell_1+\ell_2+2}\, \ell_1!\, \ell_2!} \frac{1}{2} \int_{-1}^{1} du(1-u^2)^{\ell_1} \int_{-1}^{1} dv\, (1-v^2)^{\ell_2} e^{\frac{(a'u+b'v)^2}{4}}$$

$$VP_{n+\ell_1+\ell_2}\left(\frac{a'u+b'v}{2}\right)$$

Let $$A = \frac{1}{2} \frac{1}{\zeta^{(n+1)/2}} \frac{a'^{\ell_1} b'^{\ell_2}}{2^{\ell_1+\ell_2+2}\, \ell_1!\, \ell_2!}$$

Let $\alpha = a'u$ $\beta = b'v$ and expanding $(1-u^2)^{\ell_1}$ and $(1-v^2)^{\ell_2}$,

$$J_{n,\ell_1,\ell_2}(\zeta, a', b') = A \sum_{i_1=0}^{\ell_1} \sum_{i_2=0}^{\ell_2} (-1)^{i_1+i_2} \frac{1}{a'^{2i_1+1} b'^{2i_2+1}} \binom{\ell_1}{i_1} \binom{\ell_2}{i_2}$$

$$\int_{-a'}^{a'} d\alpha \int_{-b'}^{b'} d\beta\, \alpha^{2i_1} \beta^{2i_2} e^{\frac{(\alpha+\beta)^2}{4}} VP_{n+\ell_1+\ell_2}\left(\frac{\alpha+\beta}{2}\right)$$

Letting $x = \frac{\alpha+\beta}{2}$ $y = \frac{\alpha-\beta}{2}$ $J = \begin{vmatrix} \frac{\partial\alpha}{\partial x} & \frac{\partial\beta}{\partial x} \\ \frac{\partial\alpha}{\partial y} & \frac{\partial\beta}{\partial y} \end{vmatrix} = 2$

and noting that the integrand is even under the simultaneous change of α and β to $-\alpha$, $-\beta$

$$J_{n,\ell_1,\ell_2}(\zeta, a', b') = A \sum_{i_1=0}^{\ell_1} \sum_{i_2=0}^{\ell_2} (-1)^{i_1+i_2} \frac{1}{a'^{2i_1+1} b'^{2i_2+1}} \binom{\ell_1}{i_1} \binom{\ell_2}{i_2}$$

$$4\Big[\int_0^{\frac{a'+b'}{2}} dx \int_{-b'+x}^{a'-x} dy\, (x+y)^{2i_1} (x-y)^{2i_2} e^{x^2} VP_{n+\ell_1+\ell_2}(x)$$

$$- \int_0^{\frac{b'-a'}{2}} \int_{-b'+x}^{-a'-x} dy\, (x+y)^{2i_1} (x-y)^{2i_2} e^{x^2} VP_{n+\ell_1+\ell_2}(x)$$

Defining

$$f^{\pm}(j_3,\ j,\ a',b') = \binom{j_3+1}{j}\left[b'^{\,j_3+1-j}(-1)^{j_3-j} + a'^{\,j_3+1-j}(-)^{j_3+1}(\mp)^{j_3+1-j}\right]$$

$$D_m(x) = e^{-x^2}\int_0^x e^{\sigma^2}\sigma^m\, d\sigma$$

$$DE_{j,m}(x) = e^{-x^2}\int_0^x e^{\sigma^2}\,\sigma^m \int_0^{\sigma} e^{-\tau^2}\tau^j d\tau$$

we have by straightforward integration

$$J_{n,\ell_1,\ell_2}(\zeta,a',b') = \frac{1}{\zeta^{(n+1)/2}}\,\frac{1}{2^{\ell_1+\ell_2+1}}\sum_{i_1=0}^{\ell_1}\sum_{i_2=0}^{\ell_2}(-)^{i_1+i_2}\binom{\ell_1}{i_1}\binom{\ell_2}{i_2}$$

$$a'^{(\ell_1-2i_1-1)}b'^{(\ell_2-2i_2-1)}$$

$$\sum_{j_1=0}^{2i_1}\sum_{j_2=0}^{2i_2}\binom{2i_1}{j_1}(-)^{j_2}\binom{2i_2}{j_2}\frac{1}{j_1+j_2+1}\sum_{j=0}^{k}\left(F^{+}(k,j,i_1+i_2,j_1+j_2,\ell,a',b')\right.$$

$$\left.-F^{-}(k,j,i_1+i_2,j_1+j_2,\ell,a',b')\right)$$

where for $n+\ell_1+\ell_2 = 2k$

$$F^{\pm}_{k,j,i,j',\ell}(a',b') = \Gamma(j+\tfrac{1}{2})\,e^{\frac{(b'\pm a')^2}{4}}\,f^{\pm}_{j',\ell}(a',b')D_{(2(k-j)+2i-j'+\ell)}\left(\frac{(b'\pm a')}{2}\right)$$

and for $n+\ell_1+\ell_2=2k+1$

$$F^{\pm}_{k,j,i_1,j',\ell}(a',b') = 2\binom{2k+1}{2j}e^{\frac{(b'\pm a')^2}{4}}f^{\pm}_{j',\ell}(a',b')\,DE_{j,(2k-j+1+2i-j'+\ell)}\left(\frac{b'\pm a'}{2}\right)+\binom{2k+1}{2j+1}e^{\frac{(b'\pm a')^2}{4}}f^{\pm}_{j',\ell}(a',b')\sum_{\lambda=0}^{j}\frac{j!}{(j-\lambda)!}D_{2k-j-\lambda+2i-j'+\ell)}\left(\frac{b'\pm a'}{2}\right)$$

Appendix VIII: Special Functions

(a) $$E_j(x) = \int_0^x e^{-\sigma^2} \sigma^{2j}\, d\sigma \qquad (1)$$

$E_0(x)$ is related by a multiplicative factor of $\frac{\sqrt{\pi}}{2}$ to the error function

Recursion formula: $$E_{j+1}(x) = \tfrac{1}{2}[(2j+1)E_j(x) - e^{-x^2} x^{2j+1}] \qquad (2)$$

However, for small x accuracy is lost as one goes from small i to large j. It is better to express E_j in terms of E_{j+1}. For small x, the power series expansion may be used:

$$E_j(x) = \frac{e^{-x^2} x^{2j+1}}{2j+1} \left[1 + \frac{2x^2}{2j+3}\left[1 + \frac{2x^2}{2j+5}\left[1 + \cdots\right]\right]\right] \qquad (3)$$

To evaluate $E_0(x)$ (let it be represented by y), the program interpolates from a table using a Taylor series expansion. Since

$$y^{(n+2)} = -2x\, y^{(n+1)} - 2n\, y^{(n)} \qquad (4)$$

each term in the expansion is easily evaluated. The table itself is readily created by the same means. Due to the alternating sign of (4), errors are damped out during evaluation of the grid points of the table. For large values of x, $E_0(x)$ is set equal $E_0(\infty) = \frac{\sqrt{\pi}}{2}$. The function Err3(x), defined such that

$$E_0(x) = e^{-x^2}\, x(1.0 + Err^3(x))$$

is evaluated before $E_0(x)$ in the program for small x in order to avoid loss in accuracy.

Appendix VIII-b.

(b) $$D_j(x) = e^{-x^2} \int_0^x e^{\sigma^2} \sigma^j d\sigma \qquad (1)$$

$D_0(x)$ is called the Dawson integral (see p. 298)

$$D_1(x) = \tfrac{1}{2}(1-e^{-x^2})$$

The recursion formula

$$D_{j+2}(x) = \tfrac{1}{2}(x^{j+1} - (j+1)\, D_j(x)) \qquad (2)$$

Like $E_j(x)$, accuracy is lost for small x using (2), so the inverse of (2) is used, with for some maximum value j;

$$D_j(x) = \frac{x^{j+1}}{j+1} \left(1-\frac{2}{m+3}\, x^2 \left(1-\frac{2x^2}{m+5} \left(1-\cdots\right)\right)\right) \qquad (3)$$

To evaluate $D_0(x)$, the program uses the same procedure as for $E_0(x)$. Letting the function be represented by **y**, we have

$$y^{(n+2)} = -2xy^{(n+1)} - 2(n+1)y^{(n)} \qquad (4)$$

which is very similar to (4) of VIII-a. For small values of x,

$$D_0(x) = x\left[1-\frac{2x^2}{3}\left[1-\frac{2x^2}{5}\left[1-\cdots\right]\right]\right] \qquad (5)$$

which is similar to (3) of VIII-a. For large values of x,

$$D_0(x) = \frac{1}{2x}\left(1+\frac{1}{2x^2}\left(1+\frac{3}{2x^2}\left(1+\frac{5}{2x^2}\left(1+\cdots\right)\right)\right)\right) \qquad (6)$$

The function Daws 3(x) defined such that

$$D_0(x) = x\ (1.0 + \text{Daws } 3(x))$$

is evaluated before $D_0(x)$ in the program for small x in order to avoid loss in accuracy.

Appendix VIII-c

$$(c) \qquad DE_{j,i}(x) = e^{-x^2} \int_0^x e^{u^2} u^i \int_0^u e^{-\sigma^2} \sigma^{2j} d\sigma \tag{1}$$

The recursion formula is

$$DE_{j,i+2} = \tfrac{1}{2}\left[x^{i+1} E_j(x) - (i+1)\, DE_{j,i}(x) - \frac{e^{-x^2} x^{i+2j+2}}{i+2j+2} \right] \tag{2a}$$

$$DE_{j+1,i} = \tfrac{1}{2}\left[(2j+1)\, DE_{j,i} - \frac{e^{-x^2} x^{i+2j+2}}{i+2j+2} \right] \tag{2b}$$

As for $E_j(x)$ and $D_j(x)$, for small x it is better to start with large values of i and j for $DE_{j,i}(x)$. For small x,

$$DE_{j,i}(x) = \frac{e^{-x^2} x^{i+2j+2}}{2j+1} \left[\frac{1}{m+2j+2} + \frac{2x^2}{2j+3} \left[\frac{1}{i+2j+4} + \frac{2x^2}{2j+5} \left[\frac{1}{i+2j+6} + \cdots \right] \right] \right] \tag{3}$$

To evaluate $DE_{0,0}(x)$ and $DE_{0,1}(x)$ (let them be represented by y and w respectively), the procedure is the same as for $E_0(x)$ and $D_0(x)$, with

$$\begin{aligned} y^{(n+2)} &= 2xy^{(n+1)} + 2ny^n \\ w^{(n)} &= (n-1)y^{(n-1)} + xy^n \end{aligned} \tag{4}$$

For large values of x, $DE_{j,i}(x)$ may be approximated by

$$e^{-x^2} \int_0^x du\, e^{u^2} u \frac{\sqrt{\pi}}{2} = \frac{\sqrt{\pi}}{2} D_i(x) \tag{5}$$